The role of impurities on the morphology of NaCl crystals

An atomic scale view

Radenović, Neda
The role of impurities on the morphology of NaCl crystals: An atomic scale view
PhD Thesis, Radboud University Nijmegen, The Netherlands
With summary in Dutch

ISBN-10: 90-9020220-X
ISBN-13: 978-90-9020220-4

printed by: PrintPartners Ipskamp, Enschede

Part of the experimental work described in this thesis was performed at the European Synchrotron Radiation Facility, Grenoble, France.
The work is part of the CW Programme Grant on "The role of imurities in crystal growth" and was made possible by financial support from the Netherlands Organization for Scientific Research (Nederlandse Organisatie voor Wetenschappelijk Onderzoek (NWO)).

The role of impurities on the morphology of NaCl crystals

An atomic scale view

een wetenschappelijke proeve op het gebied van
de Natuurwetenschappen, Wiskunde en Informatica

Proefschrift

ter verkrijging van de graad van doctor
aan de Radboud Universiteit Nijmegen,
op gezag van de Rector Magnificus Prof. Dr. C.W.P.M. Blom,
volgens besluit van het College van Decanen
in het openbaar te verdedigen op dinsdag 24 januari 2006,
des namiddags om 3.30 uur precies

door

Neda Radenović

geboren op 28 november 1970
te Belgrado, Servië

Promotor:	Prof. dr. Elias Vlieg
Co-promotor:	Dr. W. J. P. van Enckevort
Manuscriptcommissie:	Prof. dr. S. Speller
	Prof. dr. P. Bennema
	Dr. R.M. Geertman (Diosynth B.V. Oss)

The role of impurities on the morphology of NaCl crystals

An atomic scale view

A scientific essay in Natural Sciences

Doctoral thesis

to obtain the degree of doctor
from Radboud University Nijmegen,
on the authority of the Rector, Prof. Dr. C.W.P.M. Blom,
according to the decision of the Council of Deans
to be defended in public on Tuesday, 24 january 2006
at 3.30 p.m. precisely

by

Neda Radenović

born in Belgrade, Serbia
on 28 november 1970

Doctoral supervisor:	Prof. dr. Elias Vlieg
Co-supervisor:	Dr. W. J. P. van Enckevort

Doctoral Thesis Committee:	Prof. dr. S. Speller
	Prof. dr. P. Bennema
	Dr. R.M. Geertman (Diosynth B.V. Oss)

to my father Prof. dr. Čedomir N. Radenović

This thesis is based on work carried out at Department of Solid State Chemistry, Radboud University Nijmegen. Herewith I would like to express my gratitude to:

Dr. Willem van Enkevort, my direct supervisor, for his deep involvment and guidance throughout all the stages of my work and his carefull attention.

Prof. Dr. Elias Vlieg, for supervising the work related to Surface X-ray diffraction, as well as, support, discussions and channelling ideas through the entire project.

All co-authors of the papers presented in this thesis. Special thanks are given to Daniel Kaminski for our fruitfull collaboration.

Excellent working atmosphere and collegiality between the members of the Solid State Chemistry group were very much appreciated. Posebnu zahvalnost dugujem Dr. Jeleni Arsić na njenoj podršci od mog dolaska u Holandiju.

Contents

Chapter 1

Introduction

Crystals often exhibit exotic, but beautiful geometric shapes. Their shiny, faceted and often colorful appearances have always attracted people. This made jewelry the main application of crystals until the 19th century. Many single crystals of minerals formed in the geologic past in the course of hundreds to millions of years are found in mines and caves throughout the world. Nowadays, most crystals are produced artificially to satisfy the needs of science, technology and jewelry.

1.1. WHY THIS THESIS?

Crystallization and crystal growth are important for separation, purification and definition of solid compounds. It has been known for more than two centuries that impurities in the mother phase can have a large effect on crystal morphology [1]. A variety of studies have been reported on mostly qualitative observations of morphological changes caused by the addition of small quantities of impurity [2]. Many theories have been developed, but there is, generally, lack of experimental information which would provide fundamental understanding about the microscopic mechanisms behind this effect.

Therefore, the purpose of the present study is to obtain knowledge on the atomic / molecular scale of the effects of impurities in the growth solution on the structure and growth of a crystal surface, aiming at a better understanding of the mechanisms through which impurities alter crystal growth. For this study we used NaCl single crystal as a model system, (figure 1.1).

Figure 1.1: NaCl crystals grown from pure aqueous solution with (left crystal) and without formamide impurity (right crystal)

1.2. MORPHOLOGY AND CRYSTAL GROWTH

The geometric shapes of many crystals raised curiosity to understand why and how the different morphologies of crystals develop. Moreover, for many applications the shape of a crystal is very important. For example, product quality and product handling often depend on the outer crystal shape. In the early phase of research the first attempts to explain the wealth of different crystal shapes were based only on internal factors, i.e. the type and parameters of the crystallographic unit cell. Bravais, Friedel, Donnay and Harker made the first approach in this way, by assuming that the morphological importance of a face *(hkl)* increases with the interplanar distance d_{hkl} [3]. Later, landmark papers written by Hartman, Perdok and Bennema [4-8], gave the foundations for a quantitative determination of crystal morphology. Using their periodic bond chain (PBC) theory the authors derive the morphology of a crystal from the structural information of the building units and their interactions in the unit cell. By using only first neighbour interactions between these units, periodic chains of bonds are constructed and from them so-called connected nets. This are sets of intersecting PBC's, which are parallel to certain crystal faces. Here they distinguish three different types of faces: F(lat) faces, which have a connected net, S(tepped) faces, which have parallel non-intersecting PBCs and K(inked) faces, which have no PBC within the growth layer d_{hkl}. Calculated strengths of the connected nets generate a list of possible crystal faces. Modern versions of these theories are nowadays used for analyzing the equilibrium and growth morphology of real crystals [9, 10].

Beside internal factors, the morphology of crystals is determined by external factors, i.e. growth conditions, as well. The habit of a crystal is determined by the relative growth rates of its faces in different directions: the faster the growth in a given direction the smaller the face developed perpendicular to it. In general, a crystal grows faceted with well-defined flat faces, but in many cases some of the faces appear rounded and are rough at a molecular scale [11, 12]. A flat face turns rough above a critical temperature. This effect is known as thermal roughening. In addition, below its roughening temperature a flat face can become rough if the supersaturation exceeds a critical value. This so-called kinetic roughening results in comparably high growth rates.

Depending on growth parameters, such as temperature and supersaturation, different growth mechanisms play a role in crystal growth. Below the roughening temperature and at not too high supersaturation the growth of crystals usually occurs by the addition of growth units at the kink sites of steps that are present on the surface. A perfect crystal surface devoid of dislocations grows by formation of two-dimensional nuclei, which further expand by addition of new growth units at the step edges of the 2D islands.

However, real crystals are usually not perfect and they contain various types of lattice defects. A very common defect is the screw dislocation, which acts as a perpetual step source, resulting in the appearance of a growth spiral. Spiral growth is the most important growth mechanism on a flat crystal face at low supersaturation. Appearance and morphology of a growth spiral reflects the internal structural properties and the growth conditions and thus provides valuable information on the mechanism of crystal growth.

At highest supersaturations growth occurs by random deposition of growth units on the entire surface. This results in kinetical roughening and consequently in macroscopically rounded surfaces.

The alkali halide crystals investigated in this thesis all show a faceted growth shape and depending on the growth conditions all the above mentioned mechanisms were observed.

1.2.1. The role of impurities

Besides the above mentioned external parameters, i.e., temperature and supersaturation, crystal growth also strongly depends on impurities present in the crystallization system. For this reason, impurities are often added to crystal growth systems in order to obtain a desired crystal shape, for instance blocks instead of needles. For that purpose tailor-made additives are designed that fit at specific surface locations and thus affect the growth of particular crystallographic faces [13]. If growth solutions are pure we generally have regular, monomolecular surface steps. Addition of impurities into a growth solution often generates irregular macrosteps, which again leads to the development of liquid inclusions.

For the case of low impurity concentration Cabrera and Vermilyea [14] postulated a mechanism based on the occurrence of strongly adsorbed impurity particles distributed all over the crystal surface. If a propagating growth step hits such a particle, it stops at that point and tries to move around it, resulting in a deformation of the step edge. Steps are completely blocked if the mean distance between strongly adsorbed impurity particles is equal to or less than the size of a critical two-dimensional nucleus for the corresponding supersaturation. On the other hand, weakly adsorbed impurities at not too high concentrations retard the crystal growth by occupying and thus blocking a part of the active growth centres [15, 16]. If they are relatively small and mobile, their main effect is to reduce the number of the kinks, by occupying them. They can diffuse two-dimensionally on the surface and be expelled by the moving step. Relatively large and immobile impurities, such as organic dyes, act as an obstacle for the movement of surface steps. All this results in a reduction of the growth velocity.

If the impurities are present in high concentrations, then adsorption can take place on the terraces between the steps. This changes the surface energies of the different crystal faces and hampers the addition of growth units to the surface and step positions. As a consequence crystal growth is retarded or even blocked. In a few cases, such impurities lower step free energies or act as preferred sites for 2D nucleation. These effects stimulate crystal growth.

1.3. SODIUM CHLORIDE

Rocksalt, also known as the mineral halite, is widely distributed in nature (Figure 1.2). It makes up nearly 80% of the dissolved material in seawater. It is also found naturally in ancient bedrocks throughout the world, where vast extinct salt lakes and seas have evaporated millions of years ago, leaving behind thick deposits of salt.

Figure 1.2: Mineral halite, better known as rock salt or sodium chloride

NaCl is essential to life on earth. It is a necessary ingredient in the diets of people and animals, but it also plays a role in many industrial processes. In this thesis it is important as a model system in understanding crystal growth on an atomic level if impurities are added to the growth system.

In fact, NaCl is one of the first crystals for which the influence of an impurity was observed and investigated, see figure 1.1. Already in 1783 Rome de l'Isle reported the influence of urea on the growth morphology of NaCl in his book Cristallographie [1], which is one of the first fundamental works on modern crystallography, see figure 1.3. He reported that common salt forms octhedra instead of cubes from brines containing about 30% of urea. A hundred years later, it was found that adding $CrCl_3$ has the same effect on salt

crystallisation [17], and the same was reported for the chlorides $CdCl_2$, $ZnCl_2$ and $MnCl_2$ in the 1930's [18].

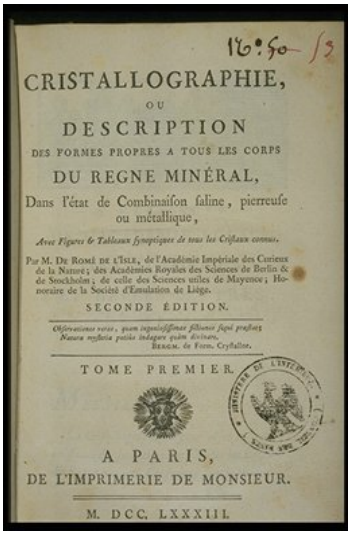
CRISTALLOGRAPHIE,
OU
DESCRIPTION
DES FORMES PROPRES A TOUS LES CORPS
DU REGNE MINÉRAL,
Dans l'état de Combinaiſon ſaline, pierreuſe ou métallique,
Avec Figures & Tableaux ſynoptiques de tous les Criſtaux connus.
Par M. DE ROMÉ DE L'ISLE, de l'Académie Impériale des Curieux de la Nature; des Académies Royales des Sciences de Berlin & de Stockholm; de celle des Sciences utiles de Mayence; Honoraire de la Société d'Emulation de Liège.
SECONDE ÉDITION.
TOME PREMIER.
A PARIS,
DE L'IMPRIMERIE DE MONSIEUR.
M. DCC. LXXXIII.

Figure 1.3: Jean-Baptiste Romé de l'Isle (1736-1790). The front page of his major contribution, *Cristallographie,* published in three volumes in 1783.

Since then, much work has been done on this issue, but the control on growth and morphology of NaCl crystals remained primarily a matter of 'mix and try'. In the 1950's and 1960's, more systematic studies were performed, in which the shape of NaCl crystals grown from aqueous solutions was determined as a function of impurity concentration [19-22]. For this crystal the stable crystallographic face changes from {100} to {111} for increasing impurity concentration. For impurities like Cd^{2+}, Mn^{2+}, Pb^{2+} and Hg^{2+} it was suggested the impurities form a fully adsorbed two dimensional layer [19, 20]. However, no direct proof was given.

The transition from the stable {100} face to the octahedral or {111} face of NaCl structure crystals is an intriguing phenomenon in the fields of crystal growth and surface science. According to the PBC analysis, the NaCl first-nearest–neighbour crystal graph [23] identifies three connected nets: one (100) connected net for the {100} orientation and the two symmetry-related $(111)_1$ and $(111)_2$ connected nets for the {111} orientation (Figure 1.4). These two $(111)_{1,2}$ connected nets correspond to one connected net with Na^+ above Cl^- and another with Cl^- above Na^+. The two $\{111\}_{1,2}$ connected nets are related to each other by an inversion point at the Na^+ and Cl^- positions, which leads to symmetry roughening as described by Meekes et al. [24]. Only considering first

order neighbour interaction and neglecting the mother phase this implies zero step energy and the {111} face should be rough and grow fast.

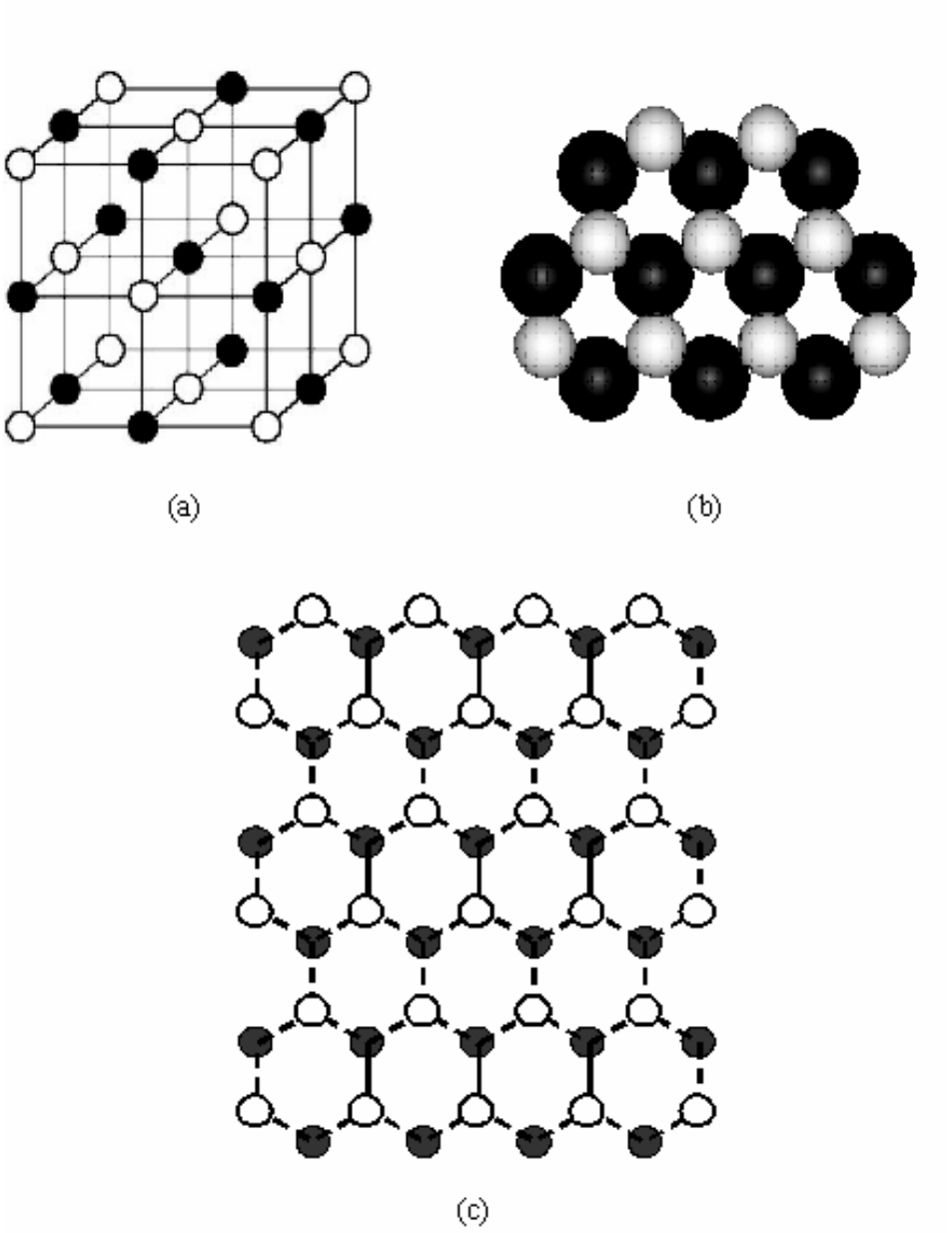

Figure 1.4: (a) The NaCl unit cell. The white spheres represent the Na^+ ions (or Cl^-), and the black spheres are Cl^- ions (or Na^+) ions. (b) Top view of the ion arrangement on the {111} plane; (c) Top view one of the two (111) connected nets for the NaCl crystal, consisting of a layer of white and a layer of black ions.

In addition to this, since the bulk structure of the NaCl crystal consists of alternating layers of cations and anions stacked along <111> directions and because of their infinitely long-range electrostatic interactions, the energy of the {111} NaCl surface should be very high. Therefore, these polar surfaces are expected to be highly unstable and should not be present in the morphology of NaCl-type crystals. A simple electrostatic explanation of the instability of the polar surfaces is given in figure 1.5. The presence of an equidistant layers charged with densities +σ and –σ induces an electrostatic field which is constant inside the bilayers and equal to zero between them. The total dipole moment is proportional to the segment thickness: $\mu = N\sigma R$ (N is number of bilayers). The electrostatic energy equals to $E = 4\pi NR\sigma^2$. As a result, we have a monotonic increase of the electrostatic potential through the sample, $V = 4\pi NR\sigma$ [25].

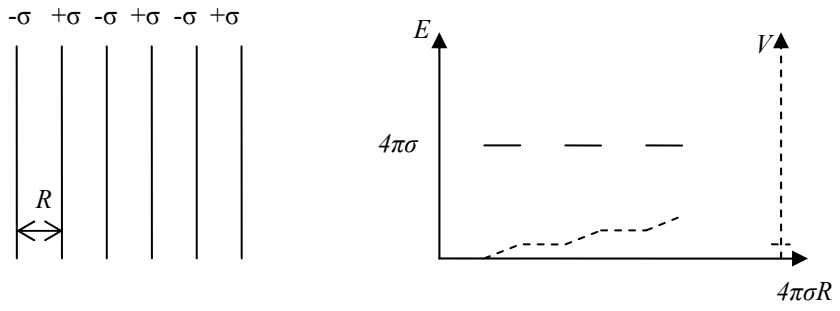

Figure 1.5: Spatial variations of the electric field E (solid lines) and of the electrostatic potential V (dashed lines) in a thin, electrostatic neutral sample cut along polar directions.

Theoretical calculations for ionic crystals with rock salt type structure suggest two possibilities for the stabilization of the {111} faces if no impurities are present: a) the bulk terminated {111} surface breaks up into neutral {100} facets upon annealing or b) this surface reconstructs [26]. Detailed information was obtained for solid - vacuum systems, of which the {111} surface of the rocksalt structure NiO was the most extensively studied case [27-31]. Some results showed the existence of an epitaxial p(2x2) overlayer [30, 32-34]. This supports the stabilization of the {111} NaCl surface by octupoles, as proposed by Lacmann 40 years ago [35]. The structural unit of such a surface is a simple cubic $(NaCl)_4$ octupolar unit, instead of the conventional face-centered cubic (f.c.c) lattice with a dipolar Na^+-Cl^- basis.

In the case of growth from solutions it was found in our group [36, 37], using AFM and SXRD, that no reconstruction occurs for the {111} NaCl surfaces. Moreover, the observed step height was $d_{\{111\},}$ which implies that,

depending on the growth conditions, one of the two connected nets is always on the top, namely Na^+ above Cl^- or opposite.

1.4. THE TECHNIQUES USED

Crystal growth is a surface process. Therefore, in this thesis we mainly used the following surface characterization techniques: differential interference contrast optical microscopy (DICM), atomic force microscopy (AFM) and surface X-ray diffraction (SXRD).

1.4.1. Optical microscopy

Optical microscopy is used to observe growth steps and all kinds of undulations on the crystal surface. As a result of height differences a light wave reflected from the crystal surface shows spatial variation in phase. Using a device in an optical microscope that translates these phase differences into intensity differences, height differences down to (sub)nanometer height can be visualized. In this way even atomic/molecular height steps can be detected. One way to do this is by using differential interference contrast.

Differential interference contrast microscopy is the most commonly used interferometric technique to image phase (height) differences. The basic principle of Nomarski DICM is given in figure 1.6. Here the incident beam is reflected from a surface with a step of height h. The reflected beam passes an optical device that splits it into two coherent waves of equal intensity, which are shifted over small lateral distance Δ ($\approx$ 1μm) and over an adjustable distance δ along the optical axis. In the region Δ near the step, the phase difference between both waves is $4\pi h/\lambda + \delta$, which differs from the value δ elsewhere. By interference of the two waves a step becomes visible as a line of different intensity in the microscope image. The method, which is capable of detecting step heights as low as 1 nm, gives only qualitative information and can be used for both *in-situ* and *ex-situ* surface observations.

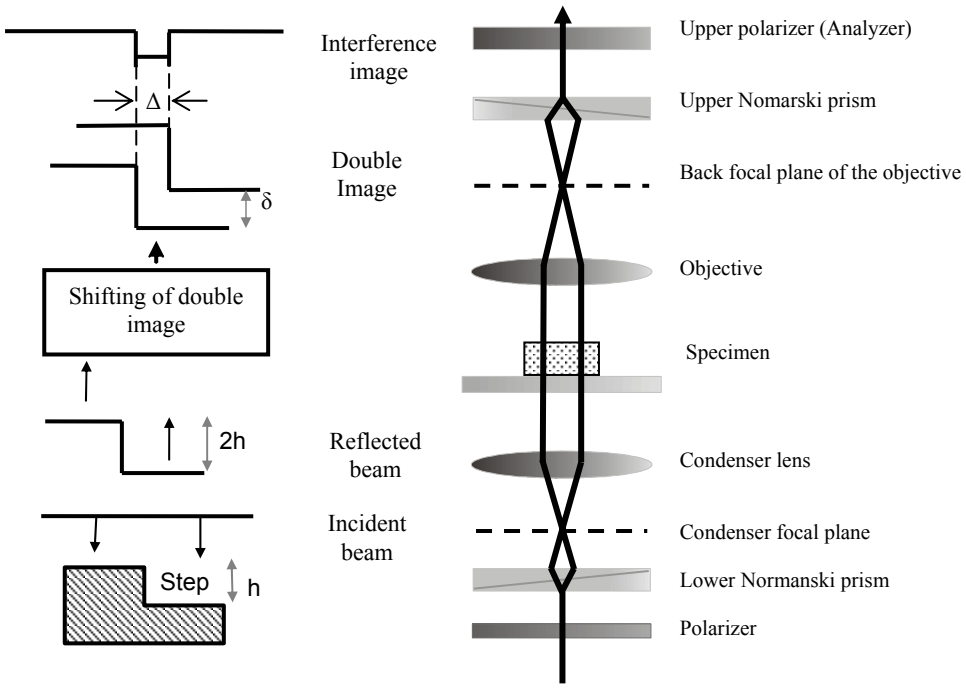

Figure 1.6: Left: Principle of DICM in reflection mode. Right: Optical layout of a DICM according to the principle of Normanski.

1.4.2. Atomic-force microscopy

This scanning probe microscope is based on scanning a surface by a sharp tip, where tip-surface interaction forces are measured as function of position. The principle of contact-mode atomic force microscopy (CM-AFM) is given in figure 1.7. A scanner made of piezo electric material is used to displace the tip-cantilever combination with respect to the sample holder, or reversed, in a controlled way. When the tip contacts the sample, the cantilever will deflect. The amount of deflection is proportional to the force between tip and sample. A laser beam reflected from the cantilever hits a position sensitive photodetector consisting of four side-by-side photodiodes. The difference between the photodiode signals indicates the position of the laser spot on the detector and thus the angular deflection (and torsion) of the cantilever. If the scanning tip encounters a height difference on the sample, the cantilever deflection will change followed by a change of the detector signal. This detector signal is fed into a feedback loop that maintains the contact force constant by adjusting the tip-sample distance until the detector signal reaches its original setpoint value. The change of z-piezo voltage needed for this is used to generate a topological

or height image, whereas recording the detector signal generates a deflection or error image. CM-AFM is capable of imaging height differences and lattice periodicities down to a few tenths of an Ångström.

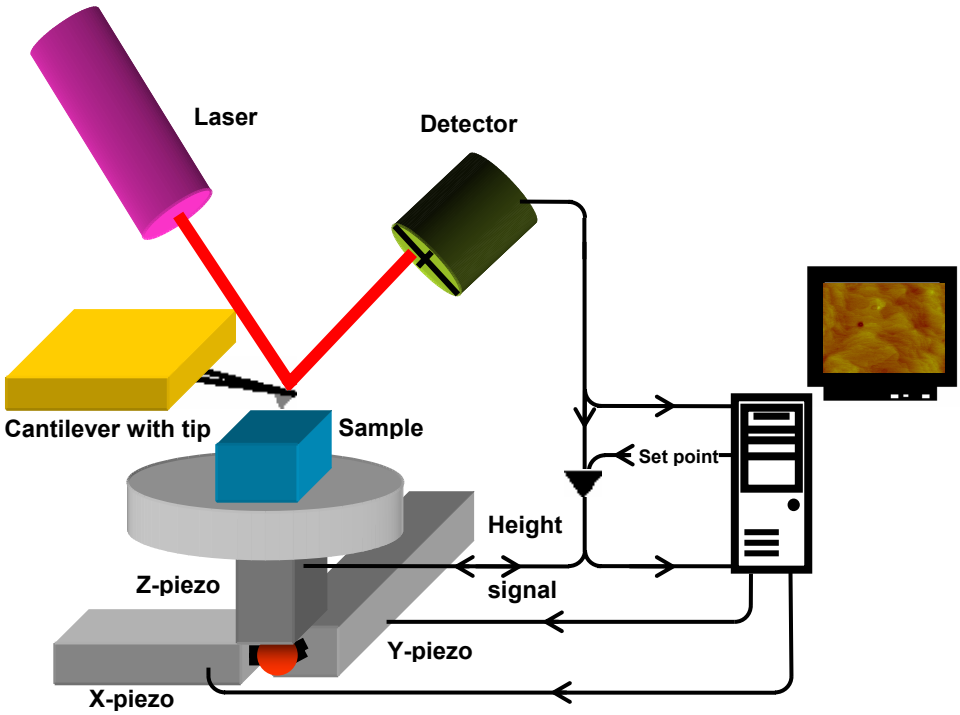

Figure 1.7: Basic principle of AFM.

1.4.3. Surface X-ray diffraction (SXRD)

Surface X-ray diffraction is a technique for the structure determination of crystal surfaces and solid-liquid interfaces by using intense X-ray beams provided by synchrotron radiation sources. This high intensity is needed in order to detect the weak signal from the surface, which is a million times less than a typical signal from the bulk. The two-dimensional nature of the surface results in rods of diffraction intensity, so called crystal truncation rods (CTRs) [38, 39], whereas three-dimensional diffraction from the bulk results in spots of high intensity, which are the so-called Bragg peaks (Figure 1.8). These Bragg peaks are denoted with three integer indices *(hkl)* and correspond to lattice points in reciprocal space. The intensity along a CTR, denoted by *(hk),* is given by the in interference sum of the bulk and surface layer. The information about the surface structure is found on a CTR at the positions between the Bragg

peaks, where the diffracted intensity mainly originates from the surface. The central (00) rod, the so called specular rod, gives the total thickness of the liquid. If this liquid layer is laterally disordered it only contributes to this rod, whereas in the case of complete ordering it will contribute to all rods.

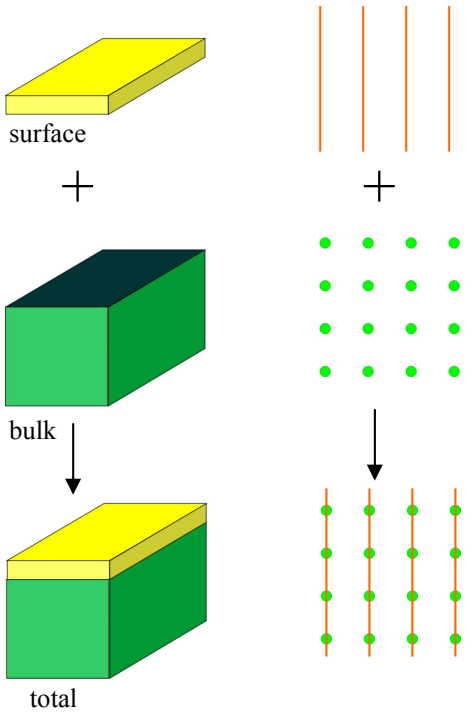

Figure 1.8:. 2D diffraction from the surface (top) results in rods in reciprocal space, whereas 3D diffraction from bulk (middle) gives Bragg peaks. A combination of both results in crystal truncation rods (bottom)

1.5. THIS THESIS

In this thesis we investigate the effect of impurities on the growth of alkali halide crystals with emphasis on NaCl. Attention is mainly focused on the morphology and atomic scale structure of the {111} faces. For that purpose octahedral NaCl single crystals of several milimeters in size were grown from aqueous solution with different impurities. The octahedral surfaces of these crystals were investigated using optical microscopy, atomic force microscopy and surface X-ray diffraction.

In the four chapters that follow we use mainly formamide as impurity. The second chapter compares the morphology of {111} NaCl faces grown from water-formamide solution with that obtained from pure water solution. AFM observations show that the formamide grown NaCl surface is not reconstructed and appears as a truncated bulk phase far below the roughening temperature. In addition, in order to get insight into the mechanism of stabilization and to ascertain if the {111} faces are again stabilized, instead of formamide we also added homologous compounds (urea, dimethylformamide and benzamide) to the NaCl-water growth solution.

In contrast to the above mentioned chapter in which only NaCl crystals in combination with different impurities are investigated, in the third chapter we study the morphology of a whole group of alkali halide crystals, but now grown only from formamide solutions. In addition to this, the (im-)possibility to obtain {111} surfaces on NaCl crystals grown from pure water solutions at high supersaturations is also investigated.

The surface structure of {111} NaCl at atomic scale is investigated using surface X-ray diffraction. These observations show that this surface is atomically flat without surface reconstruction. Chapter four describes the *in-situ* SXRD analysis of {111} NaCl surfaces in contact with water-formamide solutions at different environmental conditions. Chapter five presents AFM, optical microscopic and SXRD observations of {111} NaCl surfaces grown from aqueous solutions with small concentration of $CdCl_2$ added. Cd^{2+} is very different from formamide and is already active at far lower concentrations than formamide. In this case it is found that the octahedral surface is Cl^- terminated, with ¼ monolayer of Cd^{2+} at random Na^+ sites on top. This implies that the mechanism for the stabilization of the {111} NaCl crystal face is different in both cases. Moreover, these observations show that this surface is atomically flat without surface reconstruction.

In the last chapter we discuss the development of pyramids on the {100} NaCl crystal surface during etching in formamide. It is shown that these features are formed due to the presence of masking dust particles at the dissolving surface.

References

1. J.B.L. de Rome de l' Isle, in: *Cristallographie*, Paris, 1783) p. p. 379.
2. H.E. Buckley, in: *Crystal Growth*, (John Wiley & Sons, New York, 1951) p. 556.
3. J.D.H. Donnay and D. Harker, Am. Mineral. 22 (1937) 446.
4. P. Hartman and W.G. Perdok, Acta Crystallogr. 8 (1955) 49.
5. P. Hartman, in: *Crystal Growth An Introduction*, ed. P. Hartman, (North-Holland, Amsterdam, 1973) p. 367.
6. P. Hartman and P. Bennema, J. Crystal Growth. 49 (1980) 145.

7. P. Bennema and G. Gilmer, in: *Crystal Growth, An Introduction*, ed. P. Hartman, (North-Holland, Amsterdam, 1973) p. 272.
8. P. Bennema, J. Crystal Growth. 122 (1992) 110.
9. R.F.P. Grimbergen, P. Bennema and H. Meekes, Acta Crystallogr. 55 (1999) 84.
10. S.X.M. Boerrigter, G.P.H. Josten, J. van de Streek, F.F.A. Hollander, J. Los, H.M. Cuppen, P. Bennema and H. Meekes, J. Phys. Chem. A. 108 (2004) 5894.
11. P. Bennema and J.P. van der Eerden, in: *Morphology of crystals, Part A, Chapter 1*. Crystal Graphs, Connected Nets, Roughening Transition and Morphology of Crystals, ed. I. Sunagawa, (Terra Scientific Publishing Company, Tokyo and D. Reidel Publishing Company, Dordrecht/ Boston/ Lancaster/ Tokyo, 1987) p.
12. P. Bennema, in: *Handbook of Crystal Growth, Part 1a, Thermodinamics and Kinetics*. Growth and Morphology of Crystals: Integration of Theories of Roughening and Hartman - Perdok theory, ed. D.T.J. Hurle, (Elsevier Publishers B.V., North Holland, 1993) p. 477-581.
13. I. Weissbuch, L. Addadi, M. Lahav and L. Leiserowitz, Science. 253 (1991) 637.
14. N. Cabrera and D.A. Vermilyea, in: *Growth and perfection of Crystals*, ed. R.H. Doremus, B.W. Roberts, and D. Turnbull, (Wiley, New York, 1958) p. 393.
15. A.A. Chernov, Sov. Phys. - Usp. 4 (1961) 116.
16. A.A. Chernov, Growth of Crystals. 3 (1962) 31.
17. J.W. Retgers, Z. physik. Chem. 9 (1892) 267.
18. L. Royer, Compt. rend. 198 (1934) 585.
19. M. Bienfait, R. Boistelle and R. Kern, in: *Adsorption et Croissance Cristalline*, ed. R. Kern. Vol. 152, (Centre National de la Recherche Scientifique, Paris, 1965) p. 577.
20. R. Boistelle, *These*. 1966: Nancy.
21. R. Kern, Bull. Soc. Fr. Mineral Crist. 76 (1953) 391.
22. L. Lian, K. Tsukamoto and I. Sunagawa, J. Crystal Growth. 99 (1990) 150.
23. P. Bennema, G. Bogels, D. Bollen, T. Mussig and H. Meekes, The Imaging Science Journal. 49 (2001) 1.
24. H. Meekes, P. Bennema and R.F.P. Grimbergen, Acta Crystallogr. A54 (1998) 501-510.
25. A. Pojani, F. Finocchi, C. Goniakowski and C. Noguera, Surf. Sci. 387 (1997) 354.
26. A. Gibson, R. Haydock and J.P. LaFemina, J. Vac. Sci. Technol. A. 10 (1992) 2361.
27. M.A. Langell, C.L. Berie, M.H. Nassir and K.W. Wulser, Surf. Sci. 320 (1994) 25.
28. P.A. Cox and A.A. Williams, Surf. Sci. 152/153 (1985) 791.
29. N. Floquet and L.C. Dufour, Surf. Sci. 126 (1983) 543.
30. C.A. Ventrice Jr, T. Bertrams, H. Hannemann, A. Brodde and H. Neddermeyer, Phys. Rev. B. 49 (1994) 5773.
31. H. Hannemann, C.A. Ventrice, T. Bertrams, A. Brodde and H. Neddermeyer, Phys. Status. Solidi. 146 (1994) 289.
32. N. Erdman, O. Warschkow, D.E. Ellis and L.D. Marks, Surf. Sci. 470 (2000) 1.
33. A. Barbier, C. Mocuta, H. Kuhlenbeck, K.F. Peters, B. Richter and G. Renaud, Phys. Rev. Lett. 84 (2000) 2897.
34. A. Barbier, C. Mocuta and G. Renaud, Phys. Rev. B. 62 (2000) 16056.
35. R. Lacmann, in: *Adsorbtion et Croissance Cristalline*, ed. R. Kern, (Centre National de la Recherche Scientifique, Paris, 1965) p. 195-214.
36. N. Radenović, W.J.P. van Enckevort, P. Verwer and E. Vlieg, Surf. Sci. 523 (2003) 307.
37. N. Radenović, W.J.P. van Enckevort, D. Kaminski, M. Heijna and E. Vlieg, submitted, (2005).
38. I.K. Robinson, Phys. Rev. B. 33 (1986) 3830.
39. E. Vlieg, Surf. Sci. 500 (2002) 458.

Chapter 2

Growth and characteristics of the {111} NaCl crystal surface grown from solution

Neda Radenović, Willem van Enckevort, Paul Verwer, Elias Vlieg

ABSTRACT

The morphology of {111} faces grown from water-formamide solutions as well as from pure water solutions was investigated. Surface patterns were examined *ex-situ* and *in-situ* using bright field and differential interference contrast optical microscopy and *ex-situ* atomic force microscopy. It was shown that formamide and urea stabilize the {111} NaCl faces, whereas larger homologous molecules do not. For the {111} NaCl crystals growing from water-formamide solutions, it was observed that growth proceeds by monomolecular, stabilized layers of height $d_{\{111\}}$, with most probably Na^+ ions on top of Cl^- ions. Steps originate from spiral – dislocation growth as well as from 2D nucleation starting from the edges of the crystal. Atomic resolution imaging of NaCl {111} showed no surface reconstruction. The {111} surfaces grown from pure water solutions showed developing of shallow growth hillocks with rounded tops. It is presumed that these hillocks are related to dislocation outcrops and growth proceeds close to the roughening temperature. Growth pits develop after a longer period of {111} surface growth in water solution. Their formation is explained by the presence of a semipermeable particle at the pit bottom, which locally retards the fast {111} growth.

2.1. INTRODUCTION

Growth of a {111} polar surface of a crystal with rocksalt structure has been one of the attractive themes in the fields of crystal growth and surface science. The history goes back to 1783, when Rome de l'Isle showed that octahedrons instead of normal cubes are formed, if rocksalt is grown in the presence of urine [1]. Despite more than two centuries since this discovery, the electrostatically polar (111) surfaces of the NaCl crystal structure were long considered a mystery in surface science, because they are difficult to investigate both experimentally and theoretically. Since the bulk structure consists of alternating cationic and anionic sheets stacked along the <111> directions, the {111} surfaces must have a very high divergent electrostatic energy, which makes them theoretically highly unstable [2]. Therefore, the form {111} is not expected to occur on the morphology of NaCl - type crystals. However, if such a flat, well-ordered (111) surface can be obtained, several interesting properties, such as novel catalytic activity or a two-dimensional electron system on top of an insulating crystal might be expected [3].

In this context, the growth of {111} surfaces has been examined for various highly ionic materials. Most detailed information was obtained for solid - vacuum systems. In the recent past, the (111) surface of rocksalt structure NiO was the most extensively studied case. Langell and Berrie grew NiO on Ni (100) and (111) substrates by oxidation and characterized the grown film (three monolayers thick) by low energy electron diffraction (LEED), X-ray photoelectron spectroscopy (XPS) and high-resolution electron energy loss spectroscopy (HREELS) [4]. They found that the NiO (111) surface is stabilized by OH adsorbates and that desorption of the hydroxyl resulted in a change of the surface into a thermodynamically more stable NiO (100) thin film. Stabilization by impurities was also found for Pb [5] and Si [6] on NiO (111). Ventice et al. grew NiO on an Au (111) substrate and observed the grown film by LEED and scanning tunneling microscopy (STM) [7, 8]. Their results showed the existence of an epitaxial p(2x2) overlayer structure of 55 nm domain size, which they ascribed to a periodic arrangement of octupolar (NaCl)4 basic units. The stabilization of the {111} NaCl surface by octupoles, each consisting of one unit cell, was proposed by Lacmann, more than 35 years ago [9]. Wolf confirmed this "octupole" reconstruction hypothesis, which cancels the divergence of the electric field in the crystal, by calculations for the {111} NaCl surface in contact with vacuum [10]. Saiki *et al.* obtained the flat (111) NaCl surface for the complex heterostructure of NaCl/CuCl/CuBr/GaAs(111)Ga 2x2, which, in contrast to the previous results for the NiO(111) surface, was stable even for the thick films [11]. They found no reconstruction. Finally, using AFM, Hegenbart and Müssig observed two

additional reconstructions, namely an orthorhombic and a hexagonal one on the (111) surface of AgBr, which is isostructural with NaCl [12].

The above work only concerns with solid – vacuum systems. A major effort has also been made in investigating the occurrence of NaCl {111} faces during growth from aqueous solutions. Bienfait et al. [13] investigated the occurrence of the octahedral faces for a wide range of supersaturations and impurities. Surface topography, using ex-situ optical microscopy of {111} KCl surfaces obtained after growth in the presence of metal ion impurities, showed the occurrence of growth hillocks and macrosteps [14]. As far as known to us, no optical microscopy or AFM work was carried out for {111} NaCl, but Nozoye and Tokada found no reconstruction on the {111} faces of AgBr [15]. Plomp et al. [16] observed steps of height 1/3 <111> on the {111} faces of the same crystal, but now grown from a DMSO solution.

In our laboratory we were able to grow octahedral NaCl single crystals of several millimeters to one centimeter in size with large, flat and stable {111} faces. This opens possibilities to investigate the surface structure of these faces by optical microscopy and AFM in a convenient way. In the present paper we describe the growth and characteristics of the (111) NaCl crystal surface grown from solution.

2.2. EXPERIMENTAL PROCEDURE

The octahedral crystals used for the experiments were grown from a filtrated (0.45 μm pore width), nearly saturated aqueous NaCl solution in which 20-30 wt % of formamide was added. The crystals were obtained by slow evaporation of this solution in a desiccator with concentrated sulfuric acid as drying agent placed at the bottom of the desiccator [17]. We then selected specimens with a size of about 5 x 5 x 3 mm^3, with very flat (111) faces on the top and sides. Generally, these crystals are relatively free from liquid inclusions. Apart from quick drying using a paper tissue after separation from the growth solution, no further surface treatment was applied prior to surface examination. The surface patterns did not change when kept dry in a desiccator and were quickly observed after removal from it. In order to get insight into the mechanism of stabilization of the (111) face by formamide and to ascertain whether we can produce similar effects, i.e. the appearance of {111} faces, instead of formamide we also added homologous compounds to our growth NaCl-water solution, such as urea, dimethylformamide and benzamide.

In some experiments we submerged an octahedral NaCl crystal into a slightly supersaturated solution of NaCl in pure water or placed a droplet of the same solution on the (111) face for 15 to 30 minutes at room temperature to observe the growth features in-situ as well as ex-situ. In this way the influence

of the water molecule on the stabilization of the (111) face is established. To determine the presence of dislocations in the NaCl crystals, the {111} planes were etched using formamide. Etching was performed by placing a droplet of formamide (purity 99.5%) on a (111) face at room temperature, i.e. about 296°K. The number of etch pits formed in this way is a measure for the dislocation content.

The sample surfaces were examined *ex-situ* and *in-situ* using bright field and differential interference contrast optical microscopy (DICM) and *ex-situ* by atomic force microscopy (AFM). For the *ex-situ* AFM observations the side {111} faces were used, because of the top (111) face showed a slight shut off effect, which masks the finest details that can be seen by this scanning probe method. The AFMs used, a Digital Dimension 3100 and a Digital Instruments Nanoscope III, were operated in contact mode. In the first case, both height and deflection (error-signal) images were recorded simultaneously, whereas for the second instrument only the deflection technique was used.

2.3. OBSERVATIONS

2.3.1. General

To obtain information about the influence of the concentration of the formamide in our growth solution on the stabilization of the {111} faces of NaCl, we grew crystals from saturated water solutions without formamide, with formamide added in 10 wt % and 25 wt % and in pure formamide. In the first case, only the set of {100} faces was obtained. This implies that the growth rate of the {111} faces, $V_{\{111\}}$ is larger than $\sqrt{3}V_{\{100\}}$, where $V_{\{100\}}$ is the growth rate of the cubic faces. In the second case two sets of faces appeared, namely {100} and {111}, whereas in the third and the fourth case only octahedrons were formed. This means that, in the latter two cases the growth rate $V_{\{111\}}$, is smaller than $1/\sqrt{3}V_{\{100\}}$, which indicates a substantial change in relative growth rates. From these observations it is clear that, in contrast to growth from pure aqueous solutions, formamide stabilizes the octahedral faces with respect to the cubic faces. Similar observations have been reported earlier [13, 17, 18]. Relating the occurrence of cubo-octahedral forms at ~ 10 wt % formamide concentration with the morphodrome obtained by *Bienfait et al.*, [13] indicates that the relative superstauration in our experiments is about 7%. It is interesting to note that the quality of the crystals grown from aqueous solution with formamide added was significantly better than those grown from pure aqueous solution. The number of liquid inclusions was reduced to a large extent. Using urea as impurity in the growth solution resulted in a similar stabilization of the {111} faces as found for formamide. On the other hand, we did not observe the

appearance of octahedral faces by adding dimethylformamide and benzamide as impurities in our NaCl-water growth solution.

2.3.2. Morphology of {111} faces grown from water - formamide solutions

Figure 2.1a represents an *ex-situ* AFM image of a circular growth hillock observed on a (111) NaCl surface grown from a formamide - water solution. The radius of this hillock is ~ 30 μm, its height is ~ 70 nm. The steps of the hillock, which range in height from 3 to 11 nm, are much higher than monomolecular steps. We think that this is due to interaction of advancing steps with impurity molecules, which causes bunching in trains of steps [19]. It is suggested that the steps on the (111) surface are produced by a composite growth spiral originating from a bundle of screw dislocations, although it is difficult to prove this, because the central part could not be resolved by AFM. The type of hillock as shown in Figure 2.1 was commonly found on the crystals grown from the supersaturated water - formamide solutions. Etching of the (111) NaCl crystal surface in formamide produced a large number of etch pits ~ $4 \cdot 10^4$ per mm^2, which were persistent upon continued etching. This indicates that they are dislocation pits, and shows that a large number of dislocations are available for the creation of the spirals. Beside the typical bunched spirals, a few growth spirals with monomolecular (0.3 nm in height) steps were also observed (Figure 2.1b). The top of these spirals was easily resolved by AFM.

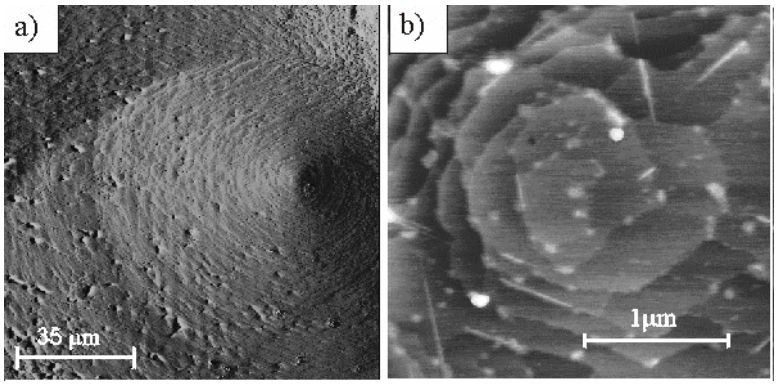

Figure 2.1: *Ex-situ* AFM images of growth spirals observed on {111} NaCl crystal surfaces grown from aqueous NaCl solution with 25 wt % of formamide added: a) Typical growth hillock, presumably originating from a dislocation bundle. Its slope is about 0.25º; the step height ranges from 3 to 11 nm; b) Spiral with monomolecular steps of height $d_{\{111\}}$= 0.3 nm. One monomolecular step consists of one Na^+ layer and one Cl^- layer.

Figure 2.2 represents an *ex-situ* optical image of a typical {111} NaCl crystal surface. On this picture it can be noticed that motion of the steps starts

from the edges of the crystal, going towards the center of the surface. Such a pattern indicates the onset of hopper growth, where due to an enhanced supersaturation steps preferentially nucleate near the edges of the crystal surface. This step motion from the edges is very often influenced by and in competition with steps that originate from the spiral hillocks.

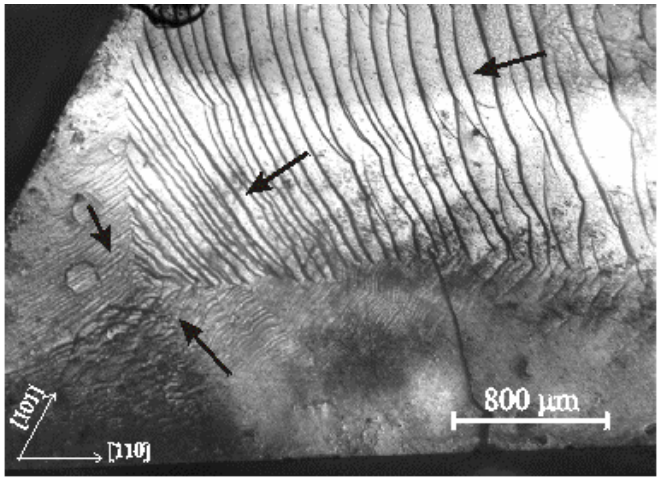

Figure 2.2: *Ex-situ* optical image of a typical {111} NaCl crystal surface grown from a water-formamide solution. It can be noticed that the motion of the steps starts from the edges of the crystal and goes towards the central depression. The directions of step flow are indicated by arrows.

Apart from higher steps, also monomolecular steps with the lowest possible heights according to the interplanar distance were observed on the (111) faces of NaCl (Figure 2.3). These steps were found on almost all side (111) faces of the crystals. AFM measurements proved the step height to be about 0.3 nm. This is in agreement with the interplanar distance, $d_{\{111\},}$ between adjacent (111) planes, which is $\frac{1}{3}\sqrt{3}a$ = 0.325 nm, with a = 0.563 nm as the cell parameter of the cubic unit cell. One monomolecular step consists of one Na^+ layer and one Cl^- layer.

Good atomic resolution is also achieved. The surfaces appear as presented in Figure 2.4, in which oriented patterns of single bright spots, referring to the positions of single ionic species are visible. Arrangements with hexagonal symmetry are the only observed structure. The observed interatomic distances are 0.39 nm, which is in excellent agreement with the calculated distance between two adjacent ions of equal sign in the (111) plane (0.395 nm). This observation shows that the surface is not reconstructed. Confirmation is recently obtained by surface X-ray diffraction on {111}NaCl crystals prepared in the same way. This will be elaborated in a forthcoming paper.

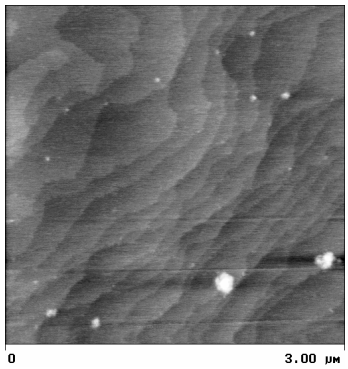

Figure 2.3: AFM image showing monomolecular steps on a (111) NaCl crystal surface grown from an aqueous NaCl solution with 25 wt % formamide. Step height is about 0.3 nm. Each monomolecular step consists of one Na^+ layer and one Cl^- layer.

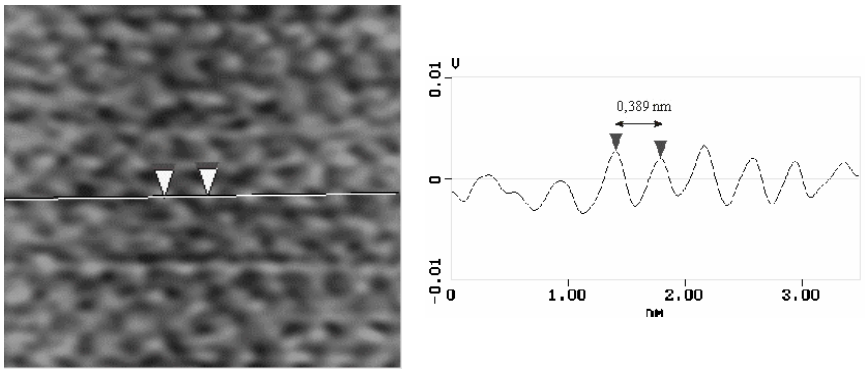

Figure 2.4: AFM image with atomic resolution of a (111) NaCl surface grown from a water-formamide solution, in which the oriented patterns of the single bright spots refer to the positions of single ionic species. The observed interatomic distances are 0.39 nm.

2.3.3. Morphology of {111} faces grown from pure water solutions

After submerging the {111} faces into a supersaturated NaCl solution in pure water, a surface morphology is obtained which is different from that obtained from water - formamide solutions. Now, shallow growth hillocks with rounded tops develop, which were also observed *in-situ* using optical microscopy. Figure 2.5 presents an optical as well as an AFM image of these protrusions. AFM observation of these hillocks showed islands of one or more unit cells high and about 150 nm wide, but no arrays of steps were observed.

After a longer period of {111} surface growth, a multitude of triangular growth pits, leading to a macroscopic roughness of the crystal surface, develop

(Figure 2.6). Careful measurement using optical microscopy shows that the side walls of the pits are inclined 36 ± 2º with respect to {111} in the zone <-110>, i.e. are ~ {114} faces. As will be elaborated in the discussion section, this indicates that the {111} faces grow faster than {100} faces.

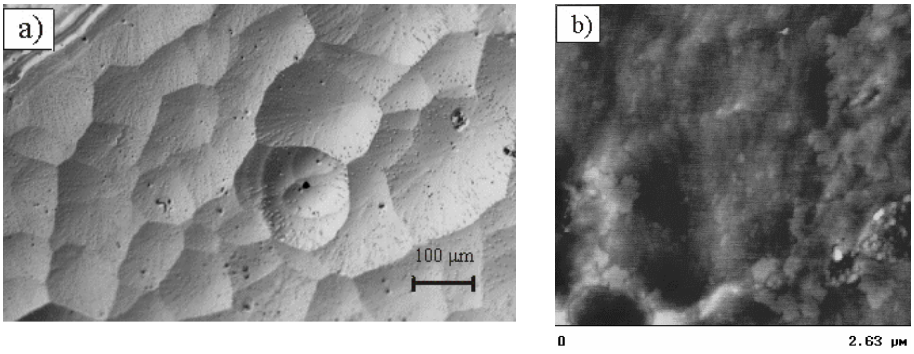

Figure 2.5: Shallow growth hillocks obtained after covering a (111) NaCl crystal surface with a droplet of a supersaturated NaCl solution in water: a) Optical differential interference contrast image recorded after 20 minutes of growth; b) AFM image of these hillocks showing islands of one or more unit cells high. No arrays of steps were observed. Both images were mapped *ex-situ.*

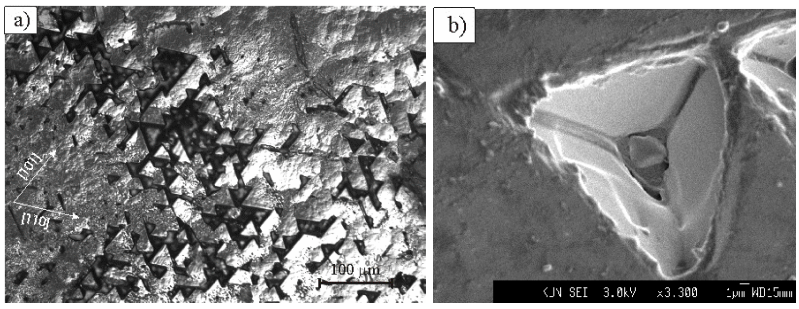

Figure 2.6: A multitude of triangular growth pits develop after a longer period of {111} NaCl surface growth from pure water solution. The side walls of the pits consist of ~ {114} faces: a) Optical image giving overview; b) Scanning electron microscope image showing one pit in detail.

2.4. DISCUSSION

2.4.1. Surface morphology of NaCl {111} grown from water-formamide solutions

Observation by optical microscopy and AFM showed that growth of the {111} faces proceeds by extended arrays of monomolecular and higher steps. This

indicates that growth occurs far below the roughening temperature. The circular shape of the hillocks and step patterns points to either growth limited by surface diffusion or to a low kink energy resulting in a high density of kinks at the steps [20]. Two mechanisms are responsible for the generation of the steps. The first mechanism is spiral growth due to the presence of screw dislocations, which are step sources allowing exactly oriented crystal facets to grow at low supersaturation. This leads to the development of spiral hillocks. In many cases we noticed a competition between different hillocks for being a dominant step source. The second mechanism is two dimensional nucleation of steps starting from the edges of the crystal surface causing step motion towards its centre.

In the case of growth from water-formamide solutions it was found, using AFM, that no reconstruction occurs for the {111} surfaces. This implies that, apart from possible relaxation, it looks like a truncated bulk phase. Here the dipole moment and electrostatic repulsive next-nearest-neighbour bond energies of the polar {111} surface are obviously compensated by solute ions, as well as by formamide molecules and, to some extent, water molecules, which both have a dipole moment. It was also observed that the lowest steps are monomolecular, i.e. consist of one Na^+ and one Cl^- layer. Never ½ $d_{\{111\}}$ steps, either corresponding to one Na^+ layer or one Cl^- layer were found. This means that always one type of ion is on top of the {111} surface. Based on a model for the electrostatics using Gasteiger atomic charges [21], see figure 2.7, we suggest that the Na^+ layer is on top of the surface. The positive charge of the sodium is stabilized more effectively by the formamide than the negative charge of the chloride, due to the fact that the negatively charged oxygen of the formamide molecule is more exposed than the buried (shielded) positive charges on the carbon atom. The NH_2 group is almost electrically neutral. Therefore, the oxygen can have a more direct interaction with neighbouring ions. The strong interaction between Na^+ ions of the {111} NaCl crystal face and electronegative O atoms of formamide results in a stabilizing adsorption of formamide on a {111} face with the Na^+ ions on top of the Cl^- ions.

We observed that formamide and urea both stabilize the {111} NaCl faces, whereas similar, but bigger molecules such as dimethylformamide and benzamide do not. Structure formulas of formamide, urea, dimethylformamide and benzamide are presented in Figure 2.7. It can be noticed that all molecules have similar charge distribution, where the charge on the oxygen is more important than the shielded charges on the carbon atoms and the NH_2 group. Formamide, with molecular volume $V \approx 41$ Å^3 and urea with $V \approx 53$ Å^3 are smaller molecules as compared to dimethylformamide ($V \approx 75$ Å^3) and benzamide ($V \approx 113$ Å^3). Molecular volume is here defined as the volume inside the Van der Waals surface. From the above, it can be concluded that the smaller molecular volume and the preferential charging of the electronegative oxygen enable nice adsorption of formamide and urea on the {111} NaCl

surface and therefore stabilize that face. For the two homologous molecules with the same charge distribution but larger molecular volume, steric hindrance prevents this effect.

We also noticed that the quality of the crystals grown from aqueous solution with formamide added was significantly better than those grown from pure water solution. This can be explained by the fact that in the presence of formamide the crystals grow considerably slower than from pure aqueous solutions, which is a result of formamide molecule adsorption on the {111} NaCl crystal surface. The slower growth reduces the extent of morphological instability caused by mass transport limited growth, and thus decreases the formation of liquid inclusions.

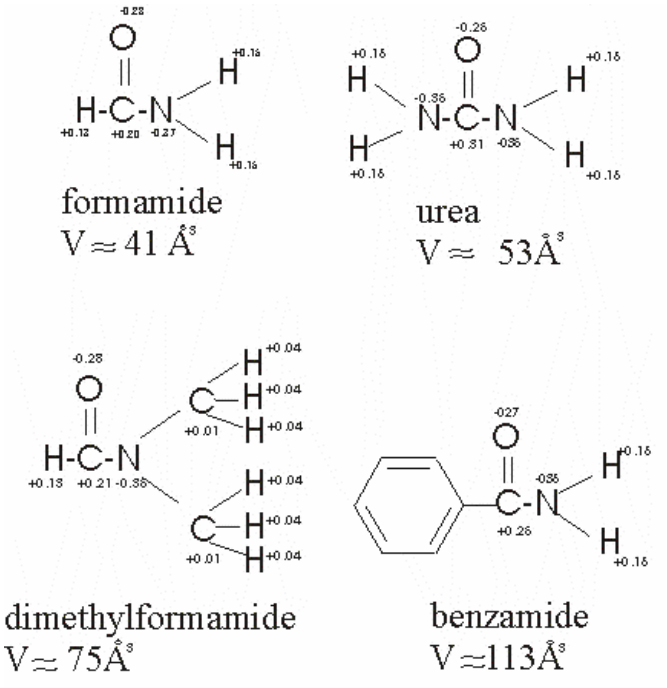

Figure 2.7: Structure formulas and calculated charge distributions of homologous compounds used in our growth solution to determine their influence on the stabilization of {111} NaCl faces.

2.4.2. Surface morphology NaCl {111} grown from pure water solutions

2.4.2.1. Growth hillocks

In the case of growth of NaCl {111} faces from supersaturated NaCl solutions in pure water, a surface morphology which is quite different from that for

growth from water-formamide solutions is obtained. We presume that the development of the shallow hillocks with rounded tops is related to dislocations and growth takes place close to the roughening temperature. Close examination of these hillocks using AFM revealed islands of one or several unit cells high. At the same time we observed no periodic steps patterns. Here 2D nucleation or even random deposition of growth units plays a main role. Monte Carlo simulations of the dislocation growth of a {100} Kossel crystal surface near the kinetic roughening transition indeed show that growth hillocks without clear concentric steps patterns develop [22]. This explanation indicates that the {111} surface grows close to its roughening transition. It causes fast growth and thus accounts for the absence of the {111} faces on the morphology of NaCl grown from pure aqueous solutions.

2.4.2.2. Growth pits

After a longer period of {111} NaCl surface growth, a multitude of growth pits, leading to a macroscopic roughness of the crystal surface develop. The side walls of the pits consist of approximately {114} faces, which are 36 ± 2º oriented with respect to the {111} growth face. Recently the concept of "velocity source" has been introduced and used to explain the occurrence of etch and growth pits, hillocks and other features on crystal surfaces [17, 23, 24]. A velocity source is a point or line on a crystal surface at which the growth / etch rate is locally different. As a consequence of this, the shape of the crystal surface adapts accordingly. In our case a masking particle, for instance a speckle of dust which locally retards growth, is the velocity source. It is situated at the bottom of the pit. The adaptation of the surface is growth pit formed.

The surface orientations around the velocity source, i.e. the side walls of the growth pits, must fulfil the connectivity relation [23, 24]:

$$\left|\vec{R}_{wall}\right| = \vec{n}_{wall} \cdot \vec{R}_{VS} \,. \qquad (2.1)$$

Here $\vec{R}_{wall}$ is the growth rate of the growth pit walls, $\vec{n}_{wall}$ the orientation of growth pit walls and $\vec{R}_{VS}$ the growth velocity of the {111} surface below the semipermeable mask (which is less than $\vec{R}_{\{111\}}$). From the connectivity condition it follows that the particle must be *semipermeable*, i.e. $\vec{R}_{VS} \neq 0$, else equation (2.1) cannot be satisfied and no growth pit will be formed. A second consequence of the connectivity condition is the fact that on the slowest growing surface of a crystal no growth pits can be formed, because then $\vec{n}_{wall} \cdot \vec{R}_{VS}$ is always less than (and never equal to) the smallest possible $\vec{R}_{wall}$. Since {100} is the slowest growing face of the NaCl crystal when crystallizing from a pure water solution, this explains why this surface never gives growth

pits. However, it is shown here that using same solution, the {111} faces grow much faster than {100}, so here the connectivity condition can be satisfied and pits are formed. The growth rate of the {100} surfaces as a sidewall of the growth pits is too slow to satisfy equation (2.1). Therefore the pit wall adjusts itself to the faster growing orientations approximately {114} to fulfil the connectivity condition.

The requirement that a pit expands during continued growing is also given in literature [25]:

$$\vec{R}_{\{111\}} \cdot \vec{n}_{wall} > \left|\vec{R}_{wall}\right| \qquad (2.2)$$

Because of the semipermeable property of the masking particle, $\vec{R}_{VS} < \vec{R}_{\{111\}}$, and from equation (2.1) it follows that condition (2.2) is always fulfilled.

According to our observations, the pits obtained during the growth of the {111} NaCl from water solutions is the reversed case of the etch pyramids obtained after formamide etching of the {100} NaCl crystal surface [17] or wet chemical etching of {100} Si [23, 24].

2.5. CONCLUSIONS

Octahedral NaCl single crystals of several millimeters to one centimeter in size with large, flat and stable {111} faces can be obtained from solution. It was shown that aqueous solutions containing formamide and urea stabilize this NaCl form, whereas larger, homologous molecules, such as dimethylformamide and benzamide, do not.

AFM and optical microscopy showed that the growth of NaCl {111} crystal faces from aqueous solutions containing formamide proceeds by monomolecular and higher layers, with most probably Na^+ ions on top of Cl^- ions. Steps originate from spiral – dislocation growth as well as from 2D nucleation starting from the edges of the crystal. Atomic resolution imaging of NaCl {111} using AFM showed no surface reconstruction.

The morphology of the {111} faces grown from pure water solutions showed different surface patterns, i.e., shallow growth hillocks with a rounded top develop. We presume that these hillocks are related to dislocations and growth proceeds close to the roughening temperature. Growth pits are formed after a longer period of {111} surface growth in pure water solution. These are produced by a mechanism which is similar, but opposite to that of the etch pyramids obtained after formamide etching of the {100} NaCl crystal surface [17].

Acknowledgements

The authors would like to thank Jelena Arsić and Sander Graswinckel for experimental assistance. This work is supported by the Dutch Organization for Chemical Research, CW-NWO.

References

1. J.B.L. de Rome de l'Isle, in: Cristallographie (Paris,1783) p. 379.
2. P.W. Tasker, Philos. Mag. A 39 (1975) 119.
3. D. Cappus, Chem. Phys. 177 (1993) 533.
4. M.A. Langell, C.L. Berie, M.H. Nassir, and K.W. Wulser, Surf. Sci. 320 (1994) 25.
5. P.A. Cox and A.A. Williams, Surf. Sci. 152/153 (1985) 791.
6. N. Floquet and L.C. Dufour, Surf. Sci. 126 (1983) 543.
7. C.A. Ventrice Jr, Th Bertrams, H. Hannemann, A. Brodde, and H. Neddermeyer, Phys. Rev. B 49 (1994) 5773.
8. H. Hannemann, C.A. Ventrice, Th Bertrams, A. Brodde, and H. Neddermeyer, Phys. Status. Solidi 146 (1994) 289.
9. R. Lacmann, in: Adsorbtion et Croissance Cristalline, ed. R. Kern. 1965, (Centre National de la Recherche Scientifique, Paris, 1965) 195-214.
10. D. Wolf, Phys. Rev. Lett. 68 (1992) 3315.
11. K. Saiki, A. Goda, and A. Koma, Jpn. J. Appl. Phys. 36 (1997) L55.
12. G. Hegenbart and T. Müssig, J. Imaging Sci. Technol. 37 (1993) 551.
13. M. Bienfait, R. Boistelle, and R. Kern, in: Adsorption et Croissance Cristalline, Vol. 152, Ed. R. Kern (Centre National de la Recherche Scientifique, Paris, 1965) p. 577.
14. L. Lian, K. Tsukamoto, and I. Sunagawa, J. Crystal Growth 99 (1990) 150.
15. H. Nozoye and H. Tokada, Jpn. J. Appl. Phys. 33 (1994) 3764.
16. M. Plomp, J.C. Buijnsters, W.J.P. van Enckevort and D. Bollen, J. Crystal Growth 209 (2000) 911.
17. N. Radenović and W.van Enckevort, J. Crystal Growth 234 (2002) 589.
18. F. Gille and K. Spangenberg, Z. Kris. Miner. Petrograd A 65 (1927) 204.
19. P. Bennema, G. Bogels, D. Bollen, T. Müssig, and H. Meekes, The Imaging Science Journal 49 (2001) 1.
20. W.J.P.v. Enckevort, in: Facets of 40 years of crystal growth. A tribute to Piet Bennema on the occasion of his retirement, Eds. W.J.P. van Enckevort, H.L.M. Meekes, and J.W.M. van Kessel, (University of Nijmegen, Nijmegen, 1997) p. 51.
21. J. Gasteiger and M. Marsili, Tetrahedron 36 (1980) 3219.
22. H.M. Cuppen, E. van Veenendaal, J. van Suchtelen, W.J.P. van Enckevort, and E. Vlieg, J. Crystal Growth 219 (2000) 165.
23. A.J. Nijdam, E. van Veenendaal, H.M. Cuppen, J. van Suchtelen, M.L. Reed, J.G.E. Gardeniers, W.J.P. van Enckevort, E. Vlieg, and J. Elwenspoek, J. Applied Physics 89 (2001) 4113.
24. E.van Veenendaal, K. Sato, M. Shikida, and J. van Suchtelen, Sensors & Actators A 93 (2001) 232.
25. R.B. Heimann, in: Auflösung von Kristallen - Theorie und Technische Anwendung (Springer, Wien, 1975) p. 3-10.

Chapter 3

Formamide adsorption and habit changes of alkali halide crystals grown from solutions

Neda Radenović, Willem van Enckevort, Paul Verwer, Elias Vlieg

ABSTRACT

The possibility to obtain {111} surfaces on NaCl crystals grown from pure water solutions was investigated in order to verify some early observations. Repeating the same experiments as reported 1953 by Kern [1] followed by detailed examination using optical microscopy and optical goniometry revealed that, independent of supersaturation, {100} is the only stable form.

We also studied the morphology of the alkali halide crystals obtained from formamide solutions. We noticed that the appearance of the octahedral form is strictly related to unit cell size. Octahedrons appear starting from NaF crystals with unit cell size 0.462 nm up to KCl with a unit cell of 0.628 nm. All the alkali halide crystals with dimensions outside this range are cubes. In addition to rocksalt structure crystals, a new, non-cubic pseudo polymorph was obtained for several alkali halide crystals grown from formamide solution. For sodium iodide this new compound was identified as NaI-1(formamide).

In addition (to this and our recent paper [2], we tried to obtain NaCl crystals with {111} faces using pyridine, aniline and glycine. In the case of pyridine and anyline we only observed cubes, whereas from aqueous solutions containing glycine we obtained crystals with well-developed faces with an average {110} orientation.

.

3.1. INTRODUCTION

The growth of electrostatically polar {111} surfaces of crystals with a rocksalt structure has attracted many studies in the fields of crystal growth and surface science. Rome de l'Isle showed already in 1783 that octahedrons instead of normal cubes are formed, if rocksalt is grown in the presence of urine [3]. Many authors have since reported this cube – octahedron shape transition for various experimental conditions. In particular, some early work reported that {111} NaCl faces can also be obtained from pure water solution [1, 4, 5]. It was observed that if NaCl and other crystals with rocksalt structure were grown at high supersaturation, octahedral crystals with well developed {111} faces appeared. On the other hand, if they were grown at low evaporation rate (or a low supersaturation) cubic crystals were formed. In our previous experimental work on the growth of NaCl crystals from water solutions [2, 6] and in many other trial experiments that we performed, we never observed {111} faces. We did observe, however, cubes resting on an {111} face which have the appearance of octahedrons and that we will refer to as "resting cubes". In the first part of this paper we will show that the claimed {111} faces at high supersaturations are most likely an artifact and that in aqueous solutions only the {100} faces are stable.

In a recent paper [2] we investigated the morphology of the {111} NaCl faces grown from water – formamide solutions. It was shown that formamide and urea stabilize the {111} NaCl faces, whereas larger homologous molecules such as benzamide and dimethylformamide do not. We concluded that molecular size as well as specific charge distribution play an important role in this stabilization of the {111} NaCl face. In the second part of the present paper we continue this investigation using pure formamide as the only solvent for all the twenty alkali halide compounds. In this, we investigate the morphology of the crystals obtained from this solution. Attention is also paid to the influence of supersaturation, which was reported to play a role in the stabilization of {111} faces if growth takes place from formamide – water solutions [5, 7]. Based on the presented model for the stabilization of the {111} NaCl faces by formamide [2], we also tried to obtain NaCl crystals with {111} faces using molecules with similar molecular volume, but with opposite charge distribution as formamide and urea. For these experiments we selected pyridine, aniline and glycine.

3.2. EXPERIMENTAL PROCEDURE

3.2.1. Growth of the NaCl crystals from water solutions

We repeated the NaCl growth experiments using the same conditions as those presented in the early work by Kern [1]. The NaCl crystals were grown from a filtered (0.2 μm pore width), initially slightly undersaturated aqueous solution. A droplet of this solution was placed on a microscope glass slide and crystals were grown by evaporation in two ways. The first one was evaporation at room temperature and ambient conditions. Evaporation was slow and took place in 30 minutes. In the second way, glass slides were heated to 80°C to increase the evaporation rate, and the droplet was evaporated in 1 to 2 minutes. In this manner we obtained a very high supersaturation in the growth solution. Although the exact values of the supersaturation are not well defined in our experiments, the conditions of very high and low supersaturation are well established. The crystal shapes were observed ex-situ and in-situ using bright field and differential interference contrast optical microscopy (DICM). The angles between crystallographic faces were determined using optical goniometry coupled with an inverted, reflection optical microscope. In this way we could operate with very small crystals and measure the angles from maximal reflection intensity for each crystal face, with a precision of ±1°.

3.2.2. Growth of the alkali halide crystals from formamide solutions

In the second experimental part, small crystals of alkali halides, with a largest dimension of up to 100 μm, were grown from solution by placing a droplet of saturated formamide solution on a glass slide and heating it to 100°C. Spontaneous nucleation occurred on the slide, which could be transferred directly to the optical microscope. Observation had to be very fast due to the fact that several of the alkali halide crystals and the formamide solutions are very hygroscopic, leading to a quick dissolution of the crystals. A typical period for nucleation and growth of the crystals was 5-15 min.

3.2.3. Growth of NaCl crystals from pyridine, aniline and glycine solutions

Since NaCl hardly dissolves in pure pyridine and aniline we used pyridine-water or aniline-water mixtures in the volume proportion 10:1 in which NaCl could be dissolved.

NaCl crystals were also grown from glycine-water mixtures. The concentration of glycine was 1.3 times that of NaCl by weight.

3.3. RESULTS AND DISCUSSION

3.3.1. Morphology of NaCl crystals grown from aqueous solutions; influence of supersaturation

Upon repeating the experiments as reported in reference [1], where NaCl crystals were grown from aqueous solution at high supersaturation, we obtained very similar results, see Fig. 3.1. When viewed from above, many crystals appear to have an octahedral shape with a (111) face on top. Such a morphology was rarely found at lower supersaturation. However, this observation does not prove that the morphology is determined by the {111} faces, because a {100}-terminated cube may give a similar appearance when it is resting on a {111} plane. In order to verify if there are visual differences in the top view appearance of octahedral crystals and the cubes resting on the {111} plane, we made a projection drawing of both cases using program Shape [8] (Fig. 3.2). Interestingly, no important differences in top view appearances of the octahedrons and the resting cubes can be seen. Therefore, they can not be distinguished when viewed from above. But we noticed that the "resting cubes" were always considerably thicker than the normal NaCl cubes, whereas if it were octahedrons they should have comparable thickness. In order to distinguish the two cases, we performed more detailed observations.

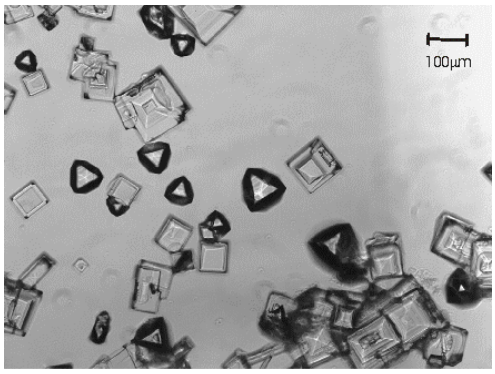

Figure 3.1: *Ex-situ* optical image of NaCl crystals grown from aqueous solution at high supersaturation showing cube shaped crystals and crystals which have the appearance of octahedrons.

Using optical microscopy, we noticed that the trigonal top faces were not flat, but were hollow in shape (Fig. 3.3). A planar trigonal {111} face at the bottom of the crystallites, which was in contact with the glass surface was observed as well. After we added a droplet of water supersaturated with NaCl to cover the crystallite completely, in-situ observation showed that these "resting

cubes", grew out into normal cubes (Fig. 3.4a and b). Upon continued growth of the cube crystal (presented in Fig 3.4b), the droplet again becomes too low leading once more to the appearance of a small triangular hollow (111) face on the top corner as explained in Figure 3.5.

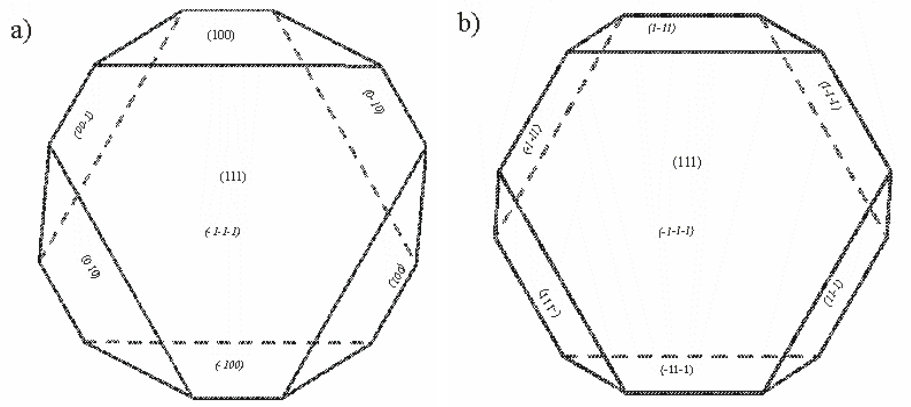

Figure 3.2: Drawing made using the program "Shape" [8] showing the virtually identical top view appearances of the cubic and octahedron form of the crystals with the rocksalt structure: a) cubic form resting on a {111} face; b) octahedral form.

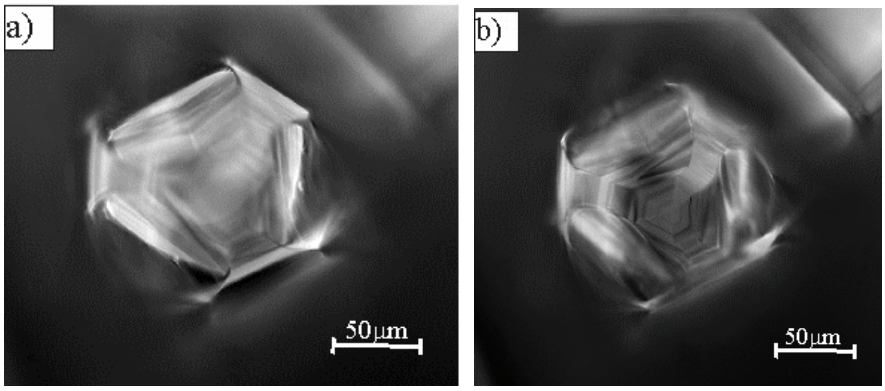

Figure 3.3: *Ex-situ* optical image showing the trigonal top of a NaCl crystal resting on a {111} face: a) focused on the hollow top of the crystal; b) focused on the flat bottom of the crystal.

To unambiguously determine the nature of the side faces we measured the angles between the triangular {111} bottom face and the adjacent three side faces of several "resting cube" crystals using the optical goniometer coupled with the inverted microscope. The measured angles were: 54.6º, 54.5º and 55.0º with an average value of 54.7º. This is in perfect agreement with the angle of

54.73º between {100} and {111} faces for a cubic structure, whereas the angle between two adjacent {111} faces for the same crystal type would be 70.52º.

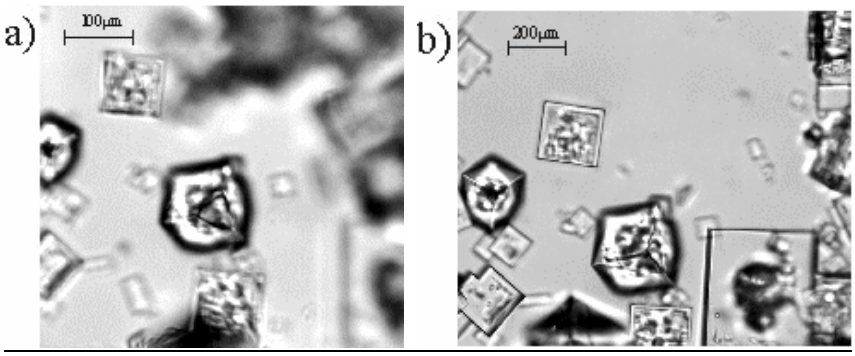

Figure 3.4: *In-situ* optical images taken after adding a droplet of supersaturated NaCl solution in water to a NaCl crystal resting on a {111} face. In the subsequent period the depressed "{111} top face" develops into the sharp top corner of a cube: a) recorded after 2 min of growth showing a reduction in size of the hollow (111) face; b) recorded after 10 min of growth showing the transformation of the hollow (111) face into the sharp top corner of the cube. The initial crystal shape was similar to the "octahedrons" as presented in Fig. 3.1.

Our observations of NaCl crystals grown from aqueous solution distinctively show that, independently of supersaturation, {100} faces are the only faces which appear. Except for the {111} faces attached to the glass substrate, we did not observe appearances of octahedral faces at high supersaturation of the droplet. This indicates that under these conditions the NaCl crystallites often nucleate on a (111) face, but during the growth the {111} faces grow faster than the {100} faces and the crystals get a cubic morphology, Fig 3.5a. Upon continued growth of the crystal, the droplet becomes too low and cannot supply the upper crystal part with solute. This results in blocking of the crystal growth due to deficit of liquid and a hollow (111) face develops on the top, Fig 3.5b. This also explains why "octahedrons" were only found in droplets and not in beakers [1].

From the above it follows that {111} faces are fast growing in aqueous solution and that the trigonal appearance of the top faces is due to the position of the crystal. Since there is no difference in the top view appearances between cubes and octahedrons, (Fig. 3.2), we think that many of the octahedrons claimed by various researchers concerns the stage at which {111} appears on top of a cube resting on a (111) plane. The trigonal appearance of these crystals in the microscope field misled the investigators.

In fact, the {111} NaCl faces can only appear in water solution in the presence of impurities

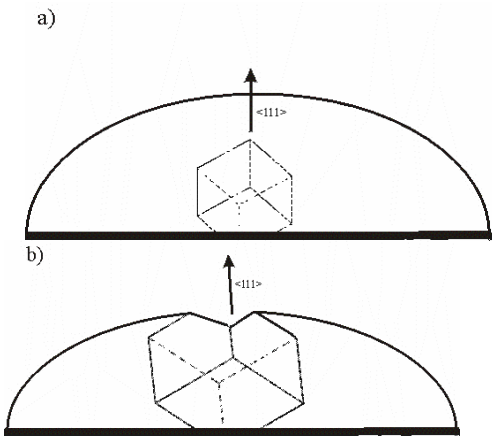

Figure 3.5: Graphic presentation explaining the formation of the false octahedrons in a solution droplet: (a) At very high supersaturation of the droplet, crystallites often nucleate on a {111} face, but during growth the {111} faces grow faster than the{100} faces and the crystal has a cubic morphology; (b) Upon further rowth, the crystal contacts the top surface of the droplet. These results in blocking the crystal growth due to deficit of liquid and a crystal with a hollow (111) top face develops.

3.3.2. Morphology of the alkali halide crystals grown from formamide solutions

3.3.2.1. Crystals with the rocksalt structure

Table 1 summarizes the results of the growth of alkali halides from formamide solutions. The occurrence of an octahedron or cubic morphology is found to be strongly correlated with the size of the unit cell. Octahedrons appear starting from the NaF crystals with the unit cell size **a** = 0.462 nm up to KCl with the unit cell of **a** = 0.628 nm. All the alkali halide crystals with unit cell dimensions within this range crystallize in the form of octahedron when grown from formamide solution. The others display a cubic shape. For three of the alkali halogenides, namely CsCl, CsBr and CsI, the cubic f.c.c. NaCl structure is metastable and after a short period the crystals transform into the stable b.c.c structure [9].

In our previous AFM study of the {111} NaCl crystal faces, it was found that no reconstruction occurs and that the lowest steps are monomolecular, with most probably the Na^+ layer on top of the surface [2]. In our proposed explanation for the stabilization of the {111}NaCl faces by formamide, we suggested that the formamide molecules stabilize the positive charge of the alkali halide cations more effectively than the negative charge of the anions. This is explained by the fact that the negatively charged oxygen of the formamide molecule is more exposed than the buried (shielded) positive

charges on the carbon atom. The NH_2 group is almost electrically neutral. Therefore, the oxygen has a more direct interaction with neighbouring ions. The strong interaction between positive ions of the {111} alkali halide crystal face and electronegative O atoms of formamide results in a stabilizing adsorption of formamide on a {111} face with the positive ions on top.

compound	unit cell size [nm]
LiF	0.403
NaF	0.463
LiCl	0.514
KF	0.534
LiBr	0.550
NaCl	0.562
RbF	0.573
NaBr	0.597
LiI	0.600
CsF	0.612
KCl	0.628
NaI	0.648
KBr	0.658
RbCl	0.658
RbBr	0.687
CsCl*	0.692
KI	0.705
CsBr*	0.725
RbI	0.733
CsI*	0.763

Table 1: Occurrences of octahedron or cube shaped alkali halide crystals grown from pure formamide solution as a function of the unit cell size. Gray fields indicate octahedral morphology; blank fields indicate cubic morphology. The CsCl, CsBr and CsI are crystallized in the metastable NaCl structure [9].

Our previous observations concerning the influence of the molecule size, where we observed that formamide and urea both stabilize the {111} NaCl faces, whereas similar, but bigger molecules such as dimethylformamide and benzamide do not, are confirmed in this study. The alkali halide crystals grown from saturated formamide solution show a clear relation between the appearance of the octahedral form and the unit cell size. This indicates that the

molecular size and fitting are as important as the charge distribution for the stabilization of the {111} alkali halide surfaces by adsorption of formamide.

For LiF, with unit cell size a = 0.402 nm, the volume of the formamide molecules is too large and steric hindrance prevents stabilization of the {111} faces. For the alkali halides with unit cell dimensions larger than a = 0.628 nm, however, there is sufficient space for the molecules to adsorb at the surface. This indicates that not only the size, but also the exact fitting of the molecules to the {111} surfaces play a role. It is known from literature that a substantial amount of the formamide molecule in the liquid phase shows a resonance structure with negatively charged oxygen and positive nitrogen atoms [10-14]. We think that the positively charged atoms in these formamide molecules show some interaction with the anionic sublayer of the alkali halide {111}faces. According to our observations the distance between the negatively charged oxygen and the positively charged nitrogen in these formamide molecules is similar to the distance between the positively charged sodium (surface layer) and the negatively charged chloride in the sublayer of the NaCl {111} face. Taking into account the atomic radii of all interacting ions this suggest that the formamide molecule in its ionic resonance structure can stabilize the {111} faces of the alkali halide crystals in the range from NaI to KCl. It is clear that the model presented in our previous paper was not complete. Surface X-ray diffraction experiments are planned to reveal the actual structure of the {111} NaCl – formamide interface.

3.3.2.2. Crystals with a needle shape

We observed that several alkali halides grown from formamide solution also crystallized in form of the needles (Fig 3.6). This phenomenon was observed for NaI, KF, LiBr and LiCl. In most cases the needles were dominant compared to the rocksalt structure crystals. Using optical polarization microscopy we noticed that the needles are optically anisotropic and show extinction in the direction parallel and perpendicular to the needle axis, whereas crystals with the rocksalt structure show extinction in all crystallographic directions. This indicates that these needles are a new, non-cubic compound which could be formed by interaction of alkali halide with formamide. For NaI we investigated the crystals in more detail. Thermogravimetric measurements of needles obtained from NaI-formamide solution, show that at 190° 25.7% of the total mass was lost. This loss of mass is almost equivalent to one formamide molecule per NaI unit and indicates that formamide is incorporated into the crystal structure. Further heating did not yield any mass loss. The incorporation of formamide is confirmed by IR spectroscopy and Raman spectroscopy of the crystals, which spectra show the presence of all important formamide peaks. Differential scanning calorimetric analysis, (DSC), of our crystals was also done and the

curve obtained is given in Figure 3.7. The DSC curve shows a sharp peak at 88.7°C, corresponding to a peritectic phase transition from $solid_1$ (our crystal) $\rightarrow$ $solid_2$ + liquid solution. The enthalpy change for this endothermic process is ΔH = -91.1 Jg-1. Further heating brings us at the region of formamide evaporation until about 190°C, which is represented by a broad endothermic peak (ΔH = -142.3 Jg-1) and finally to the melting point of the NaI at 661°C giving a sharp peak (not shown in figure 3.7). This implies that $solid_2$ is NaI. From the above analyses it can be concluded that the needle shaped crystals are a new non–cubic pseudo-polymorph NaI – 1 ($CHONH_2$).

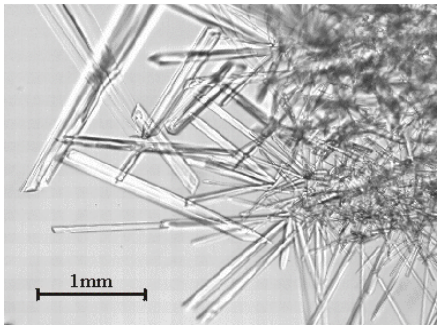

Figure 3.6: *In-situ* optical image of the needle shaped crystals formed from a NaI- formamide solution.

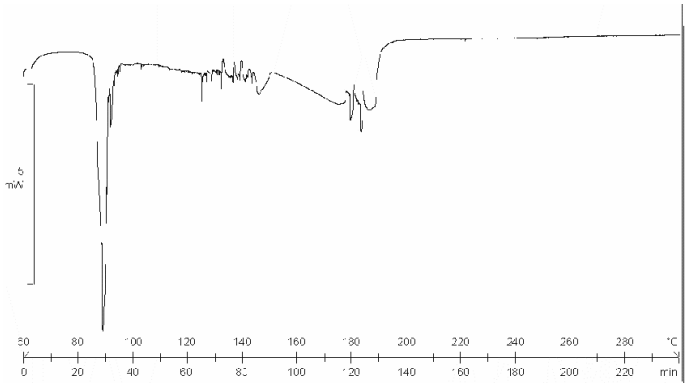

Figure 3.7: DSC curve of the needles grown from NaI – formamide solution. The sharp peak at approximately 90°C corresponds to a peritectic phase transition from our needle crystal to a NaI + liquid solution mixture. Further heating leads to evaporation of formamide up to 190°C, which is represented by a broad peak. A sharp peak at 661°C (not shown here) corresponds to the melting point of the NaI.

3.3.3. Tentative growth of sodium chloride crystals in the presence of pyridine, aniline and glycine

Based on the presented model for the stabilization of the {111} NaCl faces by formamide, we tried to obtain NaCl crystals with {111} faces using molecules with similar molecular volume but with opposite charge distribution than formamide and urea. This would provoke the appearance of the {111} faces with Cl^- ions on the top. For these experiments we selected pyridine, aniline and glycine, which have positive charge concentrated on the nitrogen atoms in the molecules. We found in the older literature references that octahedrons were observed for pyridine and aniline [15, 16], but we only observed cubes. We think that many older claims of octahedral NaCl growth suffered from the problem of cubes resting on the {111} face. In the experiments with glycine we obtained crystals with well developed macroscopic, averaged {110} faces, like observed by Bienfait et al. [5]. Closer examination showed that it is not a flat face but shows a shallow zig-zag roof structure of faces parallel to the [100] periodic bond chain (PBC) direction [17]. This is consistent with a stabilization of the {110} NaCl S-face. We will come back to it in a future paper.

3.4. CONCLUSIONS

Ex-situ and in-situ observation of NaCl crystal growth from aqueous solution show, in contrast to earlier reports, that, independently of supersaturation, {100} faces are the only faces which appear. The {111} NaCl faces can only develop in water solution if impurities are added. We noticed that for alkali halide crystals grown from saturated formamide solutions the appearance of the octahedral form is strictly related to unit cell size. Octahedrons appear starting from NaF crystals with unit cell size 0.462 nm up to KCl with a unit cell of 0.628 nm. All alkali halide crystals with the dimensions outside this range of unit cells crystallize as cubes. This confirms that apart from dipole-ion interaction, also the volume and shape of the molecules are important for the stabilization of the {111} alkali halide surfaces by adsorption. In addition to rock salt structure crystals, a new, non-cubic pseudo polymorph was obtained for several alkali halide crystals grown from formamide solution. For sodium iodide this new compound was identified as NaI-1(formamide).

Acknowledgements

The authors would like to thank Mr. Zjak van Eupen for his kind help with IR spectroscopy and thermogravimetric experiments. This work is supported by the Dutch Organization for Chemical Research, CW-NWO.

References:

1. R. Kern, Bull. Soc. Fr. Mineral Crist.. 76 (1953) 391.
2. N. Radenović, W.J.P. van Enckevort, P. Verwer, and E. Vlieg, Surf. Sci.. 523 (2003) 307.
3. J.B.L.de Rome de l' Isle, *Cristallographie*. 1783, Paris. p. 379.
4. A. Johnsen, *Wachstum und Auflösing der Kristallen*. 1910, Leipzig: Engelmann.
5. M. Bienfait, R. Boistelle, and R. Kern, *Adsorption et Croissance Cristalline*, ed. R. Kern. Vol. 152. Centre National de la Recherche Scientifique, Paris, 1965. 577.
6. N. Radenović and W.J.P.van Enckevort, J. Crystal Growth. 234 (2002) 589.
7. L. Lian, K. Tsukamoto, and I. Sunagawa, J. Crystal Growth. 99 (1990) 150.
8. E. Dowty, *Shape for Windows Professional Edition*. 1999.
9. J. Arsić, I.C. Reynhout, W.J.P. van Enckevort, and E. Vlieg, J. Crystal Growth. (2003).
10. C.C. Costrain and J.M. Dowling, J. Chem. Phys.. 32 (1960) 158.
11. R.J. Kurland and E.B. Wilson, J. Chem. Phys.. 27 (1957) 585.
12. E. Hirota, C.J. Sugisaki, G.O. Nielsen, and J. Sorerensen, Mol. Spectrosc.. 49 (1974) 251.
13. D.J. Gardiner, A.J. Lees, and B.P. Straughan, J. Mol. Struct.. 53 (1979) 15.
14. A.J. Lees, B.P. Straughan, and D.J. Gardiner, J. Mol. Struct.. 71 (1981) 61.
15. F. Gille and K. Spangenberg, Z. Kris. Miner. Petrograd A. 65 (1927) 204.
16. G.S. Korshunov and V.A. Mokievskii, Zhur. Obsch. Khim.. 18 (1948) 569.
17. P. Bennema, G. Bogels, D. Bollen, T. Mussig, and H. Meekes, The Imaging Science Journal. 49 (2001) 1.

Chapter 4

Stability of the polar {111} NaCl crystal face in solution

Neda Radenović, Daniel Kaminski, Willem van Enckevort, Sander Graswinckel, Ismail Shah, Mendel in 't Veld, Rienk Algra and Elias Vlieg*

ABSTRACT

We present a surface X-ray diffraction determination of the {111}NaCl-liquid interface structure. Using ultra-thin water and formamide liquid layers we ascertained that the crystal surface is smooth at an atomic level and is not reconstructed. Our results reveal surprisingly small differences in surface structure between the two cases, which nevertheless lead to dramatic differences in crystal morphology. We determined that the rock salt {111} surface is Na^+ terminated for both environmental conditions. A quarter to half a monolayer of laterally disordered Cl^- ions is located on top of a fully ordered Na^+ crystal surface with occupancy 0.75 to 1.0. This means that the polar surface is stabilized through the formation of an electrochemical double layer.

4.1. INTRODUCTION

It is well known that impurities can have a large effect on crystal morphology. A variety of studies have been reported on mostly qualitative observations of morphological changes caused by the addition of small quantities of impurity [1-3]. However, the atomic-scale mechanism behind these effects is usually not known. The earliest report of a habit modifier is probably from Rome de l'Isle who reported the morphology transition from cubes to octahedrons if rock salt is grown in the presence of urea [4], i.e. the stable crystallographic face of NaCl changes from {100} to {111}. We have found that the addition of at least 20 wt% of formamide to the aqueous growth solution has the same effect [5, 6].

This transition from the common {100} face to the octahedral or {111} face is an intriguing process, because the polar {111} face is not expected to be stable. Along the [111] direction the NaCl crystal consists of alternating layers of cations and anions. The resulting long-range electrostatic interactions lead to a very high energy of the {111} NaCl surface. Therefore, these polar surfaces should be highly unstable and not present in the morphology of NaCl-type crystals [7]. Theoretical calculations for ionic crystals with rock salt type structures propose two solutions to make this face stable: (1) the bulk terminated {111} surface facets into neutral {100} type faces upon annealing or (2) the surface reconstructs [8]. These two solutions are similar, since the reconstruction can be considered as faceting on an atomic scale. Results obtained for NiO(111) in vacuum confirmed these predictions [9-13].

In the case of growth from solution, recent work carried out in our group using formamide or $CdCl_2$ as impurities [14] has shown that no reconstruction or faceting occurs for {111} NaCl surfaces. For the $CdCl_2$ case, it was concluded that the surface is Cl^- terminated and that a disordered layer containing ¼ monolayer Cd^{2+} and ¾ monolayer H_2O stabilizes this surface.

For the formamide case, Atomic Force Microscopy (AFM) and optical microscopy observations were not sufficient to determine the mechanism behind the stabilization. Therefore, we here report a surface X-ray diffraction investigation. Given the known difference in stability of the {111} face in water or formamide solutions, we expected large differences in the interface structure, but this turns out not to be the case. Instead, the formation of an electrochemical double layer is the main stabilizing mechanism in both cases.

4.2. EXPERIMENTAL PROCEDURE

The surface X-ray diffraction (SXRD) technique is very suitable for the structure determination of the interface between a crystal surface and solution [15]. In SXRD, diffracted X-ray intensities along so-called crystal truncation

rods are measured [16]. These rods are tails of diffuse intensity connecting the bulk Bragg peaks in the direction perpendicular to the surface. Their exact shape is determined by the atomic structure of the solid-liquid interface.

The octahedral NaCl crystals, with dimensions 4x4x3 mm^3, were grown at our laboratory from supersaturated aqueous solution in the presence of formamide [5]. After separation from the growth solution, the crystals were quickly dried using a paper tissue. AFM was used to check the surface prior to X-ray diffraction. Using AFM we found the {111} NaCl surface to be atomically smooth and covered with steps of height d_{111}, which means that the surface is either Cl^- or Na^+ terminated. The surface patterns did not change when the crystals were kept dry in a desiccator.

The SXRD experiments were performed at the DUBBLE and ID03 beam lines of the European Synchrotron Radiation Facility (ESRF) in Grenoble, using an X-ray energy of 10 keV. The data were collected under two different environmental conditions, namely by exposing the crystal surface (i) to 75% relative humidity (RH) and (ii) to formamide vapour in a dry nitrogen atmosphere. The resulting thin solution layers lead to a much better signal-to noise ratio than obtained for thicker films. The experiments were carried out at room temperature. The addition of 30 % formamide to an aqueous solution is sufficient to stabilize the {111} face [5], but in these vapour pressure experiments we used pure vapours in order to have an unambiguous composition of the liquid film. The experimental set-up consists of a cell in which the crystal surface can be examined in a well-controlled atmosphere [17]. This cell is coupled to a (2+3)-diffractometer [18] operating in a vertical geometry in case of the DUBBLE beamline and to a horizontal *Z*-axis diffractometer [19] in case of ID03. To establish equilibrium between crystal and vapour, the system was left for at least fifteen minutes before every measurement.

In order to describe the NaCl {111} surface lattice and to index the X-ray reflections, we use a (111) surface unit cell. The lattice vectors $\mathbf{a_i}$ of this cell are expressed in terms of the conventional cubic lattice vectors by:

$$\mathbf{a_1} = \frac{1}{2}[10\bar{1}]_{\text{cubic}}, \qquad \mathbf{a_2} = \frac{1}{2}[\bar{1}10]_{\text{cubic}}, \qquad \mathbf{a_3} = [111]_{\text{cubic}},$$

with

$$|\mathbf{a_1}| = |\mathbf{a_2}| = \frac{1}{2}a\sqrt{2}, \qquad |\mathbf{a_3}| = a\sqrt{3},$$

and where a = 0.563 nm is the lattice constant of NaCl. The corresponding reciprocal lattice vectors $\mathbf{b}_j$ are defined by $\mathbf{a}_i \cdot \mathbf{b}_j = 2\pi\delta_{ij}$. The momentum transfer vector is given by $\mathbf{Q} = h\mathbf{b}_1 + k\mathbf{b}_2 + l\mathbf{b}_3$, with ($hkl$) the diffraction indices. With our choice of the surface unit cell the index l corresponds with the direction perpendicular to the surface.

The integrated intensities of the (*hkl*) reflections were measured using rocking scans. They are converted into structure factor amplitudes by applying the appropriate geometrical and resolution corrections [20]. This correction procedure puts all rods on the same relative scale, except for the specular data. The negative values for diffraction index *l* are obtained by inverting the structure factors according to Friedel's rule. The parameters describing the different models are fitted to experimental structure factors using a χ^2 minimization. Model calculations and fitting are done using the ROD program [21].

4.3. RESULTS

4.3.1. Solution layer thickness

The interface structure we measure is only representative of the situation during solution growth if the liquid layer is sufficiently thick. We therefore first determined this thickness by measuring the Kiessig fringes in the specular rod [22]. We observed these fringes for both the water and the formamide atmosphere. Note that this confirms with high sensitivity earlier results using ellipsometry about the presence of such a layer [23, 24]. The measured layer thicknesses were completely reproducible at both beam lines. We could observe the evolution of the liquid layer thickness after the crystal was exposed to either water or formamide vapour. Figure 4.1 shows this for a case in which the crystal is exposed to the vapour pressure of a saturated NaCl solution in which 50 wt% formamide was added. In this case the measured layer thickness increases from 9 Å after 10 min of exposure to approximately 40 Å after 50 min.

In order to obtain a pure aqueous film, we inserted a NaCl-saturated solution in the sample cell, which gives a relative humidity (RH) of 75 %. This yields a stable layer with a thickness of 30 Å after 35 min. In the formamide case we derived a stable layer thickness of 24 Å from the Kiessig fringes. For both conditions we obtain a film that is sufficiently thick to obtain the equilibrium structure at the solid-liquid interface. This is confirmed by the fact that the specular rod is constant in time except for the part at low *l*.

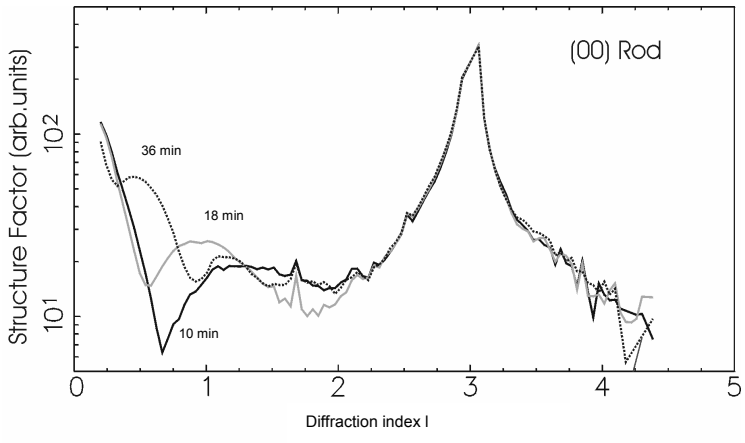

Figure 4.1: The (00) rod measured after exposure of the {111} NaCl surface to a vapour pressure of supersaturated NaCl solution where 50 wt % formamide was added. The first Kiessig fringe can be seen at $l = 1.1$ after 10 min (black solid line), at $l = 0.9$ after 18 min (grey solid line) and at $l = 0.5$ after 36 min (black dotted line). For $l > 2.2$, no changes in the rod occur.

4.3.2. Data set and model

For both environmental conditions more than 100 non-equivalent reflections were measured. The agreement factors are 7% in both cases, when averaged over equivalent reflections for all specimens used in each type of experiment. The data set consists of the (00), (10) and (20) rods; the results are shown in Figure 4.2. The specular, or (00), rod gives information about the electron density perpendicular to the surface, whereas the two other rods are sensitive to in-plane ordering as well. The (00) rod shows the largest differences between the two environmental conditions, for the other rods the differences are surprisingly small, given the fact that the {111} face is thought to be unstable in water. We conclude that the interface structure is almost the same for the two environmental conditions. From the fact that the (20)-rod, which is the least sensitive to the liquid structure, follows the profile expected for a bulk-terminated crystal, we further conclude that no reconstruction of the crystal occurs. This agrees with our AFM data [5].

In order to fit the data, we need a model that describes the entire interface. Since our data set is limited, we further need to keep our model as simple as possible. We do not know the liquid structure a priori and therefore start with a generic model in which the amount of charge density at various lattice positions can be optimized. In this way we find that we need a strong contribution exactly located at a bulk-extrapolated fcc position on top of a Na-terminated surface, for both experimental conditions. The density corresponds to approximately 0.5 monolayer (ML) Cl. We find little difference between

water and formamide, thus we do not locate the formamide directly. While we initially expected to find a well-ordered formamide layer that would in this way stabilize the {111} surface, these results imply that we have to change our point of view. The data tell us that the interface consists of a bulk-terminated crystal with approximately 0.5 ML Cl on top. As will be explained fully in the discussion section, this is an excellent way to obtain charge neutrality.

Based on this we can construct our final model, in which we add partially-ordered liquid layers further away from the crystal, see Figure 4.3. These water or formamide layers were modelled using only oxygen atoms, since X-rays are insensitive to hydrogen and do not differentiate between O, N and C at our precision level. For the crystal part we started with a bulk truncated {111} NaCl surface with a Na^+ layer on top. Above it we placed one Cl layer and two oxygen layers (O1 and O2). The various degrees of ordering in the liquid layers are modelled using anisotropic Debye-Waller and occupancy parameters. We find no lateral ordering in the layers O1 and O2, so the lateral Debye-Waller parameter for these layers is fixed at $B_{//} = 1000$ Å^2. The top three layers can relax in the direction perpendicular to the surface. In first instance, we tested the model allowing also in-plane relaxations of the Cl^- layer. As the best fits were for a fcc site, we fixed the in-plane coordinates in the final calculations. Similarly, we found no relaxation in the top Na^+ layer and fixed its position to the bulk value. The Debye-Waller, *z*-position and occupancy parameters of the top Na^+ ion and the Cl^- and liquid layers were optimised during the fitting procedure.

For each different environment condition all rods were fitted simultaneously. We used the same model for the humid and formamide environments, which makes comparison simpler. Using this model, we obtained not perfect, but physically satisfactory fits of the experimental data for the humid and the formamide conditions with χ^2 values of 3 and 5 respectively. The best fitting parameters are listed in Table 1 and the fits are shown in Figure 4.2. When can improve our fits slightly by adding more components to the model, e.g. allowing Cl to occupy both fcc and hcp positions, but given the limited size of our data set we restrict our model to the most important features. Models with Cl^- termination do not yield a satisfactory fit, showing that the {111} NaCl surface is Na^+ terminated for our experimental conditions.

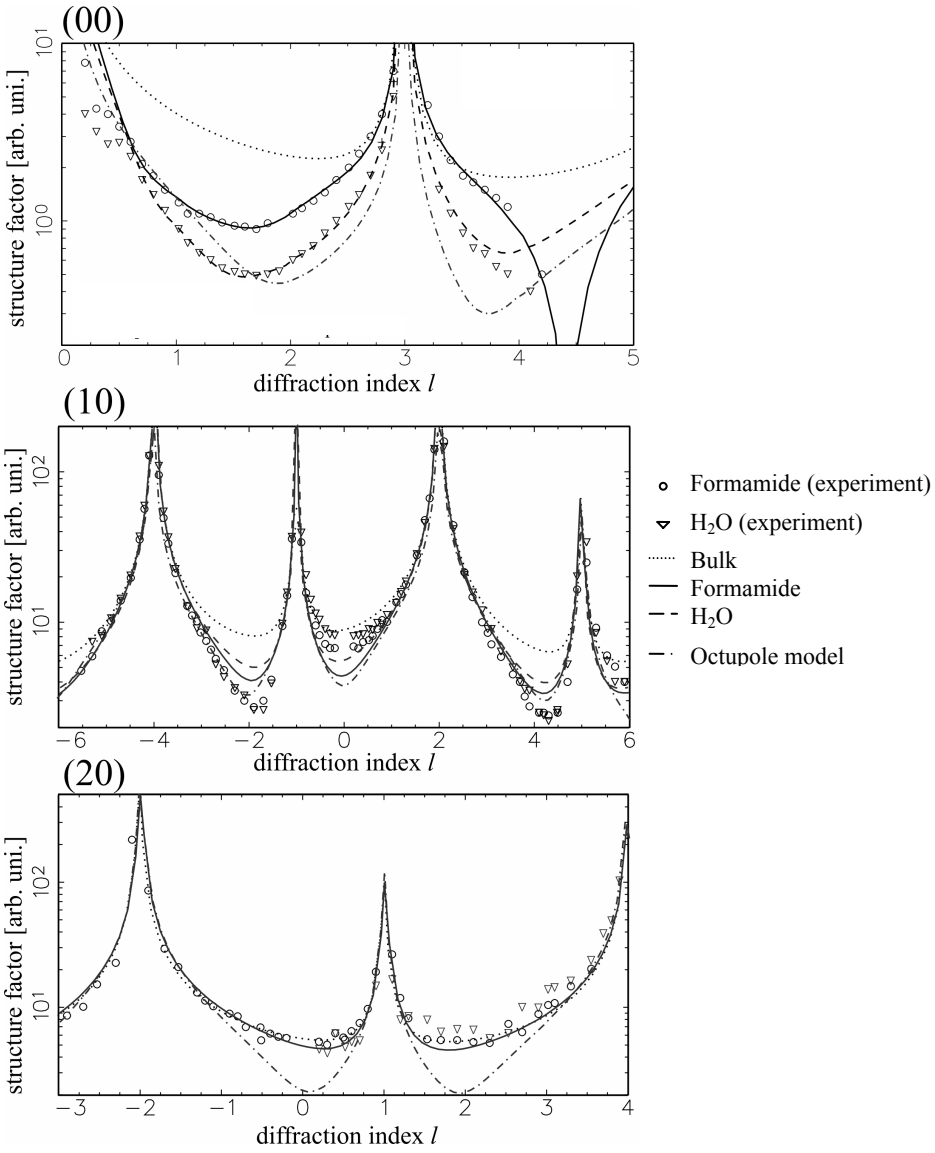

Figure 4.2: Structure factor amplitude along the (00), (10) and (20) rods. Measured structure factors are indicated by symbols. The solid curve represents the best fit for formamide, the dashed curve is for water, the dotted curve is for a bulk terminated crystal and the dash-dotted curve represents the octupole model.

4.3.3. Electron density distribution

A convenient way to visualise the liquid order adjacent to the crystal surface is to use a projection of the electron density on the z-axis in which the effective density depends on the in- plane Debye-Waller parameter $B_{\|}$ [25]. The electron density distribution $\rho(z)$ is calculated by summing all the individual contributions of atoms using:

$$\rho_z = \sum_i Z_i n_i \exp\left(-Q_{\|,i}^2 \frac{B_{\|,i}}{16\pi^2}\right) \frac{1}{\sqrt{2\pi\langle u_{\perp,i}^2\rangle}} \exp\left(\frac{-(z_i - z)^2}{2\langle u_{\perp,i}^2\rangle}\right), \qquad (4.1)$$

where Z_i is the atomic number, n_i the occupancy, $Q_{||,i}$ the parallel momentum transfer, $B_{||,i}$ the in-plane Debye-Waller factor and z_i the position of atom i. The mean vibration amplitude perpendicular to the plane is given by $\left\langle u_{\perp,i}^2 \right\rangle$ and is related to the out of plane Debye-Waller factor by $B_{\perp,i} = 8\pi^2 \left\langle u_{\perp,i}^2 \right\rangle$. The first exponential term in equation (4.1) depends on the parallel momentum transfer and shows to which extent the different rods are sensitive to the liquid structure [25]. This factor is equal to 1 for the specular rod (where the $Q_{\|} = 0$) and decreases for the other rods. For the specular rod all layers contribute, but for high in-plane momentum transfer only layers with sufficient lateral order are visible.

The calculated electron density distributions across the interface for both the water and formamide case are shown in Figure 4.4. The peak labelled Na^+ is the topmost crystal layer; its occupancy is found to lie between 0.7 and 1.0. On the liquid side we find one well-defined Cl^- layer on a fcc position for both the humid and the formamide atmosphere conditions. The in-plane Debye-Waller parameters show that this layer and the layers above are liquid-like; their contribution to the (10) rod is small. The occupancy of the Cl^- layer lies between 0.4-0.7 for both the formamide and the humid conditions. All this suggests a strong interaction of these chloride ions from the liquid side with the atoms of the topmost Na^+ crystal layer. The next liquid layers (modelled by oxygen atoms O1 and O2 in Figure 4.4) show only out-of-plane ordering. Subsequent layers have no order and correspond to the disordered bulk liquid.

atom	parameter	Formamide	Water
O-2	z [Å]	7.5(4)	4(2)
	$B_{//}$ [Å^2]	1000*	1000*
	$B_{\perp}$ [Å^2]	1100(200)	1100(200)
	Occupancy	1.5(4)	2.0(7)
O-1	z [Å]	3.4(2)	2.0(5)
	$B_{//}$ [Å^2]	1000*	1000*
	$B_{\perp}$ [Å^2]	141(80)	164(80)
	Occupancy	1.3(3)	1.0(5)
Cl	z [Å]	-0.04(3)	-0.04 (3)
	$B_{//}$ [Å^2]	71(10)	86(10)
	$B_{\perp}$ [Å^2]	7(4)	7(9)
	Occupancy	0.4 – 0.7	0.4 – 0.7
Na	B [Å^2]	0.4*	0.4*
	Occupancy	0.7 – 1.0	0.7 – 1.0
	χ^2	3.0	5.0

Table 1: Best fit parameters for the formamide and water environments. Values with * were fixed during fitting. The z positions are given with respect to an unrelaxed Cl^- top layer.

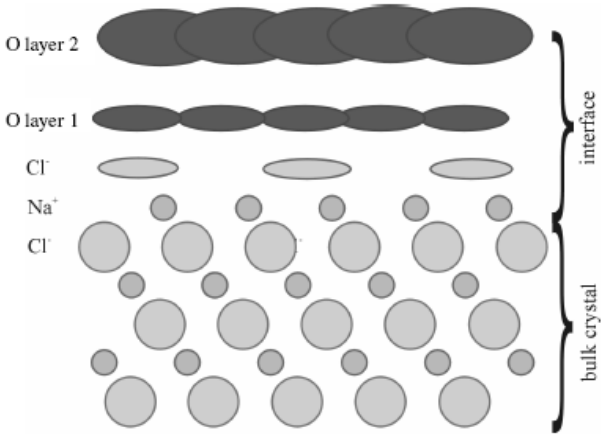

Figure 4.3: Schematic side view of the {111} NaCl face used for data modelling for the humid and formamide environments.

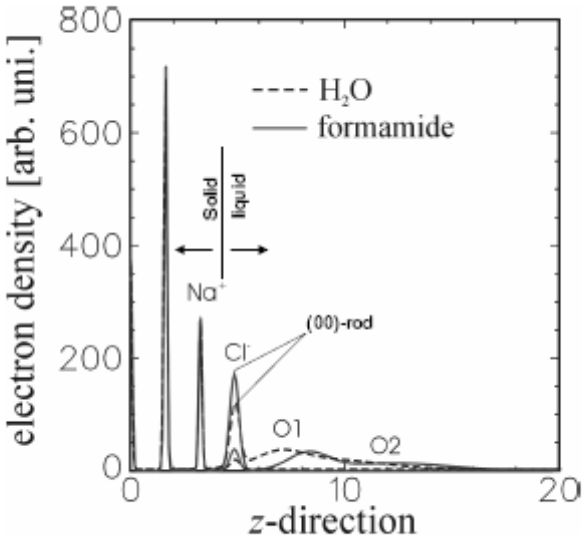

Figure 4.4: Electron density distribution across the interface for the (a) formamide (solid line) and (b) humid circumstances (dotted line). The electron density distribution is shown for two parallel momentum transfers: (00) (two highest peaks) and (10) (two small peaks).

4.4. DISCUSSION

4.4.1. Surface structure

Our SXRD observations confirm the conclusion already drawn from the AFM measurements [5], that the NaCl {111} surface is smooth at an atomic level and is not reconstructed. This supports the conclusion drawn by Brunsteiner and Price from their molecular dynamics simulation of {111} potash alum in contact with a saturated aqueous solution that an electrostatically polar surface of an ionic crystal does not need to be reconstructed to be stable [26].

As we previously mentioned, {111} NaCl is a charged (polar) surface, where the topmost layer consists of either Na^+ or Cl^- ions. Our SXRD results show that the {111}NaCl surface in the presence of formamide and water is Na^+ terminated and not reconstructed. Given these observations, a simple way to obtain charge neutrality is explained in Figure 4.5. Consider a very thin NaCl crystal with a top and bottom {111} surface. This can be made charge neutral by having the same number of Na^+ and Cl^- layers, but then the top and bottom

surface have a different termination, see Figure 4.5a. On thick crystals one observes only one type of termination, so this situation is unlikely. One can generate the same termination on both sides by removing one layer, but then the system is no longer neutral and will have a high electrostatic energy, see Figure. 4.5b. By moving half a surface layer to the opposite side, finally, one can obtain a system that is both charge neutral and has the same structure on both sides, see Figure 4.5c. Other neutral surfaces are possible, because if one removes (on both sides) the same amount of ions from the first and second layer of figure 4.5c, charge neutrality is maintained [27]. The specific case of a top layer with 0.25 ML and a second layer with 0.75 ML corresponds to the octupole reconstruction model proposed by Lacmann [28]. From our data we know that the surface is, however, *not* reconstructed. Figure 4.2 shows a calculation for this octupole model: the difference with the data is especially large for the (20) rod.

Our SXRD results show one well defined but weakly ordered Cl^- layer for both the humid and the formamide atmosphere conditions. The occupancy of this disordered and liquid-like layer (0.4 - 0.7) agrees with the 0.5 ML described in Figure 4.5c. Our data show that the charge-compensating Cl^- layer is not part of the crystal, but is part of the liquid. What we observe is in fact the diffuse half of the electrical double layer adjacent to the bulk truncated {111} Na^+ terminated surface! This situation is sketched in Figure 4.5d. Unfortunately, we cannot determine the occupancy parameter very precisely. An occupancy larger than 0.5 can be explained by the fact that the first liquid layer also contains formamide or water molecules. Since the first layer is located exactly at an extrapolated Cl position, Cl indeed has to be a main component in this layer. The uncertainty in the occupancy of the topmost Na^+ layer is also quite large (0.7-1.0). It is possible that the layer is fully occupied, as our earlier AFM observations suggest, but some vacancies could be present. A value of 0.75 corresponds to the value for the octupole model. This would imply a Cl^- occupancy of 0.25, which is within our fitted range when taking into account that in that case ~0.75 ML of water/formamide (with roughly half the charge density) needs to be added to the layer.

We find that the electrical double layer is very thin, only 5 Å for both conditions. This agrees with estimates using Grahame's equation [29, 30] for the present case. The analytical approach of calculating the properties of the electrical double layer on top of a NaCl {111} surface is described in reference [14]. The calculations further show that about 80% of the charge compensating Cl^- ions are confined to the first liquid layer.

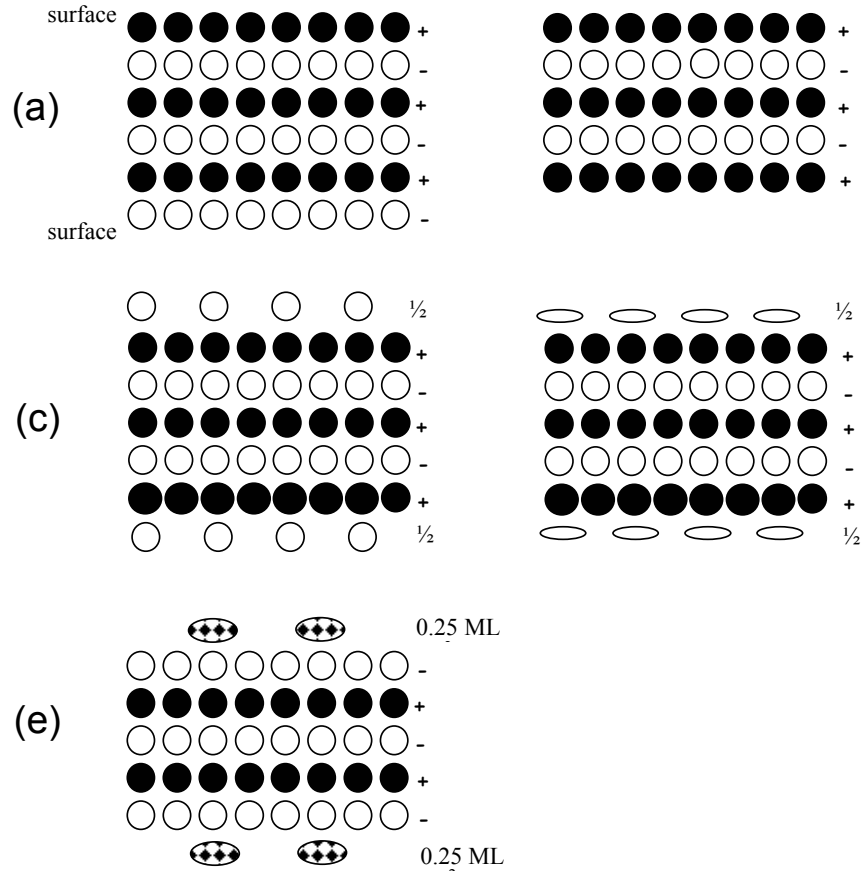

Figure 4.5: Charge distribution versus stability of the polar NaCl{111} surface. (a) The crystal is charged neutral, but its top and bottom surfaces have a different terminations. (b) The terminations of the opposite surfaces are the same, but the crystal is charged and has a very high electrostatic energy (c) By placing a charge compensating 0.5 ML Cl^- layer on top of the complete Na^+ layer for both sides, the crystal is both charged neutral and has the same termination on both sides. (d) Same as (c) but now the charge compensating layer is part of the liquid. (e) For the $CdCl_2$ impurity one has 0.25 ML Cd^{2+} on top of a complete layer of Cl^-. Also in this case the crystal is also charged neutral and has the same termination on both sides.

The model indicates that for both pure water and for formamide solutions, the main mechanism for stabilization is the compensation of the net charge of 0.5 e^+ per surface atom by the opposite charge of 0.5 ML of Cl^- in the first layer of the solution. This model can be extended to the case of Cd^{2+} impurities, which also leads to a crystal morphology with {111} faces [31]. Because of the double charge of the Cd^{2+} ions, one expects for that case 0.25 ML Cd^{2+} on top of a full Cl^- layer, see Figure 4.5e. This fully agrees with the results we obtained recently on that system[14].

4.4.2. Stabilization of the {111} face

We have found that in both aqueous and formamide solutions, the solid-liquid structures are nearly the same and that in both cases, half a monolayer of Cl^- ions stabilizes the polar {111} surface. This means, however, that we have not yet explained the dramatic change in crystal morphology from {100} to {111} which occurs when formamide is added to a pure aqueous NaCl solution. The original explanation that the {111} face is not stable in water, is found to be incorrect. So, there must be a (somewhat more subtle) difference in stability of both forms, such that the balance with respect to the {100} face changes when formamide is added. This must be related to the difference in the interaction of formamide and water with the interface.

Commonly, formamide and water are regarded as similar solvents, characterized by a large dielectric constant (ε = 109.5 for formamide and 78.36 for water), a large dipole moment (μ = 3.37 D for formamide and 1.84 D for water) and the formation of a three-dimensional hydrogen-bonded network. Molecular dynamics simulations of Na^+ and Cl^- ion solvation in aqueous mixtures of formamide [32] as well as NMR measurements [33] show that the formamide molecules interact more strongly with the Cl^- and Na^+ ions than the water molecules in forming a solvation shell. This suggests that the role of the formamide molecules in the stronger stabilization of the {111} NaCl surface compared to water could be the interaction with the first liquid Cl^- layer. This stabilising interaction is stronger for formamide than for water, and thus results in the appearance and stability of octahedral {111} NaCl crystals. This agrees with Figure 4.4, where the first liquid layer is more intense and better ordered for the formamide case. Another possible factor, which unfortunately can not be verified by SXRD, is a difference in step structure and step energy for the two cases. This may also contribute to the observed difference in surface stability. More insight into the stabilization mechanism could come from Molecular dynamics simulations of the interface, but these are challenging and reliable potentials are difficult to obtain [34].

Given the structural similarity between urea and formamide, it is likely that the explanation for the {111} morphology in the presence of urea is similar. We thus propose that also in the case of the classic observation of Rome de l'Isle [4], the {111} surface is flat and unreconstructed. Its presence in the morphology arises from the increased stability of the {111} interface thanks to the interactions of the urea with the first Cl^- layer in the liquid. Similar to formamide, we do not expect that the urea is strongly bonded to the surface.

We find that for the cases of pure water solutions, and for formamide or Cd^{2+} additives, the main stabilisation mechanism is the formation of a charge-compensating layer in the liquid, i.e., the formation of an electrochemical double layer. For charged surfaces in solution, this may be a common

mechanism, because typically there are several ionic species present in the solution. For surfaces in vacuum, nature does not have this route available to minimize the surface energy. For {111} surfaces of crystals with the rock salt structure in vacuum, indeed reconstructions have been found [9-13]. Yet another means to obtain charge neutrality was reported for triangular (111) bulk terminated NaCl islands grown in vacuum by adsorption of Na or Cl on Al(111) and Al(100). In that case the charge of the topmost layers differs from the bulk, and the islands were found to consist of two +1/2 charged Na layers with a Cl^- layer in between [35].

The large changes in morphology for NaCl as a function of impurities are not apparent from the interface structure, but this is certainly not always the case. For example, for the {101} surfaces of potassium di-hydrogen phosphate (KDP), the changes in growth velocity as a function of pH correspond with large changes in the interface structure [36].

4.5. CONCLUSIONS

By using surface X-ray diffraction, we have found that the main stabilizing mechanism for the polar {111} faces of NaCl in solution is the formation of a charge-compensating ion layer in the first liquid monolayer of the solution on top of an unreconstructed crystal surface. This also holds for pure aqueous solutions, and therefore the change in crystal morphology from {100} to {111} upon addition of impurities (formamide or Cd^{2+}) arises from interactions in the liquid that are not directly visible in the interface structure. To achieve stabilisation, nature thus chooses the formation of an electrochemical double layer. In vacuum this route is not available, and under these conditions a surface reconstruction or charge transfer is the only way to obtain a stable {111} surface on crystals with a rock salt structure.

Acknowledgements

The authors would like to thank the staff of the beamlines DUBBLE and the ID03 at the European Synchrotron Radiation Facility in Grenoble, France for their kind assistance during the measurements. Special thanks are given to Christophe Pelletier for inspiring discussions. This work is supported by the Council for Chemical Sciences of the Netherlands Organisation for Scientific Research (CW-NWO)

References

1. H.E. Buckley, in: *Crystal Growth*, (John Wiley & Sons, New York, 1951) p. 556.
2. J. Nyvlt and J. Ulrich, in: *Admixtures in Crystallization*, (VCH, Weinheim; New York; Basel; Camridge; Tokyo, 1995) p. 206-213.
3. L. Lian, K. Tsukamoto and I. Sunagawa, J. Crystal Growth. 99 (1990) 150.
4. J.B.L. de Rome de l' Isle, in: *Cristallographie*, Paris, 1783) p. p. 379.
5. N. Radenović, W.J.P. van Enckevort, P. Verwer and E. Vlieg, Surf. Sci. 523 (2003) 307.
6. N. Radenović, W.J.P. van Enckevort and E. Vlieg, J. Crystal Growth. 263 (2004) 544.
7. P.W. Tasker, Philos. Mag. A. 39 (1975) 119.
8. A. Gibson, R. Haydock and J.P. LaFemina, J. Vac. Sci. Technol. A. 10 (1992) 2361.
9. M.A. Langell, C.L. Berie, M.H. Nassir and K.W. Wulser, Surf. Sci. 320 (1994) 25.
10. P.A. Cox and A.A. Williams, Surf. Sci. 152/153 (1985) 791.
11. N. Floquet and L.C. Dufour, Surf. Sci. 126 (1983) 543.
12. C.A. Ventrice Jr, T. Bertrams, H. Hannemann, A. Brodde and H. Neddermeyer, Phys. Rev. B. 49 (1994) 5773.
13. H. Hannemann, C.A. Ventrice, T. Bertrams, A. Brodde and H. Neddermeyer, Phys. Status. Solidi. 146 (1994) 289.
14. N. Radenović, W.J.P. van Enckevort, D. Kaminski, M. Heijna and E. Vlieg, Surf. Sci. (2006) *in press*.
15. E. Vlieg, Surf. Sci. 500 (2002) 458.
16. I.K. Robinson, Phys. Rev. B. 33 (1986) 3830.
17. J. Arsić, D. Kaminski, N. Radenović, P. Poodt, S. Graswinckel, H.M. Cuppen and E. Vlieg, J. Chem. Phys. 120 (2004) 9720.
18. E. Vlieg, J. Appl. Cryst. 31 (1998) 198.
19. J. Bloch, J. Appl. Cryst. 18 (1985) 33.
20. E. Vlieg, J. Appl. Cryst. 30 (1997) 532.
21. E. Vlieg, J. Appl. Cryst. 33 (2000) 401.
22. H. Kiessig, Ann. Phys-Leipzig. 10 (1931) 769.
23. J.H. Frazer, Phys. Rev. 34 (1929) 644.
24. W. Bayh and H. Pflug, Z. Angew. Phys. 25 (1968) 358.
25. M.F. Reedijk, J. Arsić, F.F.A. Hollander, S.A.d. Vries and E. Vlieg, Phys. Rev. Lett. 90 (2003) 066103.
26. M. Brunsteiner and S.L. Price, J. Phys. Chem. B. 108 (2004) 12537.
27. The general condition for having both charge neutrality and an identical structure of the opposite {111} faces is given by $2\sum_i q_i n_i = \pm 1$. Here i is the surface layer number, starting from a fully occupied Na^+ ($\sum = -1$) or Cl^- layer ($\sum = +1$) and q_i and n_i are the ion charge and occupancy of the ions in this layer. For instance, for the octupole model [28] $q_1 = -1$, $n_1 = 3/4$, $q_2 = 1$, $n_2 = 1/4$, $n_{i>2} = 0$.
28. R. Lacmann, in: *Adsorbtion et Croissance Cristalline*, ed. R. Kern, (Centre National de la Recherche Scientifique, Paris, 1965) p. 195-214.
29. D.C. Grahame, J. Chem. Phys. 21 (1953) 1054.
30. J. Israelachvili, in: *Intermolecular and surface forces*, (Academic Press, London, 1992) p. 213-259.
31. M. Bienfait, R. Boistelle and R. Kern, in: *Adsorption et Croissance Cristalline*, ed. R. Kern. Vol. 152, (Centre National de la Recherche Scientifique, Paris, 1965) p. 577.
32. Y.P. Puhovski and B.M. Rode, Chem. Phys. 222 (1997) 43.
33. C.K. Finter and H.G. Hertz, Z. Phys. Chem. N.F. 148 (1986) 75.
34. I. Okada, Y. Namiki, H. Uchida, M. Aizawa and K. Itatani, J. Mol. Liq. 118 (2005) 131.

35. W. Hebenstreit, M. Schmid, J. Redinger, R. Podloucky and P. Varga, Phy. Rev. Lett. 85 (2000) 5376.
36. D. Kaminski, N. Radenović, M.A. Deij, W.J.P. van Enckevort and E. Vlieg, Crystal Growth & Design. accepted (2005).

Chapter 5

Structure of the {111} NaCl crystal surface grown from solution in the presence of $CdCl_2$

Neda Radenović, Willem van Enckevort, Daniel Kaminski, Maurits Heijna and Elias Vlieg

ABSTRACT

NaCl crystals grown from solution with small concentrations of $CdCl_2$ as impurity have a morphology determined by {111} faces instead of the normal {100} morphology. Optical microscopy, atomic force microscopy and surface X-ray diffraction (SXRD) observations show the {111} surface to be atomically smooth without surface reconstruction. The growth proceeds by monomolecular and higher steps, that originate from 2D nucleation starting from the edge of the crystal as well as from spiral growth. *In-situ* SXRD observations also show that at an atomic scale the {111} NaCl surface is similar to its bulk face truncated along the {111} plane. Analysis based on the SXRD results and electrical double layer theory leads to the conclusion that the polar {111} NaCl surface is stabilized by a mixed monolayer of Cd^{2+} (occupancy 0.25) and water (occupancy 0.75) in direct contact with the top Cl^- layers of the NaCl {111} underneath.

.

5.1. INTRODUCTION

The morphology of crystals grown from solution can be strongly modified if appropriate impurities are added. Many examples of such habit modifiers are known [1-3], but the atomic-scale mechanism behind these effects is usually not known. The earliest report of a habit modifier is probably from Rome de l'Isle who reported in 1783 that octahedrons instead of normal cubes are formed if rock salt is grown in the presence of urine, which was an early source of urea [2]. Despite the increasing number of theoretical and experimental studies that followed this early discovery, there are still unanswered questions about the stability of the electrostatically polar {111} surfaces of rock salt type crystals. The NaCl bulk structure consists of alternating layers of Na^+ and Cl^- ions stacked along the <111> directions. Therefore, the {111} faces must have a high divergent electrostatic energy, which makes them unstable [4]. This implies that, from theoretical point of view, the form {111} is not expected to occur on the morphology of NaCl - type crystals. Theoretical calculations for ionic crystals with rock salt type structure suggest two possibilities when no impurities are present: a) the bulk terminated (111) surface breaks up into neutral {100} facets upon annealing or b) this surface reconstructs [5]. Detailed information was obtained for solid - vacuum systems, of which the {111} surface of the rocksalt structure NiO was the most extensively studied case [6-10]. Some results showed the existence of an epitaxial p(2x2) overlayer [9, 11-13]. This supports the stabilization of the {111} NaCl surface by octupoles, as proposed by Lacmann 40 years ago [14].

A significant effort in investigating the role of impurities on the occurrence of NaCl {111} faces during growth from aqueous solutions has been made by Kern, Boistelle and Bienfait [15-17]. Cd^{2+} shows the strongest effect, because even a small concentration results in the appearance of {111} faces, which are not present in clean solutions. This morphology change is the result of a relative difference in growth rate between the {111} and {100} faces [18-20]. Hartman [21] and Bienfait et al. [17] assumed that the {111} NaCl surface is covered by an epitaxial layer (two-dimensional compound), where Cd^{2+} interacts with three Cl^- ions from the crystal side and with three Cl^- ions or three H_2O molecules from the solution side. According to this hypothesis, this epitaxial $CdCl_2$ layer is identical to pure $CdCl_2$ with a layer thickness $d_{(0003)}$, where the hexagonal unit cell has parameters a=b=3.85Å, c=17.46 Å. The a, b axes of this unit cell closely match the a, b axes (3.98 Å) of the two-dimensional, trigonal, unit cell of {111} NaCl. Based on measured adsorption isotherms, Boistelle and Simon proposed that this adsorption layer consists of $CdCl_2 \cdot 2NaCl \cdot 3H_2O$ instead of $CdCl_2$ [22]. Although epitaxial $CdCl_2 \cdot 2NaCl \cdot 3H_2O$ crystallites have been observed *ex-situ* by optical microscopy and are verified by X-ray diffraction [23], the existence during

growth of this two-dimensional epitaxial adsorption layer has not been experimentally confirmed.

In our previous AFM study of the {111}NaCl crystal faces grown using formamide as additive [23, 24], it was found that no reconstruction occurs and that the lowest steps are monomolecular, with probably the Na^+ layer on top of the surface [23]. However, Cd^{2+} is very different from formamide and is already active at far lower concentrations than formamide to produce octahedrons. This indicates that the mechanism for the stabilization of the {111} NaCl crystal face in both cases is different. In this paper we present detailed experimental data on the atomic structure of the NaCl {111}-solution interface in order to understand the role of Cd^{2+} in this case and to verify the models proposed in literature.

5.2. EXPERIMENTAL PROCEDURE

The octahedral crystals used for the experiments were grown from a filtered (0.45 μm pore width), nearly saturated aqueous NaCl solution in which up to 3 wt % of $CdCl_2$ was added. The crystals were obtained by slow evaporation of this solution in a desiccator at room temperature with concentrated sulfuric acid as drying agent placed at the bottom of the desiccator. We then selected specimens with a size of about 3 x 3 x 2 mm^3, with very flat {111} faces on the top and sides. Generally, these crystals were relatively free from liquid inclusions. Apart from quick drying using a paper tissue after separation from the growth solution, no further surface treatment was applied prior to examination. The surface patterns did not change when the crystals were kept dry in a desiccator and were quickly observed after removal.

The sample surfaces were examined *ex-situ* using bright field and differential interference contrast optical microscopy (DICM) and by atomic force microscopy (AFM). For the AFM observations the side {111} faces were used, because the top face showed a slight shut-off effect, which masked the finest details. The AFMs used, a Digital Dimension 3100 and a Digital Instruments Nanoscope III, were operated in contact mode. In the first case, height and deflection (error-signal) images were recorded simultaneously, whereas for the second instrument only the deflection technique was used.

In some experiments we placed a droplet of aqueous $CdCl_2 \cdot 2NaCl \cdot 3H_2O$ compound solution on top of a {111} NaCl face in order to verify the observations made by Boistelle and Simon [22]. The subsequent development of the crystal needles and plates on the {111} surface was observed *in-situ* using optical microscopy.

Additional information on the surface structure of {111} NaCl at an atomic scale was obtained by surface X-ray diffraction (SXRD). Using this technique diffracted X-ray intensities along so-called crystal truncation rods

were measured [25]. These rods are tails of diffuse intensity connecting the bulk Bragg peaks in the direction perpendicular to the surface. Their exact shape is determined by the atomic structure of the solid-liquid interface. The integrated intensities were converted into structure factor amplitudes by applying the necessary geometrical and resolution corrections [26]. Note that the correction procedure puts all rods on the same relative scale, except for the specular data. The negative values for diffraction index l were obtained by inverting the structure factors according to Friedel's rule. Model calculations and fitting were done using the ROD program [27]. The SXRD experiments were performed *in-situ* and *ex-situ* at beamline ID03 of the European Synchrotron Radiation Facility (ESRF) in Grenoble. The energy of the X-rays used was 10.3 keV. The experiments were carried out at room temperature. The experimental set-up consists of a growth chamber [28] coupled to a Z-axis diffractometer. For *in-situ* experiments a droplet of the Cd^{2+}-containing growth solution was placed on top of the {111} NaCl surface and then covered with a thin Mylar foil, leaving a thin layer of saturated solution between the crystal and the foil. *Ex-situ* experimental data were obtained from as-grown octahedral crystals in air.

In order to the describe NaCl {111} surface lattice and to index the X-ray reflections, we introduce a (111) surface unit cell. The lattice vectors $\mathbf{a_i}$ of this cell are expressed in terms of the conventional cubic lattice vectors by:

$$\mathbf{a_1} = \frac{1}{2}\left[10\bar{1}\right]_{\text{cubic}}, \qquad \mathbf{a_2} = \frac{1}{2}\left[\bar{1}10\right]_{\text{cubic}}, \qquad \mathbf{a_3} = \left[111\right]_{\text{cubic}},$$

$$\text{with} \quad \left|\mathbf{a_1}\right| = \left|\mathbf{a_2}\right| = \frac{1}{2}a\sqrt{2}, \qquad \left|\mathbf{a_3}\right| = a\sqrt{3},$$

and where a is the lattice constant of NaCl (a = 0.563 nm). The corresponding reciprocal lattice vectors $\mathbf{b}_j$ are defined by $\mathbf{a}_i \cdot \mathbf{b}_j = 2\pi\delta_{ij}$. The momentum transfer vector is given by $\mathbf{Q} = h\mathbf{b}_1 + k\mathbf{b}_2 + l\mathbf{b}_3$, with ($hkl$) the diffraction indices. With our choice of surface unit cell the index l corresponds with the direction perpendicular to the surface, while each rod is labeled by the indices (hk).

5.3. OBSERVATIONS

5.3.1. Surface morphology

5.3.1.1. Ex-situ observations of growth patterns

Observations made by optical microscopy showed that the octahedral faces are usually very flat and smooth without further structure (Figure 5.1a). Individual steps could not be seen by optical microscopy, suggesting that the {111} faces grow by monomolecular layers. In some cases bunched step patterns were observed close to the edges of the face, see fig 5.2. These undulated steps are sloping down towards the edges and are not present at the centre of the crystal surface. This indicates that the growth source is near the centre of the crystal face from which steps advance towards its periphery.

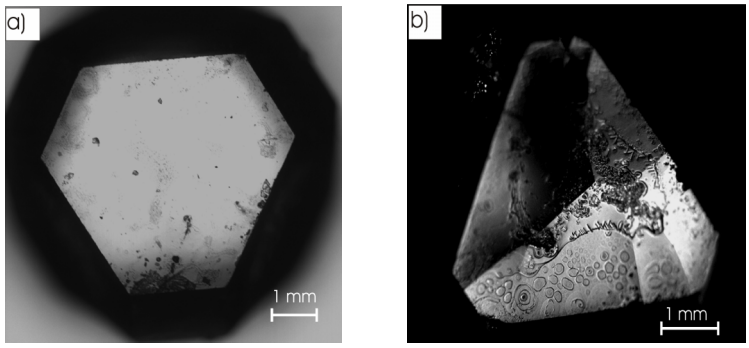

Figure 5.1: *Ex-situ* optical DICM images of a {111} NaCl crystal surfaces grown from a water solution with $CdCl_2$ added as impurity: a) Typical {111} surface; b) Depressed surface containing seams.

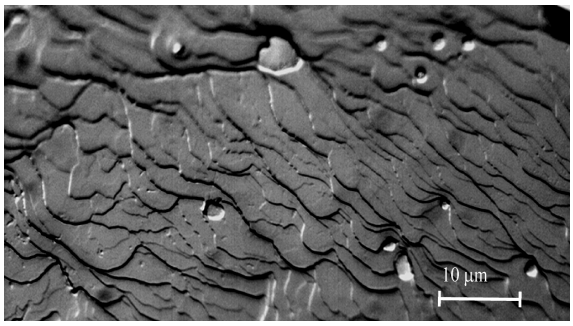

Figure 5.2: *Ex-situ* DICM optical image of a {111} NaCl crystal surface grown from a water solution with $CdCl_2$ added as impurity, showing bunch patterns close to the edges of the face. These undulated steps are not observed at the center of the crystal surface.

A few octahedral crystals have faces as shown in figure 5.1b. This surface is depressed and contains seams. This is probably due to a higher supersaturation of the growth solution close to the edges of the crystal, which provokes the generation of steps by 2D nucleation, which then propagate from the crystal edge towards the centre. If two step trains, generated from different edges of the surface collide, discontinuities in step density develop and a seam is formed.

AFM provides information on a smaller length scale. Observations of the {111} NaCl faces show the presence of numerous monomolecular steps with the lowest possible height according to the interplanar distance (Fig. 5.3). These steps were observed on almost all side {111} faces of the crystals. In all cases, the steps were undulated and did not align with a preferred crystallographic direction. The step height according to AFM measurement is about 0.3 nm. This is in agreement with the interplanar distance, $d_{\{111\}}$, of 0.325 nm. One monomolecular step therefore consists of one Na^+ layer and one Cl^- layer. We have never observed $(1/2)d_{\{111\}}$ steps (which would correspond with one Na^+ layer or one Cl^- layer), so the surface is either Na^+ or Cl^- terminated.

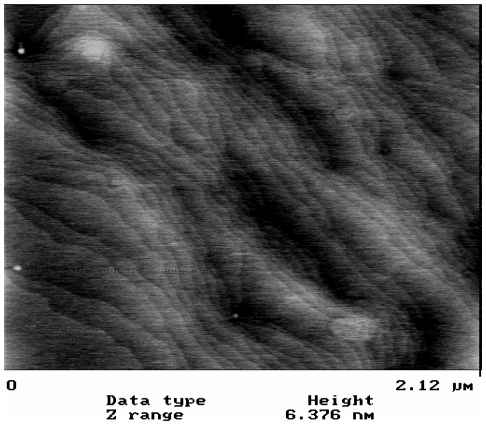

Figure 5.3: AFM image showing monomolecular steps on a (111) NaCl crystal surface grown from an aqueous NaCl solution with $CdCl_2$ added as impurity. Step height is about 0.3 nm. Each monomolecular step consists of one Na^+ layer and one Cl^- layer.

High resolution AFM always revealed oriented patterns of single bright spots with hexagonal symmetry, corresponding to the positions of single ionic species (Fig. 5.4.). The measured interatomic distances of 0.44±0.05 nm are in good agreement with the calculated distance between two adjacent ions of equal sign in the {111} plane (0.398 nm). This observation shows that the surface is not reconstructed and looks like a truncated bulk phase.

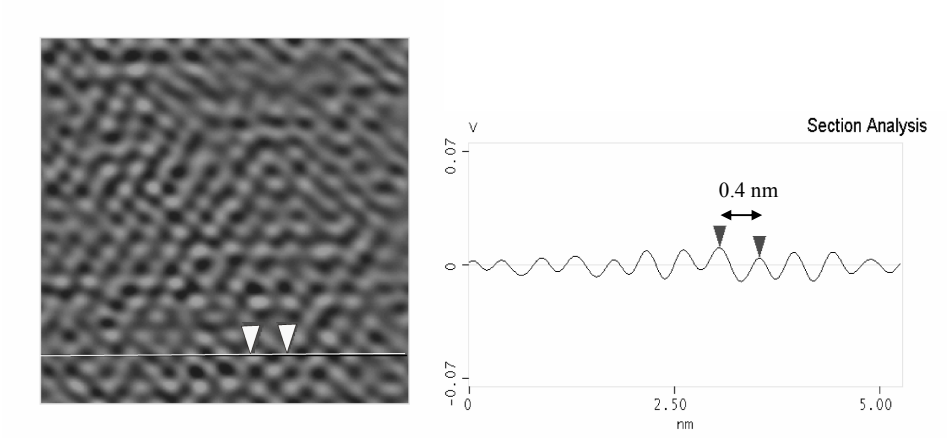

Figure 5.4: AFM image with atomic resolution of a (111) NaCl surface grown from an aqueous NaCl solution with $CdCl_2$ added as impurity. The oriented patterns of the single bright spots refer to the positions of single ionic species. The observed interatomic distances are 0.4 nm.

5.3.1.2. Epitaxial crystallites of $CdCl_2 \cdot 2NaCl \cdot 3H_2O$

In order to check observations made by Boistelle and Simon, which they used to support their proposed epitaxial adsorption model [22], we placed a droplet of $CdCl_2 \cdot 2NaCl \cdot 3H_2O$ compound solution on top of a {111} NaCl face and recorded crystal growth *in-situ* by optical microscopy. This resulted in the epitaxial growth of two types of crystals, namely needles like those shown in figure 5.5a, and hexagonal plates shown in fig. 5.5b.

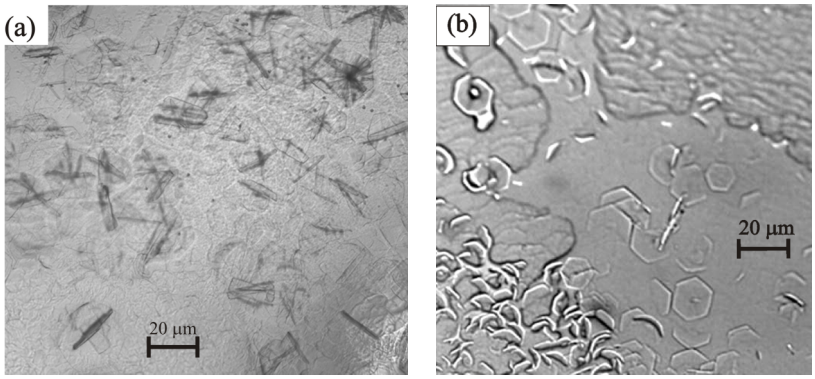

Figure 5.5: Optical image of epitaxial $CdCl_2 \cdot 2NaCl \cdot 3H_2O$ crystals: a) needle-like patterns, assigned as a twin pair (macle) consisting of a (non-visible) crystal with its basal (0001) plane parallel to the (111) substrate surface and a (visible) twin inclined with respect to that plane; b) hexagonal plates presenting non-twinned $CdCl_2 \cdot 2NaCl \cdot 3H_2O$ crystals with their basal (0001) plane parallel to the (111) NaCl surface.

The needles were identified by Boistelle and Simon [22] as $CdCl_2 \cdot 2NaCl \cdot 3H_2O$. They assigned the needles as a twin pair (macle) consisting of a (non-visible) crystal with its basal (0001) plane parallel to the (111) substrate surface and a (visible) crystal twinned on that plane. In contrast to Boistelle and Simon [22], we did observe a number of non-twinned $CdCl_2 \cdot 2NaCl \cdot 3H_2O$ crystals with their basal (0001) plane parallel to the (111) NaCl surface (Fig. 5.5b). A part of the crystals in figure 5.5b, especially those at the lower left part, are twinned.

5.3.2. Surface X-ray diffraction

The size of the data set is different for the two environmental conditions. We measured 121 non-equivalent reflections for the *in-situ* and 20 for the *ex-situ* experiments. The agreement factors are 8% in all cases, when averaged over all samples used in each type of experiment. The data set contains (00), (10), (11) and (20) rods for the case when the crystal surface was covered by a thin liquid film of saturated NaCl solution with $CdCl_2$ added as impurity. Both the *in-situ* and *ex-situ* SXRD experiments showed that the NaCl {111} surface is atomically smooth and is not reconstructed. The *in-situ* data, show little difference from the structure factors calculated for a bulk terminated {111} NaCl surface (solid curve in figure 5.6). This, unfortunately, makes the data rather insensitive to the termination of the crystal. The data disagree with the models containing large structural changes, i.e. the p(2x2) model [29] or the model with a $CdCl_2$-containing layer [22], see figure 5.6. The fact that only rods with the smallest in-plane momentum transfer, i.e. the (00) and (10) rods, show deviations from the bulk calculation means that there is only minor ordering in the interfacial liquid [30]. The (00) rod could only be obtained over a limited range and with moderate accuracy, precluding a detailed determination of the perpendicular ordering for this system. A good fit for these rods is obtained when a bulk terminated surface (either Cl^- or Na^+) is covered with one well-ordered water layer. A model that will be discussed below, namely a disordered layer consisting of $1/4Cd^{2+}$ and $3/4H_2O$, yields an equally good fit, that is given in figure 5.6. Our observations confirm the conclusion already drawn from the AFM measurements that the surface is smooth at an atomic level and is not reconstructed. This once again rules out the octupole model as well as the $CdCl_2 \cdot 2NaCl \cdot 3H_2O$ two-dimensional layer hypothesis for the {111} NaCl surface stabilization.

In addition, the specular, or (00) rod was measured *ex-situ* for the as-grown {111}NaCl surface. We observed a Bragg reflection at d_{0003}=8.84 Å, which confirmes Boistelle and Simon's observation about the existence of isolated epitaxial crystallites $CdCl_2 \cdot 2NaCl \cdot 3H_2O$ on top of the {111} face [22]. In contrast to this, such $CdCl_2 \cdot 2NaCl \cdot 3H_2O$ crystals are not present on the top of

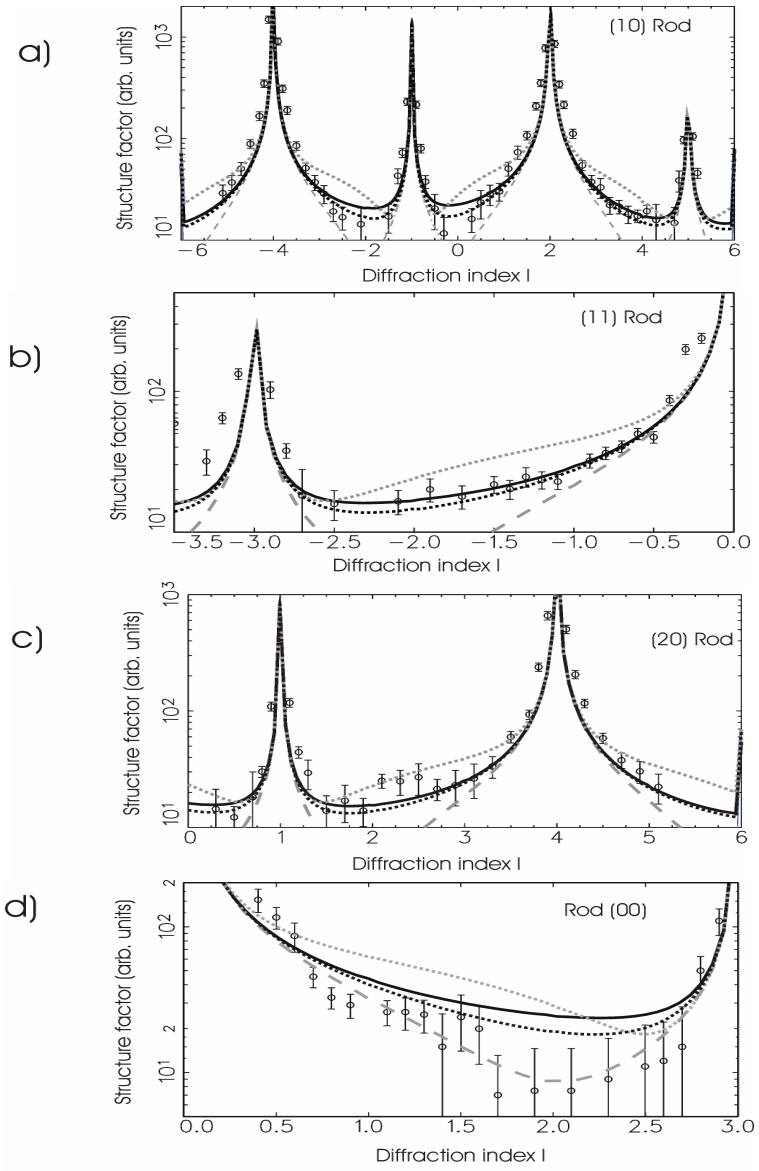

Figure 5.6: Structure factor amplitudes along the (00), (10), (11) and (20) crystal truncation rods for a {111}NaCl surface covered with a thin film of saturated solution with $CdCl_2$ added as impurity. The open circles are data measured *in-situ*. The full line is a calculation for a bulk terminated crystal, whereas the gray dotted-line and the gray dashed line show the octupole p(2x2) model and the model presented by Boistelle and Simon [22], respectively. The black dotted line presents the calculation for a disordered, mixed monolayer of Cd^{2+} (occupancy 0.25) and water (occupancy 0.75) in direct contact with the top Cl^- layers of the NaCl (111) surface underneath.

the {111} NaCl crystal surface when this is covered with the saturated, Cd^{2+} containing growth solution. This follows from the *in-situ* measurement of the specular rod profile (Figure 5.6).

5.4. DISCUSSION

Optical microscopy and AFM observations show that the growth of octahedral NaCl faces in the presence of Cd^{2+} impurity proceeds by monomolecular and sometimes higher steps. The surface morphology is essentially different from that obtained by growth from pure NaCl solutions [23], because the presence of monolayer steps shows that here growth occurs far below the roughening temperature. Two mechanisms are found to be responsible for the generation of the steps. The appearance of bunched and macrostep patterns close to the edge of the surface and never at the centre indicates that the growth source is near the centre of the crystal face. Since it is well known from X-ray diffraction topography that, in general, dislocation lines end at the central part of a crystal face [31], this suggests that the steps are generated by spiral growth due to the presence of screw dislocations. The second mechanism is two-dimensional nucleation of steps starting from the edges of the crystal surface, probably due to a higher supersaturation of the growth solution in these areas, causing step motion towards the center.

AFM data of {111} NaCl grown in the presence of Cd^{2+} show that no reconstruction occurs for this surface and that the surface looks like a truncated bulk phase. This rules out the octupole model for the stabilization of the octahedral NaCl surface, a conclusion that is confirmed by the SXRD results. The lowest observed steps are monomolecular, i.e. consist of one Na^+ layer and one Cl^- layer. $(1/2)d_{\{111\}}$ steps, corresponding to either one Na^+ layer or one Cl^- layer, were never found. This means that only one type of ion is on the top of the {111} surface. We have reported a similar observation in our earlier paper on {111} NaCl grown in the presence of formamide as additive [23]. The present data, however, do not allow to determine directly whether a Na^+ or a Cl^- layer is on top.

According to the model proposed by Boistelle and Simon [22], the {111} face is stabilized by a two-dimensional epitaxial $CdCl_2 \cdot 2NaCl \cdot 3H_2O$ adsorption layer. They did not observe this layer directly, but adsorption isotherms indicated a high concentration of Cd^{2+} close to the surface [32]. Unfortunately, AFM can not be used to distinguish between a (111) truncated NaCl bulk surface and a (0003) two-dimensional layer of $CdCl_2 \cdot 2NaCl \cdot 3H_2O$. The positions of the Cl^- and the Na^+/Cd^{2+} ions in each Cl^--Cd^{2+}/Na^+-Cl^- sandwich layer of this compound are virtually identical to that of {111} NaCl. Moreover, the ionic radii of Na^+ (0.95 Å) and Cd^{2+} (0.97 Å) are almost identical. This

makes the hypothetical epitaxial surface very similar to a truncated bulk face. However, *in-situ* SXRD can make a distinction between these two models and rules out the two-dimensional epitaxial layers. This technique also shows that epitaxial $CdCl_2{\cdot}2NaCl{\cdot}3H_2O$ crystallites are absent when the surface is covered with the thin liquid film of Cd^{2+} contaminated growth solution. While the two-dimensional epitaxial layer does not occur, we do find from optical microscopy and SXRD that three-dimensional epitaxial $CdCl_2{\cdot}2NaCl{\cdot}3H_2O$ crystallites can grow on the {111} NaCl surface. In contrast to the *in-situ* observations, *ex-situ* SXRD of a NaCl crystal removed from the Cd^{2+} contaminated NaCl solution revealed a sharp d_{0003} Bragg reflection from $CdCl_2{\cdot}2NaCl{\cdot}3H_2O$. This observation confirms the existence of a number of small epitaxial crystallites of this compound on the {111} NaCl surface in air. The fact that the d_{0003} Bragg peak is not present in the *in-situ* measurement indicates that the $CdCl_2{\cdot}2NaCl{\cdot}3H_2O$ crystallites originate from shut off effects during separation of the solution and subsequent drying of the crystals. Unfortunately, the limited data set for this condition was not sufficient to prove or disprove the presence of this compound as a two-dimensional adsorption layer on the dried {111} NaCl surface.

Two possibilities for the termination of the crystal therefore remain: either Cl^- or Na^+. In both cases some ordering of the solution at the solid-liquid interface is expected. A surface covered by Na^+, however, is highly unlikely, because such a surface will repel the Cd^{2+} ions and no effect of Cd^{2+} on the growth of {111} NaCl is expected to occur. For a Cl^- termination, Cd^{2+} ions can play a role. In electrochemical terms, there are two models for the location of the Cd^{2+} ions [33]: (a) The Cd^{2+} is in the diffuse electrical double layer adjacent to the NaCl surface, which is covered by a water layer, or (b) The Cd^{2+} ions are directly attached to the rock salt surface, i.e. are positioned in a Stern/Helmholtz layer composed of ¼ Cd^{2+} and ¾ H_2O per surface Cl^- atom.

Calculation of the ion concentration profiles in the diffuse electrical double layer adjacent to a Cl^- terminated, bulk truncated {111} NaCl surface (appendix A) suggests that the compensating charge is almost completely provided by Na^+ ions. This would imply that Cd^{2+} hardly adsorbs on the {111} NaCl surface and thus hardly affects its growth. This fails to comply with our experiments as well as with the adsorption isotherms measured by Boistelle et al. [32]. Therefore, we conclude that the Cd^{2+} ions are most likely directly adhered to the {111} NaCl surface, forming a Stern/Helmholtz layer.

Based on their adsorption isotherms Boistelle et. al. [32] concluded that at saturation the surface coverage is one Cd^{2+} for four Cl^- surface atoms. This corresponds with half a unit charge per surface atom and is identical to the compensating surface charge density of the layer adjacent to the octahedral NaCl surface, necessary to make the system solution – crystal electrically neutral (Appendix A, section A1). From their adsorption measurements

Boistelle et. al. [32] also concluded that three different kinds of Cd^{2+} adsorption sites exist on NaCl {111}. This agrees with direct adsorption on the rock salt surface, since if the species would be "floating" in the diffuse double layer, no different types of adsorption sites would be expected. The good fit of the adsorption isotherms with the Langmuir model [32] confirms the disordered nature of the Cd^{2+}/H_2O layer, as this theory does not hold for strong, ordered lateral interactions and domain structures. This model is fully consistent with the X-ray data (figure 5.6), provided the Cd^{2+}/H_2O layer does not show strong lateral ordering.

From all this evidence it is most likely that stabilization of the {111} form and its retarded growth results from Cd^{2+} directly adsorbed onto the crystal surface. This lowers the surface free energy as follows from Gibbs adsorption isotherm [31, 33]. In addition, step propagation is retarded because the adsorbed Cd^{2+} ions have to be removed prior to step advancement.

5.5. CONCLUSIONS

Octahedral single NaCl crystals of several millimetres in size with stable and flat {111} faces can be obtained from supersaturated aqueous solutions with small concentrations of $CdCl_2$ as impurity. Optical and AFM observations showed that the growth of these octahedral crystal faces proceeds by monomolecular and higher steps. Steps originate from 2D nucleation starting from the edge of the crystal as well as from spiral growth. Atomic resolution imaging of NaCl {111} using AFM and SXRD showed an atomically smooth surface without surface reconstruction. *In-situ* SXRD observation also showed that the {111} NaCl surface is similar to its bulk face truncated along the {111} plane. Analysis based on the SXRD results and electrical double layer theory leads to the conclusion that the polar {111} NaCl surface is stabilized by a mixed monolayer of Cd^{2+} (occupancy 0.25) and water (occupancy 0.75) in direct contact with the top Cl^- layers of the NaCl {111} underneath.

Acknowledgement

The authors would like to thank the staff of the beamline ID03 at the European Synchrotron Radiation Facility in Grenoble, France for their kind assistance during the measurements. This work is supported by the Dutch Organization for Chemical Research, CW-NWO.

Appendix A:

The electrical double layer adjacent to a bulk terminated {111} NaCl surface

A.1. Surface charge

An octahedral NaCl crystal can be considered as an onion-like structure composed of alternating positively and negatively charged layers (figure A1). The total charge of this crystal, Q, is equal to the sum of the charges of the individual layers, or

$$Q = \sum_{n=1}^{N} (-1)^n \phi d_0 A (d_0 n)^2 \ . \qquad \text{(A1)}$$

In this equation N is the total number of layers, ϕ the average volume charge density in each layer, d_0 the layer thickness and $A(d_0 n)^2$ the surface area of layer n. A is a geometrical constant, which is $12\sqrt{3}$ for an octahedron. Summing for $N \to \infty$ gives

$$Q \cong (-1)^N \phi d_0 A (d_0 N)^2 \ / 2 \, , \qquad \text{(A2)}$$

which is identical to half the charge of the outer layer.

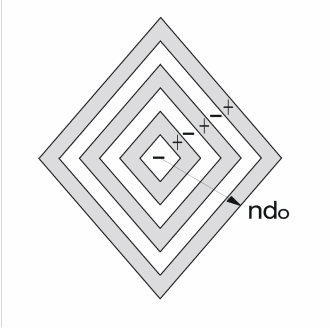

Figure A1: Octahedral NaCl crystal composed of alternating positively and negatively charged layers of thickness d_0.

The whole system crystal-solution must be electrically neutral. So, if an octahedral NaCl crystal with only one type of ion at its surface exists in the solution, then the liquid must be charged -Q. This charge will condense as excess ions near the charged outer layer of the crystal, forming an electrical double layer. Since Q is half the charge of the outer layer, the compensating charge density, σ, at the surface must correspond with half a unit charge per surface atom. For {111} NaCl $\sigma = 0.582$ C/m^2.

A.2. The electrical double layer

The distribution of the Na^+, Cd^{2+} and Cl^- ions adjacent to the {111} NaCl surface is governed by two equations [34]:

$$\rho_i(x) = \rho_i(\infty) \exp(-z_i e \psi(x) / kT) \qquad \text{(A3)}$$

and

$$\sum_i z_i e\rho_i(x) = -\varepsilon\varepsilon_0 \frac{d^2\psi(x)}{dx^2}. \quad \text{(A4)}$$

The first equation is Boltzmann's law, in which $\rho_i(x)$ is the density of ion i as a function of distance x from the crystal surface. Further, $\rho_i(\infty)$ is the concentration of ion i in the bulk solution, z_i is the charge number of ion i, $\psi(x)$ the electrical potential at x, e the electron charge and kT has the usual meaning. The second equation is Poisson's equation, in which ε is the relative dielectric constant and ε_0 the dielectric constant in vacuum. The boundary conditions are

$$\psi(\infty) = 0 \quad \text{(A5)}$$

and

$$\sigma = \int_{x=0}^{\infty} \sum_i z_i e\rho_i(x) = \varepsilon\varepsilon_0 \left(\frac{d\psi(x)}{dx}\right)_{x=0}. \quad \text{(A6)}$$

Combining equation (A3) and (A4) gives [34]

$$\sum_i \rho_i(x) - \sum_i \rho_i(\infty) = \frac{\varepsilon\varepsilon_0}{2kT}\left(\frac{d\psi(x)}{dx}\right)^2, \quad \text{(A7)}$$

and insertion of equations (A6) and (A3) into (A7) gives Grahame's equation [34, 35]

$$\sum_i \rho_i(\infty)[\exp(-z_i e\psi(0)/kT) - 1] = \frac{\sigma^2}{2\varepsilon\varepsilon_0 kT}. \quad \text{(A8)}$$

For a given compensating surface charge density, σ, and bulk concentrations of the different ions, $\rho_i(\infty)$, now the electrical potential at the surface, $\psi(0)$, can be calculated by solving equation (A8) for $\psi(0)$.

If $\psi(0)$ is known, the relation between $\psi(x)$ and x, i.e. the electrical potential as a function of distance, can be calculated by integrating equation (A7):

$$x = \left(\frac{\varepsilon\varepsilon_0}{2kT}\right)^{1/2} \int_{\psi(0)}^{\psi(x)} \left[\sum_i \rho_i(\infty)\{\exp(-z_i e\psi) - 1\}\right]^{-1/2} d\psi. \quad \text{(A9)}$$

If $\psi(x)$ is known, then the ion concentrations $\rho_i(x)$ as a function of distance x from the crystal surface can readily be obtained by using expression (A3).

A.3. Ion concentration profiles

We now consider a saturated aqueous NaCl solution contaminated with 1 wt % $CdCl_2$ in contact with a {111} NaCl crystal surface with the Cl^- ion layer on top. This impurity concentration is well beyond the saturation value for maximal Cd^{2+} surface coverage, which is one Cd^{2+} for four Cl^- ions at the surface [32].

For a Cd^{2+} contaminated NaCl solution in water adjacent to a {111} NaCl surface, the specific Grahame equation is obtained directly from the general expression (A8) [34]

$$\sigma = -\sqrt{8\varepsilon\varepsilon_0 kT}\,\sinh\left(\frac{e\psi(0)}{2kT}\right)\left\{[NaCl]_{bulk} + [CdCl_2]_{bulk}\left(2+\exp\left(\frac{-e\psi(0)}{kT}\right)\right)\right\}^{1/2} \quad \text{(A10)}$$

Using σ = 0.582 C/m^2, T = 298K, ε = 78.5, $[NaCl]_{bulk}$ = 3.938.10^{25} molecules/m^3 (5.44 mol/liter) and $[CdCl_2]_{bulk}$ = 3.28.10^{27} molecules/m^3 (6.54.10^{-2} mol/liter), this equation is numerically solved for $\psi(0)$, giving a surface potential of $\psi(0)$ = -0.0726 Volts. Then, $\psi(x)$ is obtained by numerically integrating equation (A9) starting from the known $\psi(0)$. Finally, $\rho_{Na+}(x)$, $\rho_{Cd2+}(x)$ and $\rho_{Cl-}(x)$ are calculated with the help of equation (A3) and using the computed $\psi(x)$. Figure A2-a gives the three ion concentration profiles, $\rho_i(x)$, acquired in this way. The graph in figure A2-b shows the integrated excess concentrations $\int_0^x [\rho_i(x) - \rho_i(\infty)]dx$ of the three ions close to the crystal surface.

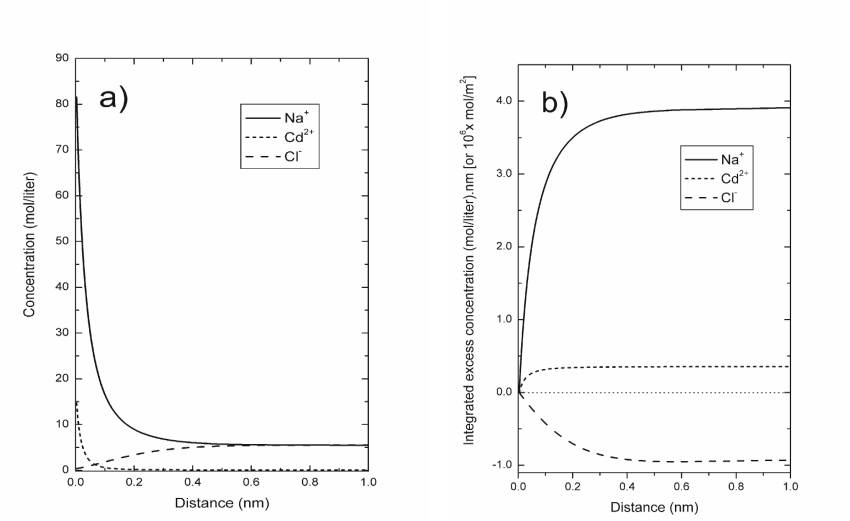

Figure A2: The calculated electrical double layer of a saturated aqueous NaCl solution contaminated with 1% of $CdCl_2$ adjacent to a {111} NaCl surface. Both the concentration (a) and integrated concentration profiles (b) of the Na^+, Cd^{2+} and Cl^- ions are shown.

It is clear that in this continuum model the diffuse electrical double layer is very thin, about 0.5 nm wide. The ratio of integrated excess concentration, i.e. the number of extra ions in the double layer, of Cd^{2+} and Na^+ is 0.091, so the compensating charge is largely covered by the Na^+ ions. Boistelle et al. [32] reported a complete 0.25 Cd^{2+} coverage for $CdCl_2$ concentrations even below 10^{-3} molar. Repeating the above calculations for the 10^{-3} molar case gives a Cd^{2+}/Na^+ integrated excess concentration ratio of $1.4 \cdot 10^{-3}$. Here the calculated amount of Cd^{2+} in the electrical double layer $\approx 6 \cdot 10^{-9}$ mol m^{-2}, which corresponds to $\approx 5 \cdot 10^{-4}$ monolayer. It is clear that this value is negligibly small and conflicts with the observed Cd^{2+} adsorption isotherm measured by Boistelle et al. [32].

Therefore, we must conclude that the Cd^{2+} is in direct contact with the crystal surface, rather than being distributed throughout the double layer.

References

1. H.E. Buckley, in: *Crystal Growth*, (John Wiley & Sons, New York, 1951) p. 556.
2. J.B.L. de Rome de l' Isle, in: *Cristallographie*, Paris, 1783) p. p. 379.
3. I. Weissbuch, L. Addadi, M. Lahav and L. Leiserowitz, Science. 253 (1991) 637.
4. P.W. Tasker, Philos. Mag. A. 39 (1975) 119; J. Phys. C: Solid State Phys. 12 (1979) 4977.
5. A. Gibson, R. Haydock and J.P. LaFemina, J. Vac. Sci. Technol. A. 10 (1992) 2361.
6. M.A. Langell, C.L. Berie, M.H. Nassir and K.W. Wulser, Surf. Sci. 320 (1994) 25.
7. P.A. Cox and A.A. Williams, Surf. Sci. 152/153 (1985) 791.
8. N. Floquet and L.C. Dufour, Surf. Sci. 126 (1983) 543.
9. C.A. Ventrice Jr, T. Bertrams, H. Hannemann, A. Brodde and H. Neddermeyer, Phys. Rev. B. 49 (1994) 5773.
10. H. Hannemann, C.A. Ventrice, T. Bertrams, A. Brodde and H. Neddermeyer, Phys. Status. Solidi. 146 (1994) 289.
11. N. Erdman, O. Warschkow, D.E. Ellis and L.D. Marks, Surf. Sci. 470 (2000) 1.
12. A. Barbier, C. Mocuta, H. Kuhlenbeck, K.F. Peters, B. Richter and G. Renaud, Phys. Rev. Lett. 84 (2000) 2897.
13. A. Barbier, C. Mocuta and G. Renaud, Phys. Rev. B. 62 (2000) 16056.
14. R. Lacmann, in: *Adsorption et Croissance Cristalline*, ed. R. Kern, (Centre National de la Recherche Scientifique, Paris, 1965) p. 195-214.
15. R. Kern, Bull. Soc. Fr. Mineral Crist. 76 (1953) 391.
16. R. Boistelle, *These*. 1966: Nancy.
17. M. Bienfait, R. Boistelle and R. Kern, in: *Adsorption et Croissance Cristalline*, ed. R. Kern. Vol. 152, (Centre National de la Recherche Scientifique, Paris, 1965) p. 577.
18. Draganova, Izv. Khim. 14 (1981) 229.
19. D. Draganova and R. Koleva, Izv. Khim. 13 (1981) 631.
20. L. Lian, K. Tsukamoto and I. Sunagawa, J. Crystal Growth. 99 (1990) 150.
21. P. Hartman, in: *Adsorption et Croissance Cristalline*. Vol. 152, (Centre National de la Recherche Scientifique, Paris, 1965) p. 477.
22. R. Boistelle and B. Simon, J. Crystal Growth. 26 (1974) 140.
23. N. Radenović, W.J.P. van Enckevort, P. Verwer and E. Vlieg, Surf. Sci. 523 (2003) 307.
24. N. Radenović, W.J.P. van Enckevort and E. Vlieg, J. Crystal Growth. 263 (2004) 544.
25. I.K. Robinson, Phys. Rev. B. 33 (1986) 3830.
26. E. Vlieg, J. Appl. Cryst. 30 (1997) 532.
27. E. Vlieg, J. Appl. Cryst. 33 (2000) 401.
28. S.A. de Vries, P. Goedkindt, W.J. Huisman, M.J. Zwanenburg, R. Feidenhans'l, S.L. Bennett, D.M. Smilgies, A. Stierle, J.J.De Yoreo, W.J.P. van Enckevort, P. Bennema and E. Vlieg, J. Crystal Growth. 205 (1999) 202.
29. D. Wolf, Phys. Rev. Lett. 68 (1992) 3315.
30. M.F. Reedijk, J. Arsić, F.F.A. Hollander, S.A. de Vries and E. Vlieg, Phys. Rev. Lett. 90 (2003) 066103-1.
31. X.Y. Liu, J. Phys. Chem. B. 105 (2001) 11550.
32. R. Boistelle, M. Mathieu and B. Simon, Growth of Crystals. 12 (1984) 99.
33. P.W. Atkins, in: *Physical Chemistry*, 6th edition ed, (Oxford University Press, Oxford, 1998) p. 708.
34. J. Israelachvili, in: *Intermolecular and surface forces*, (Academic Press, London, 1992) p. 213-259.
35. D.C. Grahame, J. Chem. Phys. 21 (1953) 1054.

Chapter 6

Pyramids on {100} NaCl after formamide etching

Neda Radenović, Willem van Enckevort

ABSTRACT

Pyramidal hillocks are often formed during wet chemical etching of silicon for micromechanics applications and prevent the production of a smooth surface. The observations of silicon pyramids led to the hypothesis that a semipermeable particle locally retards the etching, causing the pyramid formation (J. Appl. Phys. 89 (2001) 4113). The formation of pyramids is not unique to silicon and therefore the causes of the formation and stability of the hillocks cannot be sought in peculiarities of silicon. We investigated {100} NaCl etched in formamide as a model system to improve our understanding of this phenomenon. Our *in-situ* and *ex-situ* observations of pyramid growth, shape and density support the hypothesis of the semipermeable particle. We have strong evidence that a masking particle of dust at the surface is responsible for the appearance of the pyramids on the crystal surface during etching. The size of the particle is less than 300 nm.

6.1. INTRODUCTION

Wet chemical etching of silicon in strongly anisotropic etchants, such as aqueous KOH, is used for the fabrication of sensors and actuators [1]. The performance of an increasing number of micromechanical devices requires very smooth surfaces, which implies that knowledge of the morphology of etched surfaces is becoming more and more important. However, under certain conditions pyramidal etch hillocks appear on Si {100} surfaces. Since the prevention of etch hillock formation in the anisotropic silicon etching process is an issue of primary importance [2-5], this topic has been the subject of considerable study. The hillock shape is approximately pyramidal and seems to be bounded by a set of four {111} planes and four <110> ridges [6,7]. The fact that such formations can be stable during etching, appears to defy conventional understanding of etch anisotropy [8]. According to the traditional kinematic wave theory, the continuum theory of crystal growth and etching [9,10], protruding shapes on a crystal surface etch fast and should disappear after a certain period of time. The origin of pyramid formation during etching is not completely understood, but observations have led to the hypothesis that semipermeable particles – quite possibly etching products – sticking to the surface are responsible for the development of the hillocks. It is assumed that a large number of tiny masking particles are present on the surface and that these particles are automatically transported towards the protruding ridges and the top of the hillocks [11]. These semipermeable particles reduce the etch rate at the ridges and the top of the pyramidal etch hillocks making these elevations stable in time.

The formation of pyramidal hillocks during etching is not unique to silicon, but is quite a common phenomenon. It has been observed on quartz and it has also been mentioned by Tan, to occur for a number of other materials [12]. Therefore the causes of the formation and stability of the hillocks cannot be sought in the peculiarities of silicon. Because the Si–KOH system is not an ideal one for investigating etch pyramids (since hydrogen bubble formation *in-situ* makes direct observation impossible), we investigated {100} NaCl in formamide as model system to improve our understanding of this phenomenon. In the present paper, we present our observations of the morphology, distributions and properties of etch hillocks obtained on the {100} faces of NaCl crystals using formamid as an etchant. It will be proved that the semipermeable particle hypothesis for hillock formation, as proposed in ref. [8], is correct for the NaCl case. In contrast to Si-etching, here one can apply the particles to the surface on purpose and remove them by agitating the solution. It will be also be shown that the slowest etching face does not reveal pyramids.

6.2. EXPERIMENTAL PROCEDURE

The {100} planes of sodium chloride crystals were etched using formamide as an etchant to obtain steep pyramids and shallow etch pits as, for instance, shown in Figure 6.1. The crystals used for the etching experiments were grown from a filtrated (0.45 μm pore width) aqueous NaCl solution, by slow evaporation in an desiccator with concentrated sulfuric acid as drying agent placed at the bottom of the exsiccator. We then selected specimens with a size of about 5 x 5 x 3 mm^3 , with a very flat (100) face on the top and relatively free from inclusions. Apart from drying using a paper tissue after separation from the growth solution, no further surface treatment was applied. In a number of cases the surfaces were prepared by cleavage along a {100} face. To establish a possible relation between the growth method and pyramid formation also melt-grown crystals were used. In some experiments the surface of freshly cleaved, melt-grown crystals were purposely contaminated by dust particles in order to determine the possible origin of the pyramids. We also etched a {111} NaCl crystal surface to obtain possible conformation of our hypothesis on the geometrical conditions for hillock formation.

Etching was performed by placing a droplet of formamid (purity 99.5%) on the (100) face and leaving it there for 10 min at room temperature, i.e about 296°K. To verify the effects of hydrodynamics, some crystals were placed in beakers with formamid, with or without agitation of the liquid. After etching, the sample surfaces were quickly dried using a paper tissue and examined *ex-situ* using bright field and differential interference contrast optical microscopy (DICM), scanning electron microscopy (SEM) and atomic force microscopy (AFM). For SEM observations, a Jeol JSM-6330 F was used with an accelerating voltage of 3 kV. Prior to observation, the surfaces were coated with a thin platinum layer to prevent charging. The AFM, a Digital Dimension 3100, was operated in contact mode. In all cases, both height and deflection (error-signal) images were recorded simultaneously. *In-situ* observation of the etching process was carried out by placing a crystal covered by a formamid droplet under a bright field optical transmission or reflection microscope. The process was recorded on tape using standard video techniques.

To obtain information on the crystallographic anisotropy of formamide etching, hemispherical depressions were machined in single crystals of sodium chloride. These hemispherical depressions, which have a radius of 5 mm, are etched using pure and slightly undersaturated formamide. Similar to the well-known sphere experiments for growth [14], surface examination of the etched hollow hemispheres provides information on the relative etch velocities in the different crystallographic directions. The slowest etch directions appear as facets in the hemispheres.

6.3. OBSERVATIONS

6.3.1. General Features

According to results obtained by optical microscopy, AFM and SEM, pyramids on the {100} face after formamide etching are of a well-defined geometric shape. Two types of micropyramids can be observed: micropyramids with a rectangular base (figure 6.1a) and micropyramids with an octagonal base (figure 6.1b). All of them have the same approximate orientation and fulfill the 2D point group symmetry 4mm of the {100} NaCl surface. The four faces of the etch micropyramids with a rectangular base are between {2.5 1 0} and {1.2 1 0} and have an angle of inclination ranging from 20-40°.

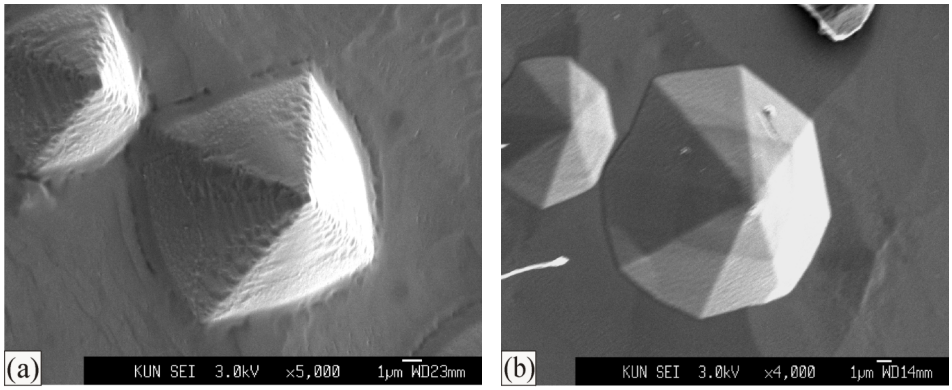

Figure 6.1: Typical etch pyramids obtained after formamide etching of a {100} NaCl surface: a) pyramids with rectangular base; b) pyramids with octagonal base.

Their edges are always parallel to the <100> and <010> crystal directions as shown in figure 6.2. In this figure it is also shown that the ridges of the octagonal pyramids projected on the {100} surface are parallel to the <100> and <110> orientations in the {100} plane. The symmetrically equivalent faces of these pyramids are inclined at angle of ≈ 40-45° to the {100} face of the etch bottom. The angle α varies from 0° to 45° (see figure 6.2). Both types of pyramids can be observed on the same sample obtained from the same etch experiment, but on the separate surface regions.

We observed pyramids in various dimensions ranging from 1 to 20 μm, randomly distributed in densities of 0 to $3 \cdot 10^4$ per mm^2. The pyramid size distribution for a typical experiment is given in figure 6.3, which shows that the elevations occur in a wide range of sizes. It was also found that the pyramids have a tendency to appear near the edges of the crystal, at the borders of opened inclusions and near scratches, which are regions slightly off from the exact

{100} orientation. Using the different microscopic methods no evident particle could be seen on the top of the etch pyramids.

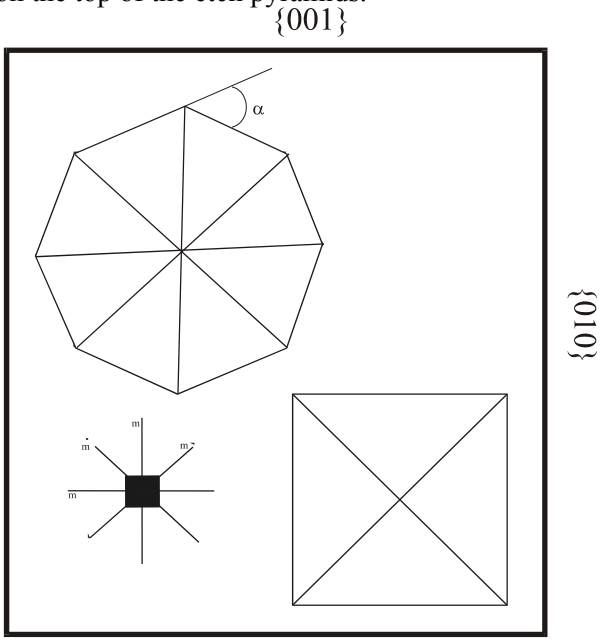

Figure 6.2: Graphic presentation showing the crystallographic orientation of the etch pyramids on a {100} NaCl surface.

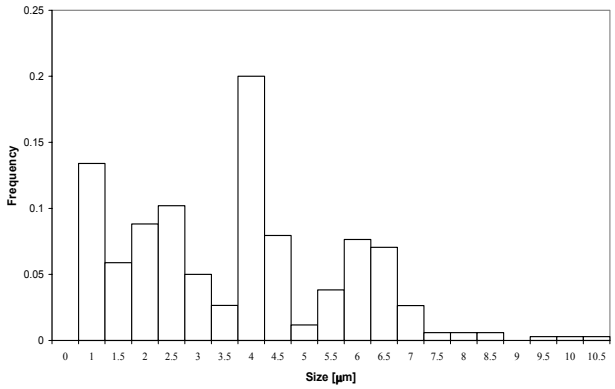

Figure 6.3: Size distribution of etch pyramids obtained after 30 minutes of etching

In addition to the pyramids, shallow pits were also found (figure 6.4). These depressions have rounded shapes and their sidewalls are inclined 4° to 9° with respect to {100}. From their persistence during etching it was concluded that these pits are related to dislocations. This was confirmed by the fact that identical etch pit patterns were obtained on the opposite cleavage faces after cleaving a crystal along {100}. The shallow pits are often arranged in rows, which probably correspond with extended arrays of dislocations, i.e. low angle grain boundaries or slip bands. No correlation was found between the occurrence and distribution of the pits and the hillocks.

Placing a droplet of formamide on a {111} NaCl crystal surface did not result in the appearance of pyramidal etch hillocks; only etch pits were formed.

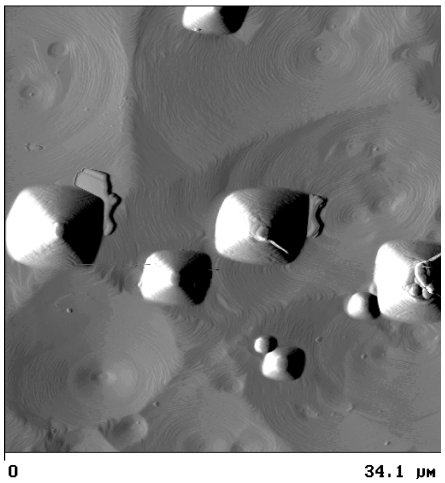

Figure 6.4: AFM image showing the shallow etch pits between a few pyramids

6.3.2. *In situ* observations

In-situ observations of the etching of a NaCl {100} face by a droplet of formamid for a period of one hour showed that most etch hillocks appeared immediately after starting of etching (figure 6.5 a, b, c), whereas a smaller number of them showed up later. During etching, the majority of the pyramids grows and becomes considerably larger, whereas some of them decrease in size and tend to disappear slowly, (figures 6.6 a, b, c). After 20 hours of etching the droplets become saturated, evaporate and growth sets in. Then the remaining pyramids showed no vertical growth, expand only laterally and become flat-topped, as shown in the *ex-situ* micrograph of figure 6.7.

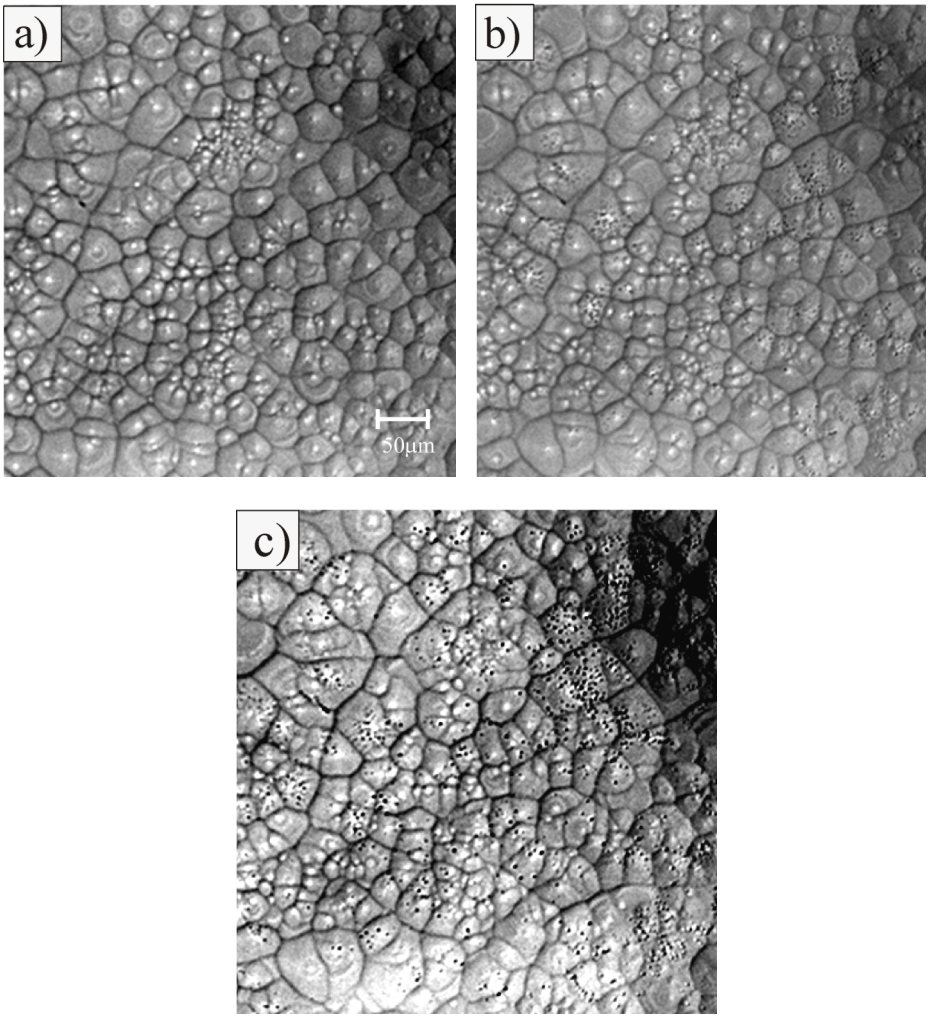

Figure 6.5: *In–situ* observation of formamide etching of a {100} NaCl surface, showing the appearance of pyramidal etch hillocks: a) Early stage without pyramids recorded after 2 minutes; b) Stage after 6 minutes; c) Stage after 15 minutes. The cellular pattern represents the shallow etch pits covering the surface; the pyramids are the black dots, which number increases going from a) to c).

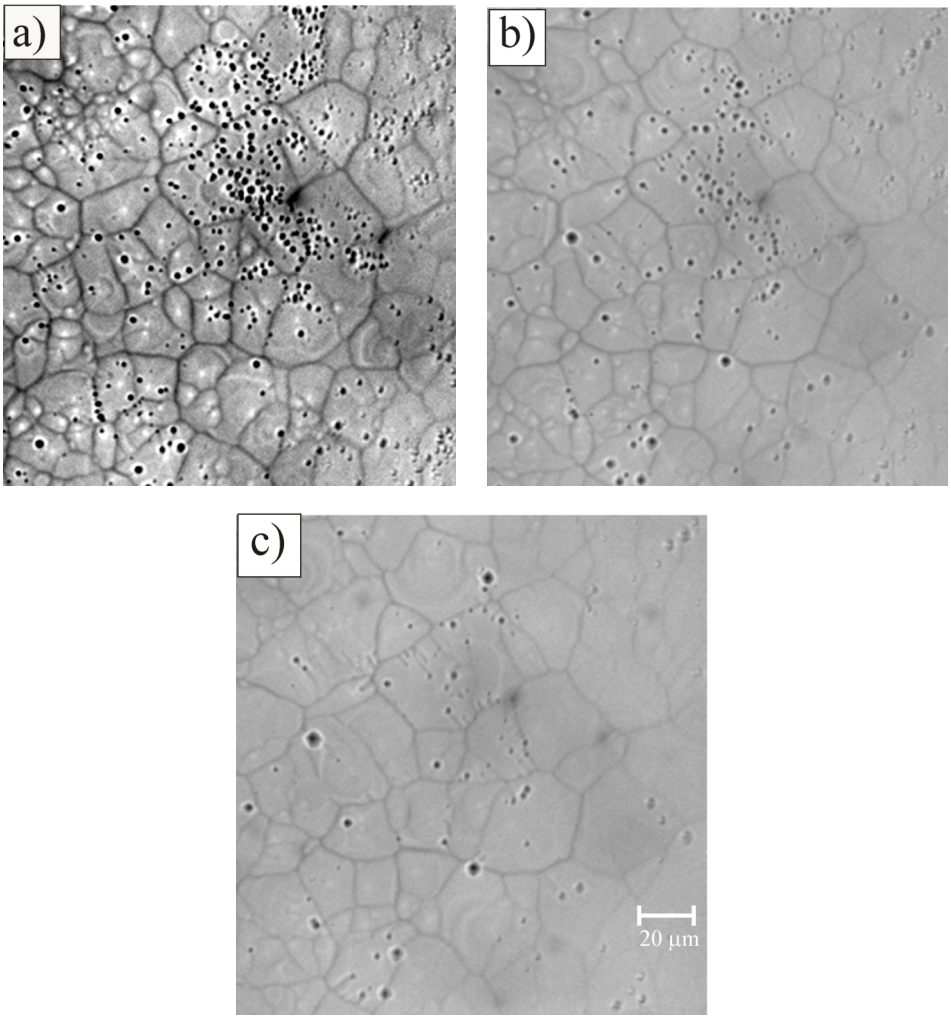

Figure 6.6: *In–situ* observations showing several stages of disappearing pyramids: a) Recorded after 20 minutes; b) Recorded after 60 minutes c) Recoreded after 120 minutes. The cellular pattern represents the shallow etch pits covering the surface; the pyramids are the black dots, which number decreases going from a) to c).

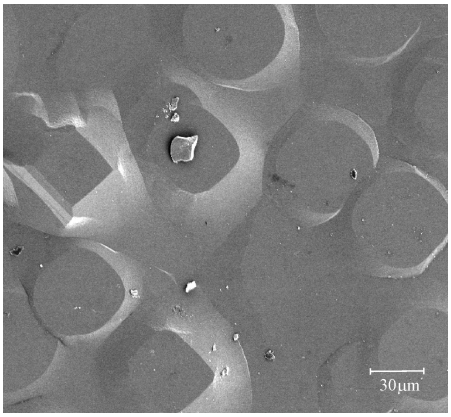

Figure 6.7: After 20 hours of etching of {100} NaCl, the formamide droplets get (super)saturated, evaporate and growth sets in, leading to lateral expansion of the pyramids without vertical growth.

6.3.3. Conditions of hillock formation

6.3.3.1. Etching of NaCl crystals grown from solution

Numerous etch pyramids are obtained by placing a droplet of formamide on the as-grown {100} face of a NaCl crystal obtained from aqueous solution. If we perform etching by submerging such a NaCl crystal into a beaker with formamide without stirring, very small pyramids in considerably smaller number are formed. They appear only at the edges of existing macrosteps and near the edges of the crystal surface. If the liquid in the beaker was stirred, only shallow dislocation etch pits can be observed and no pyramids are formed.

Application of a droplet of filtrated formamide on an as-grown {100} NaCl surface yielded the same amount of pyramids as upon using unfiltrated formamide. The pore size of the filter was 0.45 μm. Etching by placing a formamide droplet on freshly cleaved {100} NaCl faces did not generate any pyramids at all.

6.3.3.2. Etching of melt grown NaCl crystals

When we placed a droplet of formamide on a {100} face of melt-grown NaCl crystals, except for only one case, no pyramids were formed. One should realize that here the surfaces were obtained by cleavage. If the freshly cleaved surfaces were purposely contaminated with dust particles from the ambient, we obtained pyramids in all cases.

6.3.3.3. Dependence on undersaturation

To investigate a possible relation between pyramid formation and different NaCl concentrations of the formamide etchant, we performed etching of the {100} NaCl surface using solutions with low and high NaCl undersaturations. In both cases pyramids were obtained. We did not find significant differences in shape, number, sizes and size distribution of the pyramids obtained by etching with different undersaturation of NaCl in formamide.

6.3.4. Anisotropy of formamide etching

To obtain information about the influence of the anisotropy of the etching on the shape of the hillocks as well as to determine which crystallographic faces are the most stable ones in our system, we performed two different experiments: single crystal growth experiments and etching of hemispherical depressions machined in melt-grown NaCl crystals.

i) If we grow NaCl crystals from saturated water solutions with formamide added in 10 weight % as an impurity only two sets of faces appear, namely {100} and {111}. Growth from pure formamide gives octahedrons, which shows that the growth rate of the {111} faces, $V_{\{111\}}$, is smaller than $1/\sqrt{3}$ $V_{\{100\}}$, where $V_{\{100\}}$ is the growth rate of the cubic faces. This indicates that, in contrast to growth from pure aqueous solutions, formamide stabilizes the octahedral faces with respect to the cubic faces. A similar observation has been reported earlier [12, 13].
ii) Etching of the hemispherical depressions showed that in the case of etching with pure formamide only the {111} face could be observed as a facet. When using slightly undersaturated solution of NaCl in formamide, besides the {111} faces also the {100} face appeared. These experiments show that also in the case of etching, the {111} faces are stabilized.

6.4. DISCUSSION

6.4.1. The masking particle hypothesis and its verification by experiment

As will be elaborated below, our observations lead to the hypothesis that masking particles of “dirt”, adhering to the surface are responsible for the development of the etch pyramids. As explained in ref. [8,11] such a particle can not be an impermeable mask: then it would be underetched immediately and fall off. Etching under this particle is merely slowed down; therefore we refer to it as a semipermeable particle.

Arguments that the pyramids are introduced by a semipermeable dirt particle, locally retarding etching are the following. First**,** in addition to pyramid formation, the shallow etch pits can also be seen during the *in-situ* observations. This indicates that pyramids are formed during etching, and not by some growth process as was speculated in some papers [14,15]. Second, the pyramids are distributed randomly and do not correspond with dislocations as they are not related to the etch pits. This implies that the pyramids do not originate from the structural defects in the crystal. Third, after etching the {100} NaCl surface with droplets which had different undersaturations of NaCl in formamide, we did not find significant differences in the shape, number, sizes and size distribution of the pyramids. This indicates that different levels of undersaturation are not the reason for the appearance of pyramids and that, therefore, the surface characteristics must be the main reason for hillock formation. And finally, etching freshly cleaved, melt and solution grown crystals did not produce pyramids, whereas when we purposely contaminated the freshly cleaved surfaces with dust particles, the pyramids appeared. This implies that the masking particles come from the surfaces and that a large spectrum of particles can cause the formation of the pyramids, not just specific ones.

This set of experiments proves that foreign particles on the surface cause pyramid formation. These masking particles locally retard etching and pyramids develop in a similar way as shown by Monte Carlo study of silicon etching [11]. The pyramids are not due to defects in the crystals or to special properties of the liquid.

6.4.2. Properties of the masking particles

Etching the {100} NaCl surfaces with a droplet of filtrated formamide resulted in the formation of pyramids. This indicates that the masking particle does not originate from formamide or is less than 0.45 μm in size. Because no particles could be seen by AFM, SEM and optical microscopy and by measuring the width of the pyramid top using the SEM, it can be concluded that the size of the particles must be less than 300 nm.

Pyramids are not obtained if the crystal is submerged into a beaker with formamide that is stirred. This can be explained by the flow of solution, which prevents particles from becoming attached to the surface. Moreover, if crystals covered by pyramids from a previous etching experiment were submerged into the beaker with stirred formamid, the pyramids disappeared in a short time. Here, the particles that were still on the top of the pyramids are removed by flow and the pyramid is etched away.

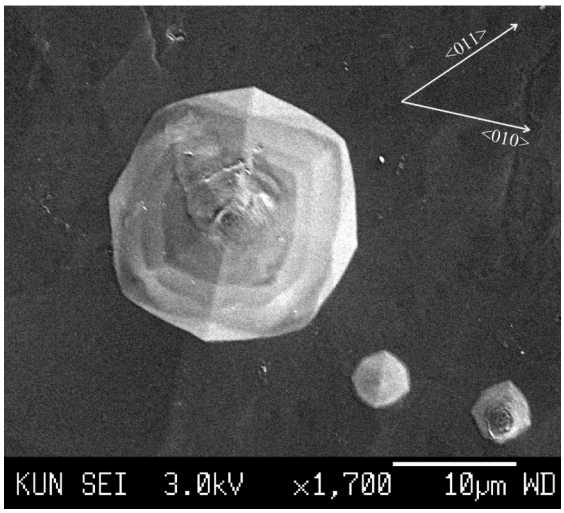

Figure: 6.8: Pyramidal etch hillock in the phase of disappearing, after removal of the masking particle.

When we submerged NaCl crystals into a beaker with formamide without stirring, pyramids are formed in very small numbers and only near the edges of the crystal and near various scratches. This indicates that even a gentle liquid flow, for instance introduced during the immersion of the crystal in the liquid, is sufficient to "wipe off" the particles from the crystal surface. The preferential formation of pyramids near the edges of the crystal surface, on the borders of opened inclusions and at various scratches is a general phenomenon, which was also encountered during the droplet experiments. Apparently these areas, which are slightly off from the exact {100} orientation, are places where the masking particles preferentially collect and become attached to the surface, producing pyramids. Such a misorientation effect was also found for pyramid formation on {100} silicon by KOH etching [8].

The *in–situ* observations showed that at the beginning of etching all pyramids were of similar size, while at later stages of etching some of them disappeared and others continued to grow. In the first case the dirt particles were removed from the pyramid top, after which the hillock was etched away, whereas in the other case the particle remained attached to the top and pyramids became considerably larger during etching. After very long periods of etching, the droplets became supersaturated, evaporated slowly and growth sets in. The remaining pyramids expanded only laterally and became flat-topped. This indicates that the masking particles do not enhance growth by fast vertical 2D contact nucleation.

The SEM image of figure 6.8 shows an octagonal etch pyramid in the phase of being etched away after removal of the masking particle. From this and similar micrographs it can be seen that the etching starts from the top of the pyramid and then proceeds downwards along the ridges. Viewed in projection on {100}, it can be seen that etching is faster in the <110> directions than along <100>. As a result of this process four faces oriented nearly {h 1 0} develop.

6.4.3. Geometrical conditions for etch hillock formation

From a purely geometrical point of view, a pyramidal etch hillock is unstable and should not exist. According to the classical kinematic wave theory of crystal growth and etching, protruding shapes on a crystal surface, $\vec{n}_0$, can only exist if the condition $\vec{R}_0 \cdot \vec{n}_{hkl} = \left|\vec{R}_{hkl}\right|$ is satisfied for all crystal orientations $\vec{n}_{hkl}$ [11]. Here $\vec{R}_0$ and $\left|\vec{R}_{hkl}\right|$ are the etching velocities of the crystal surface, $\vec{n}_0$, and of all other faces (hkl) respectively. Since this condition is not physical, the concept of "velocity source" has been introduced to explain the occurrence of etch pits, hillocks and other features on crystal surfaces [11]. A velocity source is a point or a line on a crystal surface at which the growth/etch rate is locally different. As a consequence of this, the shape of the crystal surface adapts accordingly. In our case the masking particle, which locally retards etching is the velocity source. The adaptation of the surface is the etch pyramid formed.

The surface orientations around the velocity source, i.e. the side walls of the pyramids must fulfill the connectivity relation [8, 11]:

$$\left|\vec{R}_{wall}\right| = \vec{n}_{wall} \cdot \vec{R}_{VS} \qquad (6.1)$$

Here $\vec{R}_{wall}$ is the etch rate of the pyramid walls, $\vec{n}_{wall}$ the orientation of pyramid walls and $\vec{R}_{VS}$ the etching velocity of the {100} surface below the semipermeable mask (which is less than $\vec{R}_{\{100\}}$). From the connectivity condition it follows that the particle must be *semipermeable*, i.e. $\vec{R}_{VS} \neq 0$, else equation (6.1) can not be satisfied and no pyramid will be formed. A second consequence of the connectivity condition is the fact that on the slowest etching surface of a crystal no pyramids can be formed, because then $\vec{n}_{wall} \cdot \vec{R}_{VS}$ is always less than (and never equal to) the smallest possible $\vec{R}_{wall}$. This explains why etching of the {100} face of NaCl with water never gives pyramids. Namely, in that case {100} is the slowest etching face of the NaCl crystal.

However, it is shown here that upon using formamide as etchant the {100} faces etch much faster than {111}, so that the connectivity condition can be satisfied and pyramids are formed. This is also confirmed in our experiment of formamide etching of a {111} NaCl crystal face, because we did not obtained pyramids on that slowest etching face.

Two other criteria for obtaining well shaped etch pyramids are also given in literature [16]. The first one is the requirement that a hillock expands during continued etching, or

$$\vec{R}_{\{100\}} \cdot \vec{n}_{wall} > \left|\vec{R}_{wall}\right| \qquad (6.2)$$

Because of the semipermeable property of the masking particle, $\vec{R}_{VS} < \vec{R}_{\{100\}}$, and from equation (6.1) it follows that condition (6.2) is always fulfilled. To obtain the observed hillocks on {100} NaCl with constant slope and ending with a "sharp" rim on the basal face, a second requirement [16] has to be fulfilled. Namely, for all faces (hkl) between $\vec{n}_{wall}$ and $\vec{n}_{\{100\}}$ the etch rate, $\left|\vec{R}_{hkl}\right|$, has to be larger than $\left|\vec{R}_{\lim}\right| \cdot \vec{n}_{hkl}$, in which $\left|\vec{R}_{\lim}\right|$ is defined by the two equations:

$$\vec{R}_{\lim} \cdot \vec{n}_{wall} = \left|\vec{R}_{wall}\right|$$

and

$$\vec{R}_{\lim} \cdot \vec{n}_{100} = \left|\vec{R}_{100}\right| \qquad (6.3)$$

If this condition is not satisfied, hillocks with a gradually changing slope when going downwards will be obtained, as was found for {0001} quartz etched in a HF/NH_4F mixture [11]

6.5. CONCLUSIONS

Etch pyramids are obtained by placing a droplet of formamide on a {100} NaCl crystal surface. It was shown that these protrusions originate from a local retardation of etching by particles situated on the surface. Since the particle on the top of the pyramid could not be directly imaged using AFM and SEM, its size must be less than 300 nm. Flow of the formamide leads to removal of the particle from the pyramid top and further dissolution results in the disappearance of the elevation.

This work on NaCl strongly supports the semipermeable particle hypothesis, which was used to explain pyramid formation during wet chemical etching of {100} silicon. In contrast to this model, other hypothesis for pyramid formation, such as pseudomasking by H_2 bubbles from the etch reactions [2, 7], emergence of grown-in particles during etching and pyramid formation by regrowth [14, 17, 18], do not apply to our NaCl model system.

Acknowledgements:

We gratefully acknowledge Dr. Erik van Veenendaal for many helpful suggestions and Prof. Elias Vlieg for his inspiring interest in our study. This work is supported by the Dutch organization for chemical research, CW-NWO.

References:

1. M. Elwenspoek and H.V. Jansen, Silcon Micromachining, Cambridge University Press, New York, 1999.
2. E.D. Palik, O.J. Glembocki, I. Heard, Jr., P.S. Burno, L. Tenerz, J. Appl. Phys. 70 (1991) 3291.
3. M.A. Gajda, H. Ahmed, J.E.A. Shaw, A. Putnis, Sensors & Actuators A 40 (1994) 227.
4. L.M. Landsberger, S. Naseh, M. Kahrizi, M. Paranjape, J. Microelectomech. Syst. 5 (1996) 106.
5. U. Schnakenberg, W. Bebecke, P. Lange, Proceedings Transducers '91, San Francisco (1991) 811.
6. S. -s Tan, M.L. Reed, H. Han, R. Boudreau, J. Micromech. Microeng. 4 (1994) 147.
7. T. Baum, D. J. Schiffrin, J. Micromech. Microeng. 7 (1997) 338.
8. A.J. Nijdam, E. van Veenendaal, H.M. Cuppen, J. van Suchtelen, M.L. Reed, J.G.E. Gardeniers, W.J.P. van Enckevort, E. Vlieg and M. Elwenspoek, J.Appl. Phys., 89 (2001) 4113.
9. A.A. Chernov, Sov. Phys. Crystallogr. 8 (1963) 401.
10. F.C. Frank, Growth and Perfection of Crystals, John Wiley & Sons, New York, 1958, p. 411- 419.
11. E. van Veenendaal, K. Sato, M. Shikida, A.J. Nijdam, J. van Suchtelen, Sensors & Actuators A, 93 (2001) 232.
12. F. Gille, K. Spangenberg, Z. Krist. Miner. Petrograd A 65 (1927) 204.
13. M. Bienfait, R. Boistelle, R. Kern, Adsorption et Croissance Cristalline, Colloq. Int. Centre Nat. Rech. Sci. 152 (1965) 577.
14. H.F. Buckley, Crystal Growth, Wiley, New York, 1951, p. 319.
15. K. Sangwal and S.K. Arora, J. Mater. Sci. 13 (1978) 1977.
16. R.B. Heimann, Auflösung von Kristallen - Theorie und Technische Anwendung, Springer Verlag, Wien / New York, 1975, p. 3-10.
17. S.- s. Tan, H. Han, R. Boudreau and M.L. Reed, Proc. Workshop on Micro Electro Mechanical Systems, Osio, Japan, 1994, p. 229-34.
18. S. –s. Tan, M.L. Reed, H. Han and R. Boudreau, J. Microelectromech. Syst. 5 (1996) 67.

Summary

It is well known that crystal growth and morphology are largely influenced by the presence of impurities in the growth solution. However, little is known about the actual process of impurity interaction with the growing crystal surface. In this thesis we study this influence in detail using the NaCl crystal as a model system. Attention is mainly focused on the morphology and atomic scale structure of the {111} faces, which from a theoretical point of view should not be stable.

The second chapter compares the morphology of {111} NaCl faces grown from water-formamide solution with that obtained from pure water solution. The surface patterns were examined *ex-situ* and *in-situ* using bright field and differential interference contrast optical microscopy and *ex-situ* atomic force microscopy. It was shown that formamide and urea stabilize the {111} NaCl faces, whereas larger homologous molecules do not. Atomic resolution imaging of NaCl {111} showed no surface reconstruction. For the {111} NaCl crystals growing from water–formamide solutions, it was observed that growth proceeds by monomolecular steps of height $d_{\{111\}}$. This implies that the surface is terminated by either a Na^+ or a Cl^- ion layer. The {111} surfaces grown from pure water solutions showed shallow growth hillocks with rounded tops as well as growth pits which develop after a longer period of growth. The formation of the pits is explained by the presence of a masking particle at the pit bottom, which locally retards the fast {111} growth.

In the third chapter we examine the morphology of a whole group of alkali halide crystals, which are obtained only from pure formamide solutions. We found that the appearance of the octahedral form is related to the unit cell size of the NaCl structure crystals. In addition to this, the (im-)possibility to obtain {111} surfaces on NaCl crystals grown from pure water solutions at high supersaturations is also investigated. Here we show that independently of supersaturation, {100} is the only stable form.

The atomic scale structure of {111} NaCl is further investigated using surface X-ray diffraction. Chapter four describes the *in-situ* SXRD measurements of {111} NaCl surfaces in contact with ultra-thin water and formamide liquid layers. We ascertained that the surface is not reconstructed and is Na^+ terminated for both conditions. Our results reveal small differences in surface structure between the two cases, which apparently lead to dramatic differences in crystal morphology. It was further concluded from the SXRD analysis that a quarter to half a monolayer of laterally disorderd Cl^- ions are on top of a fully ordered Na^+ crystal surface with occupancy 0.75 to 1.0. In this the surface charge is compensated and the whole crystal is electrically neutral.

A small concentration of $CdCl_2$ in the supersaturated aqueous solution results in appearance of {111}NaCl surfaces as well. This is described in chapter five, which presents AFM, optical microscopic and SXRD observations of these surfaces. Cd^{2+} is very different from formamide and is already active at far lower concentrations than formamide. This implies that the mechanism for the stabilization of the {111} NaCl crystal faces is different in both cases. *In-situ* SXRD measurement shows that at an atomic scale the {111} NaCl surface is similar to its bulk phase truncated along the {111} plane. Further analysis based on the SXRD results and electrical double layer theory leads to the conclusion that the octahedral surface is Cl^- terminated, with ¼ monolayer of Cd^{2+} at random Na^+ sites on top.

In the last chapter we discuss the development of pyramids on the {100} NaCl crystal surface during etching in formamide. Our *in-situ* and *ex-situ* observations of pyramid growth, shape and density show that these features are formed due to the presence of semipermeable, masking dust particles at the dissolving surface.

Samenvatting

Het is algemeen bekend dat de groei en vorm van kristallen in sterke mate beïnvloed worden door de aanwezigheid van onzuiverheden in de oplossing. Echter, de precieze details van hoe dit gebeurt zijn nauwelijks bekend. In dit proefschrift gebruiken we keukenzoutkristallen als modelsysteem om de interacties van onzuiverheden met een groeiend kristaloppervlak te bestuderen. Hierbij is de aandacht met name gericht op de morfologie en atomaire structuur van de {111} vlakken, die volgens de theorie niet stabiel mogen zijn.

In het tweede hoofdstuk vergelijken we de morfologie van de {111} vlakken van NaCl kristallen gegroeid vanuit water-formamide mengsels met die verkregen uit puur water oplossingen. Deze kristaloppervlakken werden *in-situ* en *ex-situ* onderzocht met behulp van helderveld en differentiële interferentiecontrast optische microscopie en *ex-situ* atomaire kracht microscopie. Het blijkt dat formamide en ureum moleculen in de oplossing de octaëdervlakken van de NaCl kristallen stabiliseren, terwijl grotere, homologe moleculen geen invloed hebben. Afbeelden van het {111} NaCl vlak met atomaire resolutie bewees dat dit oppervlak niet gereconstrueerd is. Verder bleek dat de {111} oppervlakken in water-formamide oplossingen laagsgewijs groeien met treden die één NaCl molecule hoog zijn. Dit betekent dat de bovenste, vaste oppervlaktelaag óf enkel uit Na^+ óf enkel uit Cl^- ionen bestaat. De {111} oppervlakken aangegroeid vanuit puur water oplossingen zijn bedekt met groeiheuvels met ronde toppen. Na een langere periode van groei vormen zich op de kristallen “groeiputten”, die ontstaan doordat kleine stofdeeltjes op de bodems van de putten de snelle groei van het {111} vlak plaatselijk vertragen.

In het derde hoofdstuk schenken we aandacht aan de morfologie van een hele groep van alkalihalide kristallen, die allemaal gegroeid zijn vanuit zuiver formamide oplossingen. We vonden dat het al dan niet voorkomen van de octaëdervorm sterk afhankelijk is van de grootte van de kristallografische

eenheidscel. Daarnaast werd onderzocht of {111} vlakken ook aanwezig zijn op NaCl kristallen die groeien vanuit zuiver water oplossingen met een hoge oververzadiging. Hieruit bleek dat, ongeacht de oververzadiging, alleen de {100} vlakken stabiel zijn.

Door gebruik te maken van oppervlakte röntgendiffractie metingen kan men de atomaire structuur van de {111} vlakken van de NaCl kristallen nader onderzoeken. Hoofdstuk vier beschrijft de resultaten voor deze kristalvlakken in contact met een ultradun water of formamide vloeistoflaagje. We toonden aan dat in beide gevallen het oppervlak Na^+ getermineerd is, zonder dat er oppervlakte reconstructie plaats vindt. Het verschil in oppervlaktestructuur voor beide gevallen blijkt tamelijk gering. Echter, ondanks dit geringe verschil is er toch duidelijk een grote invloed op de morfologie van de kristallen. De röntgendiffractie experimenten laten ook zien dat een kwart tot halve monolaag van lateraal ongeordende Cl^- ionen aanwezig is bovenop de geordende Na^+ toplaag, die een bezettingsgraad heeft van 75 tot 100%. Op deze wijze wordt de oppervlaktelading van het polaire {111} kristalvlak gecompenseerd en blijft het kristal elektrisch neutraal.

Als een kleine hoeveelheid $CdCl_2$ wordt toegevoegd aan de waterige groeioplossing verschijnen er eveneens {111} vlakken op de NaCl kristallen. De morfologie van deze stabiele vlakken is onderzocht met behulp van atomaire kracht en optische microscopie, terwijl de atomaire structuur is vastgelegd met oppervlakte röntgendiffractie. De resultaten zijn beschreven in hoofdstuk 5. De invloed van Cd^{2+} op de stabilisatie van de {111} vlakken is bij veel kleinere concentraties onzuiverheid merkbaar dan in het geval van formamide. Dit betekent dat het stabilisatiemechanisme in beide gevallen geheel verschillend is. *In-situ* metingen met behulp van oppervlakte röntgendiffractie toonde aan dat op atomaire schaal het {111} NaCl oppervlak nauwelijks afwijkt van de bulk fase, doorgeknipt langs het kristallografische {111} vlak. Verder uitwerken van de röntgendiffractie resultaten en toepassing van de elektrochemische dubbellaagtheorie leidde tot de conclusie dat in dit geval de {111} oppervlakken Cl^- getermineerd zijn met daar bovenop een kwart monolaag Cd^{2+} ionen op willekeurige Na^+ roosterplaatsen.

In het laatste hoofdstuk onderzoeken we de vorming van steile, piramidevormige heuvels op het {111} NaCl oppervlak, die ontstaan tijdens oplossen in formamide. *In-situ* en *ex-situ* waarneming van de groei, vorm, aantal en verdeling van deze piramides met de optische microscoop maakt duidelijk dat deze patronen ontstaan door de maskerende werking van microscopisch kleine, halfdoorlatende stofdeeltjes op het kristaloppervlak.

List of publications

1. N. Radenović, W.J.P. van Enckevort, D. Kaminski, M. Heijna and E.Vlieg *Structure of the {111} NaCl crystal surface grown from solution in the presence of $CdCl_2$,*,Surface Science, *in press*.

2. N. Radenović, W.J.P. van Enckevort and E. Vlieg. *Formamide adsorption and habit changes of alkali halide crystals grown from solutions*, J. of Cryst. Growth 263 (2004) 544.

3. N. Radenović, W.J.P. van Enckevort, P. Verwer and E. Vlieg. *Growth and Characteristics of the {111} NaCl crystal surface grown from solution*, Surface Science 523 (2003) 307.

4. N. Radenović, W.J.P. van Enckevort. *Pyramids on {100} NaCl after formamide etching*, J. of Cryst. Growth 234 (2002) 589.

5. N. Radenović, D. Kaminski, W.J.P. van Enckevort, S. Graswinckel, I. Shah, M. in 't Veld, R. Algra and E. Vlieg. *Stability of the polar {111} NaCl crystal face in solution,* submitted.

6. D. Kaminski, N. Radenović, M. Deij, W.J.P. van Enckevort and E. Vlieg. *Liquid ordering at the KDP {100}-solution* interface, Crystal Growth & Design, *in press.*

7. D. Kaminski, N. Radenović, M. Deij, W.J.P. van Enckevort and E. Vlieg. *pH-dependent liquid order at the solid-solution interface of KDP crystals,* Phys. Rew. B., *in press*

8. D. Kaminski, P. Poodt, E. Aret, N. Radenović and E. Vlieg. *Surface alloys, overlayed and incommensurate structures of Bi on Cu(111)*, Surface Science 575 (2005) 233.

9. J. Arsić, D. Kaminski, N. Radenović, P. Poodt, S. Graswinckel, H.M. Cuppen and E. Vlieg. *Thickness-dependent* ordering *of water layers at the NaCl(100) surface*, J. Chem. Phys. 120 (2004) 9720.

10. D. Kaminski, P. Poodt, E. Aret, N. Radenović and E. Vlieg. *Observation of a liquid phase with orthorhombic orientational order*, submitted.

Curriculum Vitae

Neda Radenović – Pelletier
born in Belgrade, Serbia
on 28 November 1970

1989	High School "Zemunska Gimnazija", Belgrade, Serbia
1998	Graduated physical chemist, Faculty of Physical Chemistry, University of Belgrade, Serbia Project: *Contribution to the study of membrane biopotential and its oscillations* Supervisors: Prof. dr. Dragica Minić and Prof. dr. Milorad Jeremić
1998 – 2000	Junior researcher at the Environmental Protection Laboratory, Institute of Physics, Belgrade, Serbia (working on the determination of heavy metals in atmosphere) Supervisor: Dr. Mirjana Tasić
2000 – 2005	PhD studies at the Department of Solid State Chemistry, Institute for Molecules and Materials, Radboud University Nijmegen, The Netherlands Project: *The Role of Impurities on The Morphology of NaCl Crystals: An atomic scale view* Supervisors: Prof. dr. Elias Vlieg and Dr. Willem van Enckevort